VIBRATIONAL SPECTROSCOPY OF STRUCTURAL PHASE TRANSITION AND LASER INDUCED INSTABILITIES IN SOME UNIVALENT THIOCYANATES

by

SOKKI SATHAIAH

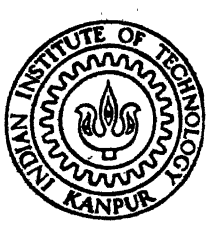

DEPARTMENT OF PHYSICS

INDIAN INSTITUTE OF TECHNOLOGY KANPUR

MAY 1990

VIBRATIONAL SPECTROSCOPY OF STRUCTURAL PHASE TRANSITION AND LASER INDUCED INSTABILITIES IN SOME UNIVALENT THIOCYANATES

A Thesis Submitted
in Partial Fulfilment of the Requirements
for the Degree of

DOCTOR OF PHILOSOPHY

by

SOKKI SATHAIAH

to the

DEPARTMENT OF PHYSICS

INDIAN INSTITUTE OF TECHNOLOGY KANPUR

MAY 1990

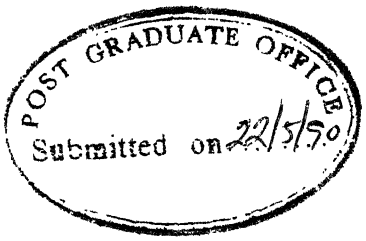

CERTIFICATE

It is certified that the work contained in the thesis entitled "VIBRATIONAL SPECTROSCOPY OF STRUCTURAL PHASE TRANSITIONS AND LASER INDUCED INSTABILITIES IN SOME UNIVALENT THIOCYANATES" by SOKKI SATHAIAH, has been carried out under the joint supervision of Dr. V.N. Sarin and myself and that this work has not been submitted elsewhere for a degree.

H.D. Bist 3.5.90

(H.D. Bist)
Department of Physics
I.I.T.Kanpur

May, 1990

SYNOPSIS

Name of Student: **SOKKI SATHAIAH** Roll No. 8410973

Degree for which submitted: **PH.D.** Department: **PHYSICS**

Thesis Title: **VIBRATIONAL SPECTROSCOPY OF STRUCTURAL PHASE TRANSITIONS AND LASER INDUCED INSTABILITIES IN SOME UNIVALENT THIOCYANATES**

Name(s) of Thesis Supervisor(s): **DR. H.D. BIST**

Month and year of Thesis Submission: **MAY, 1990**

Structural phase transitions (SPTs) in crystals between high symmetry (disordered) and low symmetry (ordered) phases occur on change of temperature, or pressure, or intensity and frequency of light, or even electric and magnetic fields applied at the sample. Recently, the focus of studies on SPTs has been on both the theoretical and experimental aspects of static and dynamic properties, their universal features and microscopic mechanisms governing them. Many interesting new areas (such as laser induced SPTs and oscillatory instabilities, PTs in laser trapped ions/atoms, incommensurate SPTs, systems containing lattice disorder due to impurities, multi critical points, quantum crystals, high T_c superconductors and quasi low dimensional systems) have emerged. One of the most novel theoretical approaches has been the application of the methods of equilibrium phase transitions to the field of synergetics or deterministic chaos. Recently, experiments on diverse physical, chemical and biological systems have been extending the concept of universality to the "transitions to chaos" in nonlinear systems and geometric phase transitions.

Among the various experimental techniques, Raman and infrared (IR) spectroscopies are the powerful micro probes to study the static and dynamic processes occurring at the molecular (or atomic) level during the SPT. Both the techniques are complementary to each other.

The thiocyanates MNCS (where M = K, Rb, Cs, Tl and NH_4) are ionic crystals consisting of univalent cations and rod shaped anions. These substances are of interest because of their simpler structures at room temperature (RT) and order-disorder type SPTs at higher temperatures. The SPTs in MNCS systems have been studied using thermal analyses, X-ray & neutron diffraction and nuclear quadrupole resonance spectroscopy on one or more of these compounds. So far, Raman & IR spectroscopic studies of SPTs have been reported only for KNCS and NH_4NCS systems. In the present work, a detailed vibrational (Raman & IR) spectroscopic investigation of SPTs in CsNCS, RbNCS and TlNCS has been carried out, for the first time. The main objectives of these studies have been a search for microscopic order parameters like soft or hard modes and other spectral manifestations of order-disorder SPTs with an eventual aim of attaining a clear understanding of the microscopic mechanisms governing the SPTs and their universality aspects. Quantities like activation energies (U) for the re-orientational motion of NCS^- ions and universal exponents, e.g., order parameter exponent (β) and correlation length exponent (ν) have been extracted from the experimental data. The most interesting and novel aspect is the observation of laser induced

temporal oscillations and cascade of period doublings as a function of laser irradiation time, near the SPT, in CsNCS crystal.

The thesis has been divided into seven chapters. Each chapter is self-contained. The chapter 1,briefly outlines the general introduction to equilibrium and nonequilibrium phase transitions (EPT and NEPTs), the relevance of EPT concepts in understanding certain complex NEPT phenomena, classification of SPTs; vibrational spectroscopies and their important role.In addition, various other topics like critical exponents, microscopic order parameters and other spectral manifestations of SPTs have been briefly reviewed. The new directions in the field of SPTs, recent developments in the experimental techniques and some important aspects of laser induced instabilities and univalent thiocyanate systems have also been discussed.

Chapter 2 contains the brief summary of the sample preparation methods, Raman & IR techniques and various factors affecting the spectra. Emphasis is given to the preventive maintenance and the methods employed for better data acquisition.

In chapter 3, Raman & IR spectra of CsNCS sample at RT and the temperature (T) dependence of various thermosensitive vibrational modes are presented. On the basis of detailed experimental studies, the orthorhombic to cubic transition in CsNCS at $T_c \simeq 470^{o}K$ has been spectroscopically characterised as an order-disorder and to be first order in nature. A remarkably consistent value of $\beta \simeq 0.35 \pm 0.04$ has been obtained from the

characteristic changes in the integrated intensity of the C-N stretching (ν_{C-N}) mode and the peak frequency of the in-plane rotatory mode, for T well below T_c. The anomalous increase in the band widths of many modes in the IR and Raman spectra have been attributed to the increased anharmonicities as precursor effects to the transition. An activation energy, $U \simeq 0.46 \pm 0.02$ ev has been calculated from the exponential increase in the bandwidth (γ_{C-N}) near T_c. The replacement of Raman external modes by a broad-band spectrum and the smeared off fine-structure in the ν_{C-N} region of IR spectrum for $T>T_c$, have been related to loss of translational invariance and emergence of dynamic disorder in the cubic phase, as both ions (Cs^+, NCS^-) are in motion.

Chapter 4 reports the novel observations, near SPT, in CsNCS single crystal. Some unusual periodic oscillations and cascade of period doublings in the scattered light were observed as a function of time, when CsNCS crystals were kept stable near the SPT temperature and irradiated by various focussed beams of constant laser powers. From the striking similarities between the observed phenomenon and the period doubling bifurcations which occur in diverse nonlinear physical, chemical and biological systems, different oscillatory regions in CsNCS crystal have been related to successive instabilities, as some internal parameter of the system changes with the irradiation time in a self-controlled manner. Considering thermal and photo-induced changes as the major sources, probable nonlinear interaction mechanisms for the observed phenomenon have been proposed.

In chapter 5, comprehensive Raman & IR studies of SPT in RbNCS are presented. The β obtained from both Raman & IR measurements ($\beta \simeq 0.45 \pm 0.04$) is strikingly consistent. In the Raman spectra, the appearance of sidebands in the ν_{C-N} and ν_{C-S} mode regions and the unusual temperature dependence of their relative strengths and splitting energies revealed the existence and gradual diminution of an internal field as the orthorhombic to tetragonal transition temperature ($T_c \simeq 439^oK$) is approached from below. Further, the internal field influences C-N and C-S oscillators in an opposite way. These results have been discussed in the context of an anharmonic oscillator model. The broad-band spectra in the external as well as internal mode regions indicate rapid head to tail fluctuations of NCS^- ions, for $T>T_c$. The activation energy, $U \simeq 0.29 \pm 0.02$ ev, has been calculated from the variations in γ_{C-N}, near T_c.

Chapter 6 reports the detailed analysis of Raman & IR spectra of TlNCS sample at various temperatures between 293 - 438^{o}K. The spectral manifestations of orthorhombic-tetragonal SPT have been found in large changes of the band profiles of many internal and external modes near T = 367^{o}K ($\simeq T_c$). More precisely, the linear variations in reduced peak intensities (I_2^r & I_3^r) of Raman external modes and the complete disappearance of ν_2 mode at T_c symbolize the progressive re-orientational disordering processes as T approaches T_c from below. Values of β obtained from these intensity measurements are 0.46 $\pm$ 0.04 and 0.45 $\pm$ 0.04, respectively. Thermal behaviour of I_3^r reveals the importance of

order-parameter fluctuations near T_c. A meanfield type correlation length exponent, $\nu \simeq 0.46 \pm 0.04$ has been computed from the characteristic T dependence of I_3^r above T_c. An abrupt increase in bandwidths of some of the internal and external modes, near T_c, has been attributed to the orientational disordering of NCS^- ions. The activation energy, $U \simeq 0.32 \pm 0.02$ ev, calculated from the large enhancement in the bandwidth (γ_3) of a librational mode is in accordance with the reported U ($\simeq$ 0.41 ev) value of KNCS system. Like RbNCS, the appearance of side bands in the ν_{C-N}, ν_{C-S} and δ_{N-C-S} mode regions of Raman spectra and the anomalous T dependence of their relative intensities and splitting energies reveal the existence and gradual diminution of an internal electric field as T approaches T_c.

Chapter 7, outlines the conclusions drawn from the present work. Comparison of present studies with known ones in other systems reveals the existence of internal fields in the orthorhombic phases of RbNCS and TlNCS. All the characteristic changes in the vibrational spectra of the samples studied suggest that the order-disorder SPTs in MNCS systems occur as both the cation and anion are in motion. It has been emphasized that the 'period doubling' like oscillatory instabilities are the unique features observed for the first time near the SPT and they may be the signatures of nonlinearities in CsNCS crystal.

ACKNOWLEDGEMENTS

I have great pleasure to express my gratitude to Professor H.D. Bist and Dr. V.N. Sarin for introducing me to the field and their stimulating guidance.

I thank Professors C.M. Bowden (USA), K.A. Nelson (USA), W. Kiefer (Germany) and D.D. Pant (DSBC, Nainital) for the encouragement and valuable suggestions on the subject during their short visit to this place. I am also thankful to all my colleagues and friends for their co-operation.

I wish to thank Mr. K. Rajagopalan for recording IR spectra and all others in graphic arts, CELT Office, Physics Office, Central Library, Workshops, Glass Blowing etc. for their timely help.

I thank Mr. S.K. Khullar and Mr. B.P. Pant for excellent typing. I am very much thankful to Mr. R.K. Bajpai, Mr. A.K. Bhargav and Mr. G.S. Thapa for tracing the figures.

I take this opportunity to express my deep sense of gratitude to all my family members, especially, my mother who showed great patience and encouraged me during the entire period of my research.

S. Sathaiah

To my parents

TABLE OF CONTENTS

LIST OF TABLES

LIST OF FIGURES

LIST OF PUBLICATIONS

(A) JOURNALS

1) Vibrational studies of structural phase transitions in Caesium thiocyanate.
S. Sathaiah, V.N. Sarin, and H.D. Bist, J.Phys: Condensed matter 1, 7829 (1989).

2) Temporal oscillations in the scattered light in CsNCS single crystal near the structural phase transition temperature, .
S. Sathaiah, V.N. Sarin and H.D. Bist., Phys.Lett.A 140 (6) 348 (1989).

3) Structural phase transitionand internal fields in Rubidium thiocyanate probed through vibrational spectroscopy,
S Sathaiah and H D Bist, J. Chem. Phys. (Submitted)

4) Vibrational spectroscopy of structural phase transitions and Raman evidence of librational fluctuations in TlNCS,
S Sathaiah and H D Bist, J. Chem.Phys. (Submitted)

5) Raman scattering studies of structural phase transition and polimerization in S_8,
S Sathaiah and H D Bist (to be communicated)

(B) CONFERENCES

1) Phase transition studies of CsNCS by Raman Spectroscopy,
S. Sathaiah, V.N. Sarin and H.D. Bist, Proc. Solid st.Phys. Symp.India, 30(A), 334 (1987).

2) Raman spectroscopic studies on the phase transition of thallium thiocyanate (TlNCS).
S.Sathaiah, V.N. Sarin and H.D. Bist, Proc. Int. Conf. Raman Spectr. XI, England, 459 (1988).

3) Raman scattering studies of NaNCS single crystal above room temperature.
S. Sathaiah, V.N. Sarin, and H.D. Bist, presented at Int.Conf.Raman Spectr. Calcutta (1988).

4) Novel observations on phase transitions probed through Laser Raman Spectroscopy.
H.D. Bist, S. Sathaiah and V.N. Sarin, in
"RECENT TRENDS IN RAMAN SPECTROSCOPY" eds:
S.B. Banerjee and S.S. Jha (World Scientific, Singapore, 1989) P.340-360.

5) Raman evidence of internal field in Rubidium Thiocyanate [RbNCS].
S. Sathaiah, V.N. Sarin and H.D. Bist, Int.Conf. Raman Spectr. XII Columbia, 496 (1990).

(C) OTHERS

1) V Pilaniappan, S Sathaiah, H D Bist and U C Agarwala, J.Am.Chem.Soc. 110, 6403 (1988)

2) P S R Prasad, S Sathaiah and H D Bist,Chem.Phys.Letts. 142(5), 341 (1987)

CHAPTER 1

INTRODUCTION

Abstract

This chapter outlines the general introduction to equilibrium and nonequilibrium phase transitions (EPT and NEPTs), the relevance of EPT concepts in understanding certain complex NEPT phenomena, classification of SPTs, vibrational spectroscopies and their important role in the detection of SPTs. In addition, various other topics like critical exponents, microscopic order parameters (soft and hard modes) and other spectral manifestations of SPTs have been briefly reviewed. A brief discussion has also been done on the new directions in the field of SPTs, recent developments in the Raman techniques and some important aspects of laser induced instabilities and univalent thiocyanates.

1.1 Phase Transitions

By varying the temperature or pressure, or the intensity and frequency of the incident light and/or the applied electric or magnetic fields, many solids change their crystal structures, certain dielectric crystals become spontaneously polarized, paramagnetic materials become magnetically ordered, samples of certain metals and ceramics become superconducting loosing all resistance to the flow of electric current and certain homogeneous mixture of liquids become immiscible dividing to form two distinct liquids seperated by a meniscus [1-8]. All these phenomena are familiar examples of equilibrium phase transitions (EPTs). A sample of matter is said to be in a certain phase (e.g. solid phase or the superconducting phase) when it has a well defined set of macroscopically observable properties (such as hardness or lack of resistivity). In general, the phase is an indication of the degree of order (or disorder) inherent in the microscopic constiuents (e.g. atoms, molecules etc.) of which the given system is composed. Every physical system tends towards a equilibrium state by making compromises between the lowest internal energy and the highest entropy. In general, this competition between low energy and high entropy underlies the formation and stability of various phases of matter [9].

1.1.1 Non-equilibrium Phase Transitions (NEPTs)

Phase transitions are not limited to systems in thermal equilibrium. Similar phenomena occur in systems subjected to a continuous influx of energy or non equilibrium systems. In recent

years it has become more and more evident that there exist numerous examples in physical, chemical and biological systems where well organised spatial, temporal or spatio-temporal structures arise out of chaotic (or disordered) states [10,11]. These ordered structures develop spontaneously and they are self-organising. Moreover, radically different systems described above exhibit striking similarities when passing from the disordered to ordered state suggesting that functioning of all the systems obey the same basic principles [12,13].

1.1.2 Order Parameter

All the systems described above possess an enormous number of subsystems (or degrees of freedom). The determination of the detailed behaviour of any individual subsystem is in general, very difficult. So, the search for a relevant parameter (called order parameter) which represents the macroscopic behaviour of the system, is a crucial step in the phase transition studies. The order parameter (η) is zero in the disordered phase and acquires a maximum value in the completely ordered state. In general, η is an observable quantitative property of the system such as magnetization (M) of a spin system undergoing magnetic phase transition or polarization in the case of a ferroelectric phase transition. In structural phase transitions (SPTs) η measures the extent to which the atomic geometry in the less symmetrical phase differs from that of the more symmetrical phase. It should be emphasized, however, that the recognition of the

macroscopic order parameter in SPTs and NEPTs is not always straight forward. A brief list of phase transforming systems and their η's are summarized in Table 1.1.

1.1.3 Order of the Transition

When η varies continuously with respect to an external variable such as temperature (T) {or pressure, or applied field etc.} the transition is called *second order*. Whereas, if η drops discontinuously to zero at T_c, then the transition is *first order*. In SPTs and NEPTs both (first and second order) types of transitions can be found. At a first order SPT two different states are in equilibrium (i.e. two phases co-exist) but there is no predictable symmetry relationship between them. There occur a large hysteresis in the T_c values, dicontinuous changes in volume and entropy; and there is a latent heat associated with such transitions. In second order SPTs, the states of the two phases tend to become identical as the transition is approached and it follows that the symmetry of the system at T_c must contain all the symmetry elements of both the phases. Order parameter, entropy and volume of the system change continuously, there occurs discontinuous change in specific heat, isothermal volume compressibility and isobaric volume expansivity but there is no latent heat associated with the second order transition. The λ-transition is a special case of second order transition [5,14].

1.1.4 Critical Exponents and Universality

The most striking feature of the second order EPTs is the occurrence of large correlated fluctuations of η near the

stability limit (or critical point) of the two phases concerned. The critical fluctuations can be quantified interms of a quantity called *correlation length* ξ, which defines the extent to which microscopic constituents (spins, dipoles etc) at a distance of 'r' are correlated. As the temperature approaches T_c, ξ grows rapidly, the maximum size of the order parameter fluctuations increases, but the smaller fluctuations are not suppressed, they merely become a finer structure superimposed on the larger ones. At the critical point ξ diverges and fluctuations of all the sizes ranging from macroscopic down to atomic scales can be seen [15,16]. Due to these co-operative fluctuations and the correlation lengths being much larger than the range of the inter-particle forces all the physical observables become independent of inter-particle interactions. Hence, widely diverse systems (e.g. superconductors, fluids, ferromagnets, ferroelectrics etc) exhibit identical critical behavior [17,18]. This universal behavior can conveniently be described interms of the quantities called critical exponents α,β,γ,ν which express the temperature dependence of the specific heat (C_p or C_v), order parameter (η), response function (χ) and correlation length (ξ), near T_c, respectively. Their functional relationships are given by

$$\begin{aligned} C &\propto |\varepsilon|^{\alpha} \\ \eta &\propto |\varepsilon|^{\beta} \\ \chi &\propto |\varepsilon|^{-\gamma} \\ \text{and } \xi &\propto |\varepsilon|^{-\nu} \end{aligned} \qquad (1.1)$$

where $\epsilon = \left[\frac{T-T_c}{T_c}\right]$ defines temperature width of the critical region. Critical exponents calculated from different theoretical models like classical mean field theories; Ising, XY and Heisenberg models are given in Table 1.2. It is very interesting to note that radically different systems with same lattice dimensionality (d) and number of components of η (n) show identical critical exponents representing one universality class. Moreover, there exist certain universal relations among the critical exponents [6,19].

1.1.5 Present Trend

The phase transition and critical phenomenon is an interesting and well studied among many complex problems (like turbulent motion, Kondo problem etc) in physics in which the events at many length scales make contributions of equal importance [16,20]. Since all these problems involve very many coupled degrees of freedom analytical solutions exist only for a few special examples. However, the experimental findings are very helpful in simplifying and testing the theoretical models and thus getting deeper insight into the phenomena. Recent experiments on diverse non-linear physical, chemical and biological systems showed that transitions to chaos, in these non-equilibrium systems, occur in some universal ways [10-13]. "Period doubling" is one of the well established universal routes to chaos [21]. Additionally, there has been a great interest in extending the concept of universality to several non equilibrium phenomena such

as aggregation, gelation, fracture, viscous fingering [22] and self organised criticalities [23]. Profound analogies have been found between NEPTs and EPTs [24]. The most novel theoretical approach has been the application of methods of EPTs to the field of synergetics (a subject which treats all the NEPT problems in an unified frame work) [10,11].

Apart from the academic interest, EPT (or NEPT) studies play an important role in finding new materials (or non linear systems) with optimum qualities (or performances) needed for various technological applications. For example, a normal ceramic material (or amorphous Carbon) could be turned into one of the most useful materials, superconductor (or the hardest known material - Diamond) under appropriate conditions of temperature and pressures [8,25]. There are vast varieties of materials with innumerable applications. To mention few of them, ferroelectrics can be used as peizo electric components, pyroelectric detectors and various other nonlinear optical components. Ferromagnetic materials can be used in computer core storage, liquid crystals in liquid crystal displays and, superionic conductors in solar cells [26-28]. Thus, the experimental, theoretical and applied aspects of phase transitions have acquired added importance.

1.2 Structural Phase Transitions

1.2.1 Classification of SPTs

SPTs have been classified into following general categories [29]:

(i) **Reconstructive SPT :** in which the original linkages of the periodic network are disrupted and a new lattice is constructed;

graphite to diamond or amorphous to crystalline phases being the classical examples.

(ii) **Martensitic SPT :** lattice positions of the two phases are related by shear deformations. These are found in metallic systems, primarily.

(iii) **Distortive SPT :** in which the lattice is distorted slightly without disrupting the original linkages of the periodic network. The distortive SPTs have been further divided into displacive and order-disorder SPTs.

In displacive SPTs, only small displacements of atoms or molecular units take place over low potential barriers as in $BaTiO_3$, $SrTiO_3$ and TeO_2. In order-disorder SPTs disordering (orientational or positional) of atoms or molecular groups, which have several equivalent orientations (or positions) separated by large potential barriers, takes place with large anharmonicities and/or displacements [1,2]. If n_1 and n_2 denote the number of equivalent positions (or orientations) in the ordered and disordered phases respectively, the increase in the entropy (Δs) during an order-disorder transition is given by $\Delta S = R \ln (\frac{n_2}{n_1})$ where R = Boltzmann constant (per mole). Typical examples of orientational order-disorder SPTs are NH_4Cl, $NaNO_2$ and KCN etc. whereas the typical positional disordering systems are Fe_3O_4, AgI etc. Likewise, there could occur electronic or spin disorder involving Jahn-Teller distortions (as in $TbVO_4$, Nb_3Sn) or charge density wave fluctuations (as in $NbSe_2$).

The analysis of several systems has been attempted by ideal categorizations into above sub-systems. However, the actual

SPTs could be a combination of more than one of the above categories.Recently, many interesting new areas such as laser induced SPTs and oscillatory instabilities [3,4,30,31], PTs in laser trapped ions/atoms [32,33], in-commensurate SPTs, systems containing lattice disorder due to impurities quantum crystals and quasi low dimensional systems [1] have emerged. In addition the large number of nonequilibrium analogs to EPTs (as mentioned earlier), interesting class of SPTs which qualitatively display NEPT phenomena have been explored [34,35]. In the present thesis, the orientational order-disorder type SPTs and laser induced *period doubling* like instabilities have been dealt with.

1.2.2 Landau Theory

It is one of the classical mean field theories which assumes that each particle moves in an average potential of all other particles. Although, critical fluctuations of η are not included, the mean field theories are successful in explaining many important features of phase transitions. Especially the singular behaviours of SPTs in ionic crystals (which display long-range forces or very small critical regions [36]) can be conveniently described in terms of mean field exponents [Table 1.2].

According to the Landau theory, the free energy (F) of the system can be expanded interms of η, since η is small near a continuous transition.

$$F = F_o + A\langle\eta\rangle + B\langle\eta^2\rangle + C\langle\eta^3\rangle + D(\langle\eta\rangle^4) + E\langle\eta^5\rangle + G\langle\eta^6\rangle + \cdots \quad (1.2a)$$

Where the coefficients A,B,C,D,... are functions of temperature (or pressure). For symmetry reasons A = C = E = 0; and D > 0 for second order transition [5,14]. Substituting these and neglecting higher order (i.e. η^6, η^8...) terms, in Equation (1.2) the stability of the system is given by

$$F = F_o + B\langle\eta^2\rangle + D\eta^4 \qquad (1.2b)$$

and

$$\frac{\partial F}{\partial \eta} = 2B\eta + 4D\eta^3 = 0 \text{ and } \frac{\partial^2 F}{\partial \eta^2} = 2(B+6D\eta^2) > 0 \qquad (1.3)$$

$$\text{or } \eta = 0,\ \eta^2 = \frac{(-B)}{2D} \text{ and } (B+6D\eta^2) > 0 \qquad (1.4)$$

From Equation 1.4 it follows that the state with $\eta = 0$ is stable only for $B \geq 0$. For $B < 0$, the stable state corresponds to $\eta \neq 0$. In otherwords, the flip in the sign of B which occurs due to variations in the temperature (or pressure, or any control parameter) changes the stability of the system.

i.e. $B = a\,(T - T_c)$ with a = const (>0)

or $\eta = o$ for $T \geq T_c$

$$\eta = b\,(T_c - T)^{1/2} \text{ for } T < T_c \qquad (1.5)$$

where $b = \sqrt{\frac{a}{2D}}$ = constant (>0).

Similar analysis for the first order transition can be done [5]by considering the η^6 term with G>o and D<o in Equation (1.2a).

1.2.3 Probes for SPTs

There are various experimental techniques to monitor the

changes in the macroscopic or microscopic properties of the system undergoing a SPT. Macroscopic measurements such as specific heat, DTA, DSC, thermal expansion, susceptibility, resistivity, dielectric and elastic constants have been extensively used to classify and comprehend different aspects of SPTs in solids. Whereas the static and dynamical processes occurring at the atomic or molecular level in SPTs can be probed by microscopic techniques such as diffraction (x-ray, or neutron, or electron), optical measurements (refractive index, or birefringence; or absorption, or fluorescence - UV,VIS and IR; or scattering - Raman, Brillouin and Rayleigh; or nonlinear optical measurements), inelastic scattering (neutrons, or x-rays) and magnetic resonance studies (EPR, or NMR, or NQR, or Mossbauer) [1,2,5].

Most of these techniques are quite often complementary to each other. The accuracy and importance of each technique depends upon the information wanted in a particular case and the availability of the crystals with various sizes.

The major microscopic techniques used in SPT studies are

(1) Raman Scattering

(2) Infrared absorption spectroscopy

(3) Inelastic neutron scattering

Among them, Raman scattering is the most versatile and occupies a unique position as far as the studies of longer wavelength ($\mathbf{k}=0$) phonons are concerned. It provides the high spectral resolution and sensitivities. With recent techniques very small (micron size) crystals and coloured samples can be studied within ultra short ($\simeq 10^{-14}$s) time scales. Additionally,

second order vibrational excitations in Raman and IR spectroscopies, involving **k**=0 phonons are very much useful in the SPT studies of low dimensional systems. Neutron scattering is also an important tool from the point of view of pure phonon spectroscopy, because it samples the complete frequency wave vector (**k**) space. But the main disadvantages are (i) it requires large crystals, (ii) longer measurement times, (iii) poor spectral resolution and (iv) low sensitivities for frequencies greater than $200cm^{-1}$.

1.3 Vibrational Spectroscopy

1.3.1 Raman Scattering

When the light (with frequency ω_o) interacts with the medium, an oscillating dipole polarization is induced, which inturn, emits the spectrum of scattered radiation consisting of many pairs ($\omega_o \pm \omega_R$) of sidebands symmetrically disposed around the elastically scattered radiation. Sir C.V. Raman and his coworkers [37,38] were the first to discover and appreciate the importance of this inelastic light scattering phenomenon. The origin of inelastic scattered components ($\omega_o \pm \omega_R$) was attributed to the modulation of polarizability (α) of the medium by the molecular or crystal vibrations (ω_R). Since then, the inelastic scattering of light became a sensitive vibrational spectroscopic tool to investigate structure, symmetry and dynamical properties of solids, liquids and gaseous systems [14,39-41] and is known as Raman scattering. The scattered frequencies at ($\omega_o - \omega_R$) and ($\omega_o + \omega_R$) are called Stokes and anti-Stokes components, respectively.

The general expression for the polarization field ($\vec{P}$) induced in medium by an incident electromagnetic field (with $\vec{E} = \vec{E}_o e^{i(\vec{k}.\vec{r}-\omega_o t)}$ is given by

$$\vec{P} = \alpha \vec{E}(t) \qquad (1.6)$$

where α is electronic polarizability tensor and is modulated by the vibrations present in the sample. So, the components of α can be expanded interms of generalized normal co-ordinates $Q(k,t)$ of molecular or crystal vibrations, i.e.

$$\alpha_{mn} = \alpha_{mn}^{(o)} + \sum_i \left[\frac{\partial \alpha_{mn}}{\partial Q_i}\right] Q_i + \sum_{ij} \left[\frac{\partial^2 \alpha_{mn}}{\partial Q_i \partial Q_j}\right] Q_i Q_j + \ldots$$

$$= \alpha_{mn}^{(o)} + \alpha_{mn}^{(1)} + \alpha_{mn}^{(2)} + \ldots\ldots\ldots \qquad (1.7)$$

The constant term $\alpha_{mn}^{(o)}$ gives rise to Rayleigh scattering with a range of frequencies 10^{-9} to 10^{-4} cm^{-1}. $\alpha_{mn}^{(1)}$ leads to first order Raman Scattering (range 10 to 4000 cm^{-1}), if in the scattering process an optical phonon is created or destroyed; or Brillouin scattering (0.05 to 1 cm^{-1}) if an acoustic phonon is involved. All other terms correspond to higher order processes involving two or more phonons, and normally, their contributions are negligibly small. Typical range of phonon excitation wave vectors (k) in the light scattering process is zero to 3×10^4 cm^{-1}. That is the upper limit of k is three orders of magnitude less than the typical k_{max} ($\simeq 3\times10^7 cm^{-1}$) that lies in the Brillouin

zone. So, the Raman Scattering is essentially due to long wavelength (or $k \simeq 0$) phonons.

The spectrum $I(\omega_R)$ of the Raman scattered light is obtained from the Fourier transform of the auto-correlation function, $\langle \alpha^{(1)}(k,t)\ \alpha^{(1)}(k,o)\rangle$. More precisely,

$$I_{mn}(k,\omega_R) \propto \frac{1}{2\pi}\int_{-\infty}^{\infty} dt\ e^{-i\omega_R t} \langle \alpha^{(1)}_{mn}(k,t)\ \alpha^{(1)}_{mn}(k,0)\rangle \qquad (1.8)$$

The final expression for the spectral differential cross section $\left(\frac{d^2\sigma}{d\Omega d\omega_S}\right)$ which represent the observed Raman line shape of a Stokes component (ω_S) is given by [14].

$$\frac{d^2\sigma}{d\Omega d\omega_S} = \frac{\left[\hbar\ \omega_o \omega_S^3\ V' V n_S \left\{ \left| \varepsilon_S^m\ \varepsilon_o^n \left(\frac{\partial \alpha_{mn}}{\partial Q_i}\right)\right|\right\}^2 \{n(\omega_R)+1\}\ g_R(\omega)\right]}{\left\{(4\pi\varepsilon_o)^2 2c^4 N\ \omega_R n_o\right\}} \qquad (1.9)$$

Here $\frac{d^2\sigma}{d\Omega d\omega_S}$ denotes the rate of removal of energy from the incident beam (I_o) as a result of its scattering in volume V' into a solid angle $d\Omega$ with scattered frequencies between ω_S & $\omega_S + d\omega_S$ divided by the product of $d\Omega d\omega_S$ & I_o. n_o, n_S are refractive indices of the medium for the incident and scattered light. ε_o and ε_S are unit vectors parallel to incident and scattered electric fields.

$$g_R(\omega) = \frac{\gamma_R/2\pi}{(\omega_R-\omega)^2 + (\gamma_R/2)^2}$$

determines the Lorentzian shape of the Raman line which has a full width γ_R at half maximum intensity. The factor V/N is fixed by

the temperature via Bose-Einstein thermal factor $n(\omega)$ $= \left[\exp\{\hbar\omega_R / K_B T) - 1\}\right]^{-1}$.

An analogous expression $\frac{d^2\sigma}{d\Omega\ d\omega}_{AS}$ can be found for the antistokes component. In general, Stokes and anti-Stokes components are related by

$$\frac{d^2\sigma}{d\Omega\ d\omega}_{AS} \left\{n(\omega_R)+1\right\} = n(\omega_R) \quad \frac{d^2\sigma}{d\Omega\ d\omega}_{S} \qquad (1.10)$$

1.3.2 Infrared Absorption

When the broad band infrared (IR) radiation incident on the medium part of the radiation, matching with the characteristic vibrational frequencies of the medium, gets absorbed. So, the analysis of the transmitted (or reflected) light in the IR ($10-10^4$ cm^{-1}) region provides an invaluable information regarding the vibrational levels, symmetries and structural characteristics of solids, liquids and gaseous systems [42-44]. IR spectroscopy is essentially a complementary technique to Raman scattering.

The IR absorption occurs through the changes in the dipole moment (μ) of the medium during the molecular (or crystal) vibrational excitations [43]. Like in the Raman scattering case, the components of μ can be expanded interms of generalized normal co-ordinates Q(k,t) of molecular or crystal vibrations,

$$\mu = \mu^{(o)} + \Sigma \frac{\partial \mu}{\partial Q_i} Q_i + \ldots\ldots\ldots$$

$$= \mu^{o} + \mu^{(1)} + \ldots\ldots\ldots + \ldots\ldots \qquad (1.11)$$

The intensity (I) of the absorption line is given by,

$$I \propto |\mu_{mn}|^2 \qquad (1.12)$$

where, μ_{mn} is the matrix element of the dipole moment associated with the absorption (transition from m to n vibrational level).

1.3.3 Selection Rules

From the lattice dynamics there are (3n-3) optical and three acoustic phonons in a crystal having n atoms per unit cell. For a crystal having no spatial symmetry elements one would expect (3n-3) pairs of Raman & (3n-3) IR modes in the vibrational spectra. But Raman (or IR) spectra for different polarizations of the incident and scattered (or absorbed) light are often related by the spatial symmetry of the medium and some vibrational lines are required to vanish for certain polarizations depending on the nature of excitations.

The spatial symmetry of the medium is specified by its symmetry group, (a group of all spatial transformations that leave the medium invariant). Individual atom (or molecules) have spatial symmetries characterized by a point group consisting of rotations and reflections that leave atoms or molecules invariant. The atomic (or molecular) arrangements in a regular crystal are characterized by a space group that contains translational symmetries in addition to reflections and rotations [14].

In general, the selection rules for Raman (or IR) spectra are determined by the symmetry properties of α (or μ) for the excitation concerned [45]. The group theoretical

criterion which determines whether or not a phonon mode is active in the first order Raman (or IR) spectrum is the condition that particular mode transforms in the same way as tensor components α_{mn} (or μ_{mn}) under the point or space group of the lattice. More precisely, the condition for a mode to be Raman (or IR) active is that the irreducible representation according to which it transforms must be contained in the reducible representation for which the tensor components α_{mn} (or μ_{mn}) form a basis [46,47].

1.3.4. Lattice Dynamics

Although the symmetry properties of molecular or crystal vibrations are obtained from a brief calculation, the derivations of their frequencies is a difficult task [14]. Approximate numerical expressions exist for only the simplest lattices, with many drastic assumptions regarding the inter-atomic and inter-molecular forces.

In the simplest microscopic model of ionic crystals, the ions can be treated as unpolarizable, undistortable point charges attracted by long-range coulomb forces and held apart by short range overlap forces [48]. In the harmonic approximation a lattice vibration can be considered interms of a uniform distortion of the crystal in which the positive ions move against a rigid sub-lattice of negative ions. But to explain all the experimental results a large number of extra forces of unknown origin must be postulated. On the otherhand, the experimental findings of Raman and IR spectra are very much useful in determining various fitting parameters involved in potential

energy (P.E) function, and thus elucidating the correct forms of inter-atomic and inter-molecular forces.

a) Internal and External Modes

In many crystalline solids it is often possible to identify molecular (or ionic) groups for which the inter-atomic forces in the same molecule (or ion) are stronger than those between atoms in different molecules (or ions). The vibrations in which different molecules (or ions) suffer internal distortions are called internal modes. Whereas, the vibrations in which different molecules (or ions) are displaced relative to one another without internal distortion are called external modes. Generally, internal modes have higher frequencies compared to external modes. The external modes are further divided into translational and rotational (or librational) modes which involve translations and quasi rotations of the molecular (or ionic) groups about their centers of gravity.

b) Harmonic Interactions

In the simplest case of a free diatomic molecule, the vibrational energy levels are obtained by solving the Schrödinger equation [49] for a given potential V(x)

$$\frac{d^2\psi(x)}{dx^2} + \frac{2m}{\hbar^2}\{E_{vib} - V(x)\}\,\psi(x) = 0 \qquad (1.13)$$

where $x = r - r_e$ represents the change in the inter-atomic distance around the equilibrium position, m is the reduced mass of the oscillator and V(x) can be written as

$$V(x) = \frac{1}{2} k_e (x^2 + a_1 x^3 + a_2 x^4 + \ldots\ldots) \qquad (1.14)$$

where k_e is the force constant. For small x, $V(x) \simeq \frac{1}{2} k_e x^2$ and the vibrational frequencies (ν) of the molecule are given by eigen-frequencies of harmonic oscillator i.e.

$$\nu = \nu_e (n+\frac{1}{2}) \qquad (1.15)$$

where $\nu_e = \frac{1}{2\pi}\sqrt{\frac{k_e}{\mu}}$ and n = 0,1,2,3 ....

In general, one may have to deal with polyatomic molecules; and the crystalline environment greatly affects their vibrational spectra.

The general expression for P.E associated with the unit cell of a crystal in the harmonic approximation [48,50], is given by

$$V = \sum_j (V_j^o + V_j') + \sum_{jk} (V_{jk}) + V_E + V_{Ej} \qquad (1.16)$$

where the summations extend over all the molecules in the unit cell. The various terms are as following

$V_j^{(o)}$ is the P.E. which determines the frequencies and selection rules of the free j^{th} molecule. V_j' is the perturbation to V_j^o due to the equilibrium field of the crystal at the site of j^{th} molecule. It may lead to changes in the frequencies and selection rules of free molecule. As a result, some of the

inactive modes may become active and degenerate modes may split (known as site group or static field splitting).

V_{jk} represents the coupling between internal vibrations of different j and k molecules. It introduces an additional splitting called factor-group or correlation field splitting. If the number of molecules in the cell is n, a non degenerate mode will split into n components.

V_E represents P.E. which determines the frequencies of external modes. The last term V_{Ej} represents the vibrational coupling between external and internal modes.

c) Anharmonicity

Experimental evidences in the number of modes, large bandwidths and their temperature dependence revealed that the harmonic P.E. approximation, which predicts the appearance of a limited number of sharp fundamentals, is inadequate. One must consider the effects of anharmonicities. There are two types of anharmonicities, namely, mechanical and electrical. Deviations from the harmonic P.E lead to mechanical anharmonicities. Whereas, the electrical anharmonicity arises due to the nonlinear variation of α (or μ) with the normal co-ordinate (Q) of vibrational mode [48-51). The general expressions for V & X ($\equiv \alpha$ or μ) are given by

$$V = \frac{1}{2} \sum_i \lambda_i Q_i^2 + \sum_{ijk} \lambda_{ijk} Q_i Q_j Q_k + \sum_{ijkl} \lambda_{ijkl} Q_i Q_j Q_k Q_l + \ldots\ldots$$

$$X = \sum_i X_i' Q_i + \sum_{ij} X_{ij}'' Q_i Q_j + \sum_{ijk} X_{ijk}''' Q_i Q_j Q_k + \cdots \quad (1.17)$$

where i,j,k ... refer to different normal co-ordinates, hence coupling of different phonons. Ingeneral, $(n+1)^{th}$ order term in V and/or n^{th} term in X allow n-phonon transitions to occur. So that if one particular phonon mode is excited it will in time decay into other modes and the peaks are broadened as a result of the finite lifetime of the modes. For example if a cubic anharmonicity leads to the decay of a phonon of frequency ω_o into two phonons of frequency $\omega_o/2$ [52] the thermal broadening of the mode due to this process can be expressed as

$$\gamma_{cubic} \propto \left[\left\{ \exp\left(\frac{\hbar\omega_o}{2K_B T} \right) - 1 \right\}^{-1} + \frac{1}{2} \right] \quad (1.18)$$

Similarly, for quartic process one can assume that ω_o decays into three phonons of frequency $\omega_o/3$ which then gives [53]

$$\gamma_{Quartic} \simeq B \left[\left\{ \{\exp\left(\frac{\hbar\omega_o}{3k_B T} \right) - 1\}^{-1} + \frac{1}{2} \right\}^2 + \frac{1}{12} \right] \quad (1.19)$$

In the high temperature limit, anharmonic contribution to bandwidth (γ) upto quartic processes is given by

$$\gamma_{anharmonic} \simeq a + bT + cT^2 \quad (1.20)$$

Where a,b & c are constants, independent of temperature.

1.4 Vibrational Studies of SPTs

As described earlier, the number of Raman (or IR) active modes depend on the number of formulae units in the primitive cell, as well as on the symmetry elements of the crystal. Since both these features are apt to change across a SPT the spectra will differ on either side of the transition. Namely, new lines can appear and degenerate modes in the higher symmetry phase can be splitted into several components due to the transition to a lower symmetry phase. In general, the temperature dependence of peak frequencies, intensities, bandwidths* and splitting energies of vibrational modes yield information regarding the ultimate structure and dynamics of a solid undergoing a SPT.

1.4.1 Soft Modes

SPTs in solids are quite often accompanied by an observable fall in the peak frequencies of certain normal modes. Raman and Nedungadi [54] were the first to notice such a strong decrease in the peak frequency of a totally symmetric optical phonon ($\simeq$ 220 cm^{-1}) near the α to β transition in quartz. Later it has been realized that every SPT can be regarded as an instability of the crystal for a certain normal mode of vibration called *soft mode* whose frequency decreases as T approaches T_c [55-57]. Although more general theoretical reports are available [1,2,5,58], the connection between the order parameter (η) and the soft mode (ω) can be made by regarding the Landau's free energy (F), (Equation 1.2), as the potential of a one dimensional

oscillator expanded in powers of the displacement η. In the harmonic approximation

$$\frac{\partial^2 F}{\partial \eta^2} = m\omega^2 = 2B \qquad (1.21)$$

From Equations (1.5) and (1.21) $\omega^2 = 2B/m = \text{const}\,|T_c - T|$

The nearly - harmonic lattice dynamical theories explain, most of the features of purely displacive SPTs. However, in order-disorder SPTs anharmonic contributions are large. Soft modes in such systems are not quantized small amplitude displacement waves but can be considered as pseudo-spin excitations by analogy with magnetism [59]. Frequency of a soft mode decreases and saturates at a finite value as T approaches T_c. Above T_c the excitation spectrum shows relaxational character and is centered around $\omega = 0$ [1,2,5].

1.4.2 Hard Modes

The existence of soft modes in vibrational spectra is the most interesting manifestation of SPTs. But it is by no means the striking spectral change induced by SPTs. The most striking spectral manifestations of SPTs occur for some of the modes which are not directly involved in the phase transition [44]. These modes are called *hard modes* and they consist in either activation of silent modes and/or splitting of degenerate modes below T_c. A qualitative information on the effects like number of new lines expected, existence of splittings etc. can be deduced from a group theoretical comparison of symmetries of space groups, G & G_o of

low and high temperature phases. A quantitative account of mode splittings, relative strengths of vibrational modes and their temperature dependences can be made on the basis of an evaluation of the coupling between the order parameter (η) and relevant degrees of freedom. For example in a meanfield (or Landau) type transition G is a sub group of G_o. Knowing G & G_o one can evaluate [60] uniquely the symmetry reduction condition

$$G_o \longrightarrow \left[\gamma^{(k,j)}, \{C_i\}\right] \longrightarrow G \qquad (1.22)$$

The knowledge of the active irreducible representation $[\gamma^{(k,j)}, \{C_i\}]$ gives possibility to write down the free energy (F) expansion interms of the invariants of η and to establish all possible couplings.

As a rule, variations in the mode strengths and frequencies are proportional to some positive integer power of spontaneous value of η. A method, to determine this power by group theoretical means of searching the lowest invariants in the F, that describes the effects induced by SPTs, has been reported by Petzelt & Dvorak [61]. Recently, Bruce et al [62] have developed a general theory for the Raman activity of hard modes. According to this theory, the total Raman intensity (I) of the hard mode can be expressed as

$$I = I^{LR} + I^{CP} + I^{PH} \qquad (1.23)$$

where I^{LR} is the long-range contribution to the first order

scattering in the ordered phase and is proportional to η^2, I^{CP} is the central peak contribution to the first-order hard mode scattering induced by short range order, and I^{PH} represents the contributions from two-phonon processes involving hard and soft-phonon quasi-harmonic interactions.

1.4.3 Orientational Disorder and Activation Energies

As described earlier, the molecular ions in solids may have several equivalent orientations which are separated by a potential barrier of different multiplicities depending on the molecular and site symmetries of the lattice occupied by the ion [63]. If the re-orientational motion is treated approximately as a jump motion between the available orientational sites, the angular jumps may occur randomly taking the ion from one configuration to an equivalent one where it resumes all its normal vibrations over again [52]. The effect of these head to tail orientational fluctuations on the vibrational line shapes have been analysed by several workers [64-68]. In general, IR line shape remain unaffected. Raman line shape reflects the symmetry adopted $\mathbf{k} = 0$ states in the ordered phase and optical density of states in a totally disordered phase [68]. Moreover, the phase interruptions to the vibration make a contribution $\gamma_{re\text{-}ori}$ to the Raman bandwidth. The temperature dependence of a Raman linewidth due to this re-orientational process can be expressed by an Arrhenius type equation [52,64,67]

$$\gamma_{re\text{-}ori} = \gamma_o \exp\left(-U/K_B T\right) \qquad (1.24)$$

Where U is an activation energy corresponding approximately to the height of the potential barrier [66], K_B = Boltzmann constant and γ_o is a constant prefactor.

In general the experimentally observed Raman bandwidth γ is given by

$$\gamma = \gamma_{instrumental} + \gamma_{vibrational} + \gamma_{anharmonic} + \gamma_{re\text{-}orientational} \qquad (1.25)$$

Where $\gamma_{instrumental}$ & $\gamma_{vibrational}$ are independent of temperature $\gamma_{anharmonic}$ is given by Equation (1.20); and $\gamma_{re\text{-}orient}$ by Equation (1.24). Near an order-disorder transition, $\gamma_{re\text{-}orient}$ may become dominant due to rapid re-orientational fluctuations of ions. So, the activation energy (U) can be calculated from the large enhancement in the bandwidths, using Equation (1.24).

1.4.4 Effect of η Fluctuations

Fluctuations of order parameter (η) are comparable with the saturated values of η_s near the order-disorder transitions [61]. So, they are expected to play a dominant role on the vibrational intensities. Except for a few SPTs [58,69], where strong interactions amongst the phonon modes are expected, the Ornstien-Zernike theory of fluctuations developed within the Landau formalism [70], is valid [71-73]. In long-wave length

($k \to o$) limit, the pair correlation function G(r) for atoms at separation r in a cubic crystal is given by

$$G(r) \propto \frac{\exp(-r/\xi)}{r} \qquad (1.26)$$

Where ξ is the correlation length for the fluctuation and

$$\xi \propto (|T-T_c|)^{-\nu} \qquad (1.27)$$

with a correlation length exponent $\nu = 0.5$

The scattered intensity I(k) can be related to Fourier transform of G(r) by [74]

$$I(k) \propto \frac{T}{k^2 + \xi^{-2}} \qquad (1.28)$$

On the similar lines, Dultz [75] calculated the contribution from fluctuations to the Raman Scattering intensity(I), near an order-disorder transition. According to that the reduced Raman scattered intensity $[I^r = \frac{\omega I}{(n(w)+1)}]$ of disorder allowed phonons which have a wave vector inside a small sphere of radius k_o around the critical wave vector k_c is given by

$$I^r(\omega) = \sum_j \rho_j(\omega) \left[a_j + b_j \left\{ 1 - \frac{\tan^{-1} k_o \xi}{k_o \xi} \right\} \right] \qquad (1.29)$$

Where $\rho_j(\omega)$ refers to one-phonon density of states of the phonon branch j ; and a_j and b_j are temperature independent parameters. I^r only depends on temperature via ξ. So that the intensity

enhancing second term represent the contribution from η fluctuations, near T_c. Whereas the first term is due to self-correlation which contributes to the spectrum even in a completely disordered crystal with $\xi = 0$.

1.4.5 Recent Developments in Raman Techniques

Raman scattering is a weak effect with a typical scattering cross section 10^{-30} cm^2 and conversion efficiency $\simeq$ 10^{-8}. Early experiments were carried out with powerful mercury lamps surrounding the sample, prism spectrographs, and the spectra were recorded by hours-long photographic exposures. As mentioned earlier, Raman & Nedungadi observed soft mode in quartz as early as 1940 [54], with their indigenous efforts. But to record the spectra below 100 cm^{-1} was almost impossible at that time because of unavoidable stray light.

The invention of laser (1960) which provides an intense, monochromatic, (ultrashort pulses and tunable frequencies when desired) and highly collimated beam of light has been major important factor for the renaissance in the field of Raman spectroscopy of SPTs. Additionally, the developments in the design and construction of double, triple and tandem monochromators with holographic gratings, perfect data acquisition techniques with optical multi channel analysers, image intensifier tubes, low dark current phtomultiplier tubes and dedicated computers have created new exciting perspectives for Raman spectroscopy by improving the resolution, accuracy, sensitivity and fast data acquisition capabilities.

Now the Raman spectroscopy is a powerful nondestructive method for the study of SPTs. The whole range of inter and intra molecular phonon frequencies can be studied with utmost sensitivities. With the advent of microtechniques the studies of micro crystals with spatial resolutions of 10^{-6}m are possible. Additionally, time resolved Raman spectroscopy provides real time (upto 10^{-14} sec) information regarding the dynamical changes in crystals undergoing SPTs [76]. The invention of dye lasers has made the possibilities of resonance Raman and non-linear coherent Raman scattering studies of coloured samples. Unwanted fluorescence could easily be descriminated by these techniques [41].

1.5 Laser Induced Instabilities

As mentioned earlier (Section 1.1.1) there exist many nonequilibrium systems which show rich variety of spatial, temporal and spatio-temporal patterns as some control parameters involved are varied. Formation of pattern means the former structure cannot persist any longer, i.e. it becomes unstable [11]. The phenomena of pattern formation are often called instabilities or bifurcations. In addition to many examples of pattern formations in nonequilibrium systems there exist a few ferroelectric crystals which exhibit nonlinear responses and period doubling bifurcations near their equilibrium phase transition temperatures [77,78].

Recently, there is a lot of interest in the laser induced instabilities and structural transitions [3,4,30,31].

Interestingly, some of the amorphous semiconductors [31,79] and chalcogenide glasses [30,80] show quasi-periodic temporal oscillations in their optical properties. The periods of the oscillations have been found to depend on the laser intensity, frequency and irradiation time [79]. But there are no controlled experiments which may reveal the regular temporal patterns in these materials. Present thesis reports (for the first time) on the observation of "period doubling" like oscillatory instabilities as a function of irradiation time near the SPT in CsNCS crystal.

1.6 Univalent Thiocyanates

There has been a great interest [1,2,5,81,82] in orientationally disordered ionic (or molecular) solids which occupy an unique intermediate position between crystalline and amorphous materials. The thiocyanates MNCS (where M = Na, K, Rb, Cs, Tl and NH_4) are ionic crystals consisting of univalent cations and rod shaped anions. These substances are of interest because of their simpler structures at room temperature and order-disorder type SPTs at higher temperatures in which some of them adopt one of the alkali halide structures through orientational disorder of anions. In other words, anions order with a definite orientation below T_c and become uncorrelated above T_c. Because of their different orientations from cell to cell, the translational symmetry is destroyed. The wave vector **k** need no longer be conserved in the light scattering process and phonons of any **k** in Brillouin zone that feel the disorder can contribute to the Raman

spectrum. Moreover, the random distribution of orientations leads to the random modulation of crystal polarizability [68]. Thus, Raman line shapes are very sensitive to the orientational disorder.

The order-disorder SPTs in MNCs systems have been studied earlier using adiabetic calorimetry [83], DTA [84,85], DSC [84], X-ray diffraction [86-94], neutron diffraction [95,96], infrared spectroscopy [85,97,98], Raman spectroscopy [98-101] and NQR spectroscopy [102] on one or more of these compounds. So far, Raman & IR spectroscopic studies of SPTs have been reported only for KNCS and NH_4NCS systems. In the present work, a detailed vibrational (Raman & IR) spectroscopic investigation of SPTs in CsNCS, RbNCS and TlNCS has been carried out, for the first time. The main objectives of these studies have been a search for microscopic order parameters like soft or hard modes and other spectral manifestations of order-disorder SPTs with an eventual aim of attaining a clear understanding of the microscopic mechanisms governing the SPTs and their universality aspects. Quantities like activation energies (U) for the re-orientational motion of NCS^- ions and universal exponents, e.g., order parameter exponent (β) and correlation length exponent (ν) have been extracted from the experimental data. The most interesting and novel aspect is the observation of laser induced temporal oscillations and cascade of period doublings as a function of laser irradiation time, near the SPT in CsNCS crystal.

REFERENCES

[1] K.A. Müller and H. Thomas (eds.), "Structural Phase Transitions I" (Springer-Verlag, Berlin, 1981).

[2] Z. Iqbal and F.J. Owens (eds.), "Vibrational Spectroscopy of Phase Transitions" (Academic press, Orlando, 1984).

[3] S.M. Arakelian and Yu. S. Chilingarian, "Nonlinear Optics of Liquid Crystals" (Nauka, Moscow, 1984).

[4] P.C. Taylor, in "Laser Spectroscopy of Solids II", (ed.) W.M. Yen (Springer-Verlag, Berlin, 1989), p. 274.

[5] R. Blinc and B. Zeks, "Soft Modes in Ferroelectrics and Antiferroelectrics" (North-Holland, Amsterdam, 1974).

[6] H.E. Stanley, "Introduction to Phase Transitions and Critical Phenomena" (Oxford Univ. press, London, 1971).

[7] M. Ausloos and R.J. Elliott, "Magnetic Phase Transitions" (Springer-Verlag, Berlin, 1983).

[8] K. Watanabe, H. Yamane, H. Kurosawa, T. Hirai, N. Kobayashi, H. Iwasaki, K. Noto and Y. Muto, App. Phys. Lett. 54, 575 (1989).

[9] J.S. Walker and C.A. Vause, Sci. Am. 256(5), 98 (1987).

[10] H. Haken, "Synergetics" (Springer-Verlag, Berlin, 1977).

[11] H. Haken, "Advanced Synergetics: (Springer-Verlag, Berlin, 1983).

[12] P. Cvitanovic, "Universality in Chaos" (Hilger, Bristol, 1984).

[13] I. Procaccia, Nature, 333(6174) 618 (1988).

[14] W. Hayes and R. Loudon, "Scattering of Light by Crystals" (John Wiley, New York, 1978) p. 202.

[15] L.P. Kadanoff, Physics 2, 263 (1966).

[16] K.G. Wilson, Sci. Am. 241, 158 (1979).

[17] M.E. Fisher, Rep. Prog. Phys. 30, 615 (1967).

[18] L.P. Kadanoff, in "Critical Phenomena", proc. Int. Sch. Phys. "Enrico Fermi", Varenna, Italy (1970).

[19] S.K. Ma, "Modern Theory of Critical Phenomena" (Benjamin, New York, 1976).

[20] K.G. Wilson, Rev. Mod. Phys. 55(3), 583 (1983).

[21] P.Cvitanovic, in "Optical Instabilities", (eds.) R.W. Boyd, M.G. Raymer and L.M. Narducci (Cambridge Univ. press, England, 1986) p. 151.

[22] R. Jullien, L. Peliti, R. Rammal and N. Boccaro (eds.), "Universalities in Condensed Matter" (Springer-Verlag, Berlin, 1988).

[23] C. Tang and P. Bak, Phys. Rev. Lett. 60(23), 2347 (1988).

[24] J.F. Scott, in "Frontier of Nonequilibrium Statistical Physics" (eds.), G.T. Moore and M.O. Scully, NATO ASI Series B135 (Plenum, New York, 1986) p. 465.

[25] A.E. Alexenko, V.S. Gorelik, B.V. Spitzin and T.F. Faizullov, proc. ICORS XI, (eds.), R.J.H. Clark and D.A. Long (John Wiley, Chichester, 1988) p. 209.

[26] K.A. Muller and E. Pytte, IBM. J. Res. Develop. 25(5), 811 (1981).

[27] F.B. Saeva (ed.), "Liquid Crystals - The Fourth State of Matter", (Dekker, New York, 1979)

[28] M.B. Salamon (ed.), "Physics of Superionic Conductors" (Springer, Berlin, 1979).

[29] M.J. Buerger, in "Phase Transitions in Solids" (eds.), R. Smoluchowski, J.E. Mayer and W.A. Weyl (John Wiley, New York, 1951) p. 133.

[30] I. Abdulhalim, R. Beserman and R. Weil, Phys. Rev. B 39(2), 1081 (1989) and references therein.

[31] J. Hajto and I. Janossy, Phil. Mag. B 47(4), 347 (1982).

[32] F. Diedrich, E. Peik, J.M. Chen, W. Quint and H. Walther, Phys. Rev. Lett. 59, 2931 (1987).

[33] S. Gilbert, J. Bollinger and D. Wineland, Phys. Rev. Lett. 60, 2022 (1988).

[34] O.G. Vlokh, B.V. Kaminskii, I.I.Polovinko and S.S. Sveleba, Sov. Phys. Solid st. 29(5), 880 (1987).

[35] J.F. Scott, in "Frontiers of Nonequilibrium Statistical Physics" (eds.), G.T. Moore and M.O. Scully, NATO ASI B135 (Plenum press, New York, 1986), p. 473 and references therein.

[36] V.L. Ginzberg, Sov. Phys. Solid St. 2, 1824 (1960).

[37] C.V. Raman and K.S. Krishnan, Nature, 121, 501 (1928).

[38] C.V. Raman, Indian J. Phys. 2, 387 (1928).

[39] G. Landsberg and L. Mandelstam, Naturwiss 16, 557 (1928).

[40] J.G. Grasselli, M.K. Snavely and B.J. Bukin, Phys. Rep. 65, 231 (1980).

[41] S.B. Banerjee and S.S. Jha (eds.), "Recent Trends in Raman spectroscopy" (World Scientific, Singapore, 1989).

[42] G. Herzberg, "Molecular Spectra and Molecular Structure", vol.II (Van Nostrand, Princeton, New Jersy, 1945).

[43] K. Nakamoto, "Infrared and Raman spectra of Inorganic and Co-ordinated Compounds" (John Wiley, New York, 1978).

[44] J. Petzelt and V. Dvorak, in "Vibrational spectroscopy of phase transitions", (eds.), Z. Iqbal and F.J. Owens (Academic press, Olando, 1984), pp 56-151.

[45] G. Turrell, "Infrared and Raman Spectra of Crystals" (Academic press, London, 1972).

[46] S. Bhagavantam and K.Venkatarayudu, "Theory of Groups and its Applications to Physical Problems" (Academic press, London, 1969).

[47] J.R. Ferraro and J.S. Ziomek, "Introductory Group Theory and its Applications to Molecular Structures" (Plenum press, New York, 1975).

[48] P.M.A. Sherwood, "Vibrational Spectroscopy of Solids" (Cambridge Univ. Press, London, 1972).

[49] G. Herzberg, "Spectra of Diatomic Molecules" (Van Nostrand, New York, 1950).

[50] S. Krimm, in "Infrared Spectroscopy and Molecular Structure", (ed.) M. Davies (Elsevier, Amsterdam, 1963).

[51] R.C. Herman and K.E. Shuler, J. Chem. Phys. 22, 481 (1954).

[52] A.K. Sood, A.K. Arora, V. Umadevi and G. Venkataraman, Pramana, 16, 1 (1981).

[53] T. Sakurai and T. Sato, Phys. Rev. B4, 583, 1971.

[54] C.V. Raman and T.M.K. Nedungadi, Nature, 145, 147 (1940).

[55] W. Cochran, Phys. Rev. Lett. 3, 412 (1959).

[56] V.L. Ginzburg and A.P. Levanyuk, JETP, 39, 192 (1960).

[57] J.F. Scott, Rev. Mod. Phys. 46, 83 (1974).

[58] R.A. Cowley, in "Raman Spectroscoy Sixty Years on", vol.17A, (eds.), H.D. Bist, J.R. Durig and J.F. Sulivan (Elsevier, Amsterdam, Netherlands, 1989).

[59] R. Brout, K.A. MQller and H. Thomas, Solid St. Commun. 4, 507 (1966).

[60] O.V. Kovalev, "Irreducible Representations of Space Groups" (Gordon and Breach, New York, 1965).

[61] J. Petzelt and V. Dvorak, J. Phys. C: Solid St. Phys., 9, 1571 (1976).

[62] A.D. Bruce, W. Taylor and A.F. Murray, J. Phys. C: Solid St. Phys., 13, 483 (1980).

[63] A.L. Verma, in "Raman Spectroscopy Sixty Years on", vol.17A, (eds.) H.D. Bist, J.R. Durig and J.F. Sullivano (Elsevier, Amsterdam, Netherlands, 1989).

[64] A. Ben Reuven, in "Advances in Atomic and Molecular Physics", vol.5, (eds.), D.R. Bates and I. Emstermann (Academic press, New York, 1969).

[65] F.J. Bartoli and T.A. Litvovitz, J. Chem. Phys., 56(1), 404 (1972).

[66] P. da R. Andrade, A.D. Prasad Rao, R.S. Katiyar and S.P.S. Porto, Solid St. Commun., 12, 847 (1973).

[67] Y. Cho, M. Kobayashi and H. Tado Koro, J. Chem. Phys. 84(8), 4643 (1986).

[68] J.P. Lemaistre, R. Ouillon, B. Perrin and P. Ranson, in "Dynamical Processes in Condensed Molecular Systems", (eds.) J. Klafter, J. Jortner and A. Blumen (World Scientific, Singapore, 1989).

[69] D.A. Bruce and W.G. Stirling, J. Phys. C: Solid St. Phys. 16, 841 (1983).

[70] L.D. Landau and E.M. Lifshitz, "Statistical Physics", Part I, (Pergamon, Oxford, 1980).

[71] V.L. Ginzburg, A.P. Levanyuk and A.A. Sobyanin, Phys. Rep. 57(3), 151 (1980).

[72] J.C. Toledano and P. Toledano, The Landau Theory of Phase Transitions" (World Scientific, Singapore, 1987).

[73] V.L. Ginzburg, A.P. Levanyuk and A.A. Sobyanin, Ferroelectrics, 73, 171 (1987).

[74] J.B. Sokoloff, Phys. Rev. B5, 4962 (1972).

[75] W. Dultz, J. Chem. Phys. 65(7), 2812 (1976).

[76] K.A. Nelson, in "Raman Spectroscopy Sixty Years on", vol.17B, (eds.) H.D. Bist, J.R. Durig and J.F. Sullivan (Elsevier, Amsterdam, Netherland, 1989) p. 83.

[77] J. Jefferies, Phys. Lett. A90(6), 316 (1982).

[78] J.Y. Huang and J.J. Kim, Phys. Rev. B34(11), 8122 (1986).

[79] I. Abdulhalim, R. Beserman, Y.L. Khait and R. Weil, App. Phys. Lett. 51(23), 1898 (1987).

[80] I. Abdulhalim, R. Beserman and R. Weil, Phys. Rev. B (to be published).

[81] J.N. Sherwood (ed.), "The Plastically Crystalline State" (John Wiley, New York, 1979).

[82] J. Ortiz-Lopez and F. Luty, Phys. Rev. B37(10), 5452 (1988).

[83] Y. Kinsho, N. Onodera, M. Sakiyama and S. Seki, Bull. Chem. Soc. Jpn. 52, 395 (1979).

[84] W. Klement Jr. and C.W.F.T. Pistorious, , Bull. Chem. Soc. Jpn. 49, 2148 (1976).

[85] M. Sakiyama, H. Suga and S. Seki, Bull. Chem. Soc. Jpn., 36, 1025 (1963).

[86] W. Bussem, P. Gunther and R. Tubin, Z. Phys. Chem. B24, 1 (1934).

[87] S. Manolatos, M. Tillinger and B. Post, J. Solid State Chem. 7, 31 (1973).

[88] Y. Yamada and T. Wantabe, Bull. Chem. Soc. Jpn. 36, 1032 (1963).

[89] C. Akers, S.W. Peterson and R.D. Willett, Acta. Crystallogr. B24, 1125 (1968).

[90] J.W. Bats, P. Coppens and A. Kvick, Acta. Crystallogr. B33, 1534 (1977).

[91] J.W. Bats and P. Coppens, Acta Crystallogr. B33, 1542 (1977).

[92] R. Lippman and R. Rudman, J. Chem. Phys. 79(7), 3457 (1983).

[93] S. Yamamoto, M. Sakuno and Y. Shinnaka, J. Phys. Soc. Jpn. 56(7), 2604 (1987).

[94] S. Yamamoto, M. Sakuno and Y. Shinnaka, J. Phys. Soc. Jpn. 56(12), 4393 (1987).

[95] M.A. Irving, M.M. Elcombe and T.F. Smith, Aust. J. Phys. 38, 85 (1985).

[96] B.K. Moss, S.L. Mair, C.J. Mcintyre and R.K. Mcmullan, Acta. Crystallogr. B43, 16 (1987).

[97] A. Tramer, J. Chem. Phys. 59, 232 (1962).

[98] Z. Iqbal, L.H. Sarma and K.D. Moller, J. Chem. Phys. 57, 4728 (1972).

[99] S.V. Karpov, A.V. Khassan Ali and A.A. Shultin, Sov. Phys. Solid St. 24, 39 (1982).

[100] H. Kanamori, H. Okamoto and K. Urabe, J. Phys. Chem. Solids, 42, 197 (1981).

[101] G.D. Tewari, D.P. Khandelwal and H.D. Bist, J. Chem. Phys. 82(2), 5624 (1985).

[102] T. Asaji, R. Ikeda and D. Nakamura, J. Magn. Reson. 31, 437 (1978).

Table 1.1 Partial list of phase transforming systems and the order parameters (η) associated with them.

(a) Equilibrium Phase Transitions :

Phase transforming system	Order parameter
Fluid near critical point	Density difference between phases
Ferromagnet	Magnetization
Ferroelectric	Lattice polarization
Antiferroelectric	Sub lattice polarization
Superconductor	complex gap parameter
Superfluid	Condensate wave function
Mixture of liquids near consolute point	Concentration difference
Crystal near structural phase transition	Normal co-ordinate of soft mode

(b) **Non equilibrium Phase Transitions :**

Phase transforming system	Order parameter†
Laser near the threshold	Electric (optical) field strength
Chemical (or Bio-chemical) reaction near an instability point	Concentration of molecules (which may depend on space and time)
Tunnel diode near an instability point	The number of electrons representing the capacitance, charge on the tunnel diode

† Taken from [10]

Table 1.2 : Critical exponents calculated from four theoretical models † [2]

			Lattice d = 3		
			Ising	XY	Heisenberg
Property	Exponent	Mean field (any d)	(n =1)	(n = 2)	(n=3)
Order parameter	β	0.5	0.325	0.346	0.365
Suceptibility	γ	1.0	1.240	1.316	1.387
Specific heat	α	0	0.110	-0.007	-0.115
Correlation length	ν	0.5	0.630	0.669	0.705

† d and n correspond to the dimensionality of the lattice and orderparameter, respectively.

CHAPTER 2

EXPERIMENTAL

Abstract

This chapter briefly summarizes the various experimental techniques used for the present work, sample preparation methods and factors affecting the spectra of samples under study. In addition to the brief description of apparatus, emphasis is given on the preventive maintenance and methods employed for better data acquisition.

2.1 Sample Preparation

Extra pure MNCS (M = Na, Rb, Cs and Tl) and S_8 samples used for the present studies were obtained from K&K laboratories (USA). All the samples were further purified by recrystallizing twice or thrice from saturated aqueous solutions. Every time good quality crystals were taken out, dissolved in fresh double distilled water and again kept for recrystallization. Transparent single crystals with well developed planes were obtained by slow evaporation of saturated aqueous solutions kept, at constant temperature and dry atmospheric conditions. These single crystals were cut along their crystal axes with the help of low speed diamond wheel saw crystal cutter (SBT:650). Properly polished crystals (or finely ground polycrystalline samples) were used for room temperature (RT) and temperature dependent spectral studies. In some possible cases, single crystals were thinned down to microplatelets and used for IR (Infrared) transmission measurements. Since some of these samples are very hygroscopic, they were always kept in dry condition. The humidity of the room was maintained below 45% while polishing, cutting, mounting the crystals and recording their spectra.

2.2 Laser Raman Spectrometer

The general layout of the equipment used for recording the Raman spectra is shown in Figure 2.1. Spectra physics Argon ion laser was used to excite the sample and a Spex Ramalog system consisting of a lasermate, a UVISIR sample compartment, a 1403

double monochromator, a thermoelectrically chilled photomultiplier (c-31034) and a photon counting system in conjunction with a compudrive and a linear chart recorder provided an automatic recording of the spectra.

2.2.1 Excitation Source

The optical source has two main parts namely, model 165 laser head and 265 exciter. The laser head contains a plasma tube (closed at both ends by Brewster's angle windows), a solenoid and an optical resonator formed by a spherical reflector at the output end and a prism (to select wavelengths) assisted by a flat mirror at the back end. The operating wavelengths and power ratings are given elsewhere [1]. The 265 exciter contains all the necessary electronic circuits to create and control the ion discharge in the plasma tube; to control the output power; and to supply and regulate the solenoid current. A constant output power can be obtained by operating the laser in light control (L.C.)mode. While operating in this L.C. mode, 1% of the beam will be splitt from the beam splitter and sensed by the light stabilizer, which in conjunction with the plasma current regulator controls the tube current, so that the output intensity always remains constant. The necessary cooling of laser head and 265 exciter is achieved by Neslab HX-500 recirculating (distilled water) heat exchanger. An automatic voltage stabilizer EMS-10, 20 KVA provides the stabilized 3 phase (400V, phase to phase) A.C. power to the laser transformer and single phase 220V to all other electronic systems

and cryostats. More details of the equipment can be found elsewhere [1,2].

2.2.2 Preventive Maintenance

Generally, gas lasers operate with gain margins of a few percent, so the losses due to any minute dust particle on optical (mirrors, windows etc.) surfaces and slow diffusion of contaminants which are negligible in ordinary optical systems can easily prevent these lasers from operating at all. This places a great demand on the periodic (atleast once in three months at the places like Kanpur) cleaning of all the optical components to maintain optimum laser performance. Periodic cleaning of all other optical components in the sample compartment and other accessories is also a must.

Similarly periodic cleaning of water filter systems, all water flowing tubes in and around the chiller plant and replacement of the distilled water are also very essential. Although pure double distilled water was used in the continuous flow recirculating chiller plant, yet after a long run (a year or so) all the filters narrow passage ways around the plasma tube and some of the interlocking flow switches can be blocked by small particulate matter (due to dust, corrosion, scale deposition etc). If these factors were ignored, in day to day working an apparent reduction in the cooling efficiency of the chiller plant can be felt. To compensate it if one (unknowingly) increases the inlet water flow rate, then the water flowing tubes (around the plasma

tube, inside and outer sides of the 265 exciter) may blast or some cracks may develop due to high pressure created by the partial blocking at narrow passage ways. To prevent these hazards regular cleaning of complete water cooling system and replacement of fresh distilled water inside the chiller plant were done periodically once in a year or so.

2.2.3 Experimental Setup

As illustrated in the optical line diagram (Figure 2.2), a linearly polarized light from an Ar^+ laser enters the lasermate via 90^o beam deflector. Lasermate being a mini monochromator, eliminates the unwanted plasma lines from the beam. The beam is then focussed onto the sample vertically from below. The typical diameter of the focussed spot is around 30 μm and the power at the sample reduces to $\simeq$ 1/3 of the initial laser power. The scattered light from the sample is collected (in an usual 90^o geometry) and focussed onto the entrance slit (S_3) of the double monochromator by an elliptical mirror M_8 in combination with a plane mirror M_9. After passing through the double monochromator, the dispersed light falls on C-31034 GaAs photomultiplier tube (PMT) for detection.

The PMT has a broad plateau in the quantum efficiency curve in the visible region as shown in Figure 2.3 (inset) An extremely small dark count $\simeq$ 30 counts/sec can be achieved by operating the PMT at -30^oC. It takes nearly 90 minutes to attain that temperature by thermo-electric cooling. The decrease in the

dark count as a function of cooling time is given in Figure 2.3. The PMT converts the optical signal to a proportionate electrical signal then digitalized and fed to DPC-2 electronics system for analysis. The output is recorded on a linear recorder. Compudrive runs the chart in synchronism with monochromator gratings.

The standard lines of low pressure Hg^+ lamp were used to calibrate the wavenumber. The maximum spectral purity I/I_o (or stray light reduction); resolution; wavenumber accuracy and repeatability achievable with 1403 double monochromator are 10^{-14} at ν=20 cm^{-1} (at 5148 A^o); 0.15 cm^{-1} (FWHM at Hg^+ 5791 A^o); $\pm$ 1 over 10000 cm^{-1}; and $\pm$ 0.2 cm^{-1}, respectively. The more detailed description of the apparatus is given elsewhere [3].

Different sample holders attached to a high precision three way moving platform can be nicely accommodated in the sample compartment. The line diagrams of different cell holders used for high temperature Raman studies are given in Figure 2.4. All the details can be found elsewhere [4].

2.2.4 Polarization Studies

For room temperature (or high temperature) polarization studies properly cut and polished single crystal was mounted on a Goniometer head (or high temperature cell holder) in such a way that one of the crystal axes coincides with the propagation vector of the incident beam. The light scattered in the 90^o geometry passes through an analyser (a plane polarizer placed before the elliptical mirror M_8) and the resultant plane polarized light will

be converted into circularly polarized light by a polarization scrambler placed before the entrance slit S_2. The plane of polarization of the incident light can be altered by 90^0 by keeping a polarization rotator before the lasermate.

The laboratory co-ordinate system was chosen such that x, y and z axes coincide with the crystal axes, a, b and c, respectively. A polarized spectrum corresponding to a polarizability tensor component α_{xy} can be determined experimentally by arranging the crystal geometry in such a way that the incident light is polarized in x-(or a) direction and allowing only the y-component to enter the monochromator. The polarizability character of the spectrum in that geometry is represented by z(xy)x, where z and x outside the parenthesis correspond to the propagation axes of incident and scattered light, respectively.

2.2.5 Recording Conditions

To get a good spectrum in a reasonable time compromise between various combinations of sensitivity, integration time, chart scale, chart (or monochromator) scanning speeds etc. has to be made. Selection of proper slit widths, optimum powers and good alignment greatly improves the resolution and spectral quality (i.e. high S/N). Figure 2.5 shows the Raman spectrum of TlNCS powder in the NCS^- bending region. The spectrum was recorded with very low power $\simeq$ 6 mw and slit width $\simeq$ 1.6 cm^{-1}. One can see the clear resolution of the weaker and closely spaced modes around

456, 460 and 463 cm^{-1}. One may get a spectrum without much trouble using large powers and slitwidths. But it is very essential to use low powers, (especially for temperature dependent studies of solids and coloured samples), to minimize local laser heating effects at the irradiated spot. On the other hand, one wants to put lower slitwidths to reduce the instrumental slitwidth contribution to the bandwidths of Raman modes. Instrumental broadening can be eliminated by recording the spectra at smaller and smaller slitwidths until no change is observed in the band profile. In the present studies low powers and minimum slitwidths have been used as far as possible; good spectral regions (i.e. high S/N) with well resolved bands (obtained after proper alignment), were monitored to investigate SPTs and other local changes occurring in the crystals.

2.3 Infrared Spectrometer

Perkin Elmer model 580 double beam ratio recording infrared (IR) spectrophotometer was used for recording the IR spectra of all the samples under investigation. The simplified block diagram of the apparatus is given in Figure 2.6. Broad band IR radiation from the source (ceramic tube heated to $\simeq 1200^{o}C$) is divided into reference and sample beams by the action of the first chopper mirror C_1. The sample absorbs radiation from the sample beam of wavenumber corresponding to its characteristic vibrational frequencies; whilst the reference beam passes through unaffected. The beams are then recombined at the second chopper

C_2 and enters into the monochromator. Then the dispersed light is focussed onto the thermocouple (gold leaf) detector. The incident radiation is strongly absorbed by the gold leaf and an increase of leaf temperature occurs. This produces a thermoelectric voltage proportional to the incident intensity. The alternating signal from the detector is amplified and then demodulated by the signal processing electronics to give separate sample and reference beam signals. The ratiometer produces the ratio of the two signals which corresponds to the transmittance value of the sample. The ratio signal is then filtered to reduce the noise level. Base line adjustment, off-setting and scaling operations are performed on the signal in the ordinate functions unit. After further amplification this signal is supplied to the recorder. The wavenumber scan motor drives both the recorder and the grating monochromator scan mechanisms in synchronism. In addition to the transmittance mode the spectra can be recorded in absorbance mode also. The detailed optical diagram is shown in Figure 2.7. More detailed description of the apparatus is given elsewhere [5]. All the recorded IR spectra were calibrated with the standard spectrum of polystyrene film.

2.3.1 Factors Affecting IR Transmission Spectra

IR transmission measurements on transparent single crystal platelets are more useful and accurate in phase transition studies as compared to the bulk reflectivity measurements because they are much more sensitive to changes in the optical constants

[6]. But it is not always possible to prepare thin transparent single crystal platelets. For CsNCS sample, a thin transparent platelet was prepared and its temperature dependent IR transmission measurements were performed. For all other systems, the powdered samples were mixed with KBr (or CsBr) matrices and then the finely ground mixture was pressed into transparent pellets. Since, there are several factors (like particle size, refractive index of the matrix, adsorption, chemical reaction and mixed crystal formation etc.) affecting the sample spectra [7,8] in the pellet method, care had been taken in the interpretation and quantitative analysis of the data. The possibilities like adsorption, chemical reaction and mixed crystal formations have been ruled out by comparing the pellet spectra with the sample spectra recorded with Nujol mull technique. Significant losses were found due to scattering which depends on the particle size, refractive index and wavelength. When the particle sizes (in a transparent pellet) are sufficiently large there will be strong reflections (i.e. pellet will be opaque) in the shorter wavelength region and a little scattering (i.e. higher transmission) in the longer wavelength region. On the other hand, if the particle sizes are comparable to the wavelengths of the radiation, the rapid changes in the refractive index of a substance in the vicinity of a few absorption bands often give rise to the famous christiansen effect [9,10]. This characteristic effect, resulting in a asymmetry of the IR absorption bands, with high transmittance

on the shorter wavelength side of C-N stretching modes has been observed for the present thiocyanate systems. But all these effects can be eliminated by properly grinding the particles to an average size less than the lowest wavelength (λ_{min}) being employed. Figure 2.8 shows how a large asymmetry in the shape of ν_{C-N} mode (of e.g. TlNCS sample) for larger particle sizes {Figure 2.8(a)} has been gradually eliminated {Figure 2.8(b) and (c)} by grinding the sample particles to smaller and smaller sizes. Finally, for an extremely smaller enough grain sizes the anomalous transmittance on the high frequency side of ν_{C-N} mode completely disappeared {Figure 2.8(d)}.

2.3.2 Temperature Dependent IR Studies

For IR temperature dependent studies a thin single crystal platelet (or a transparent pellet) of the sample was mounted on a special sample holder (metallic strip with a circular hole at the centre) and fixed into the pellet holder of the Specac variable temperature cell. The Specac cell in conjunction with a temperature controller and copper-constantan thermocouple were used to vary, control, and measure the sample temperatures with an accuracy of $\pm$ 1^{o}K.

2.3.3. Variable Temperature Cell

The line diagram of the Specac variable temperature cell is shown in Figure 2.9. It works on a dewar principle utilising a vacuum pressure of 0.5mm Hg. As illustrated in the figure the

sample cell holder is fitted directly to the base of the stainless steel refrigerant chamber. Facilities for vacuum pump connection and electrical leads are arranged on the top plate. The sample holder is fitted with heaters which enable to raise the temperature of the sample from $83^{o}K$ to $523^{o}K$. The temperature $83^{o}K$ is obtained from a refrigerant (Liquid Nitrogen). A small hole drilled into the metal block of the sample holder accommodates the junction end of a thermocouple. Further details are given in [11].

References

[1] Instruction manual, model 165 ion laser with model 265 power supply (Spectra physics, USA, 1980)

[2] Instructions and operating manual, HX-500 refrigerated recirculating heat exchanger (Neslab, USA, 1980).

[3] Instruction manual, Ramalog 1403 spectrometer (Spex, USA, 1980).

[4] M. Pal, Ph.D. Thesis, Indian Institute of Technology, Kanpur (1984).

[5] Instruction manual, model 580 infrared spectrophotometer (Perkin-Elmer Ltd., England, 1977).

[6] J. Petzelt and V. Dvorak in: "Vibrational spectroscopy of phase transitions", eds. Z. Iqbal and F.J. Owens, (Academic Press, Orlando, 1984) p. 81.

[7] A.W. Baker, J. Phys. Chem. 61, 450 (1957).

[8] G. Roberts, Anal. Chem. 29, 911 (1957).

[9] W.C. Price and K.S Tetlow, J. Chem. Phys. 16, 1157 (1948).

[10] G. Duyckaerts, Analyst 84, 201 (1959).

[11] Instructions and operating manual, model 20.100 temperature controller (Specac, England, 1980).

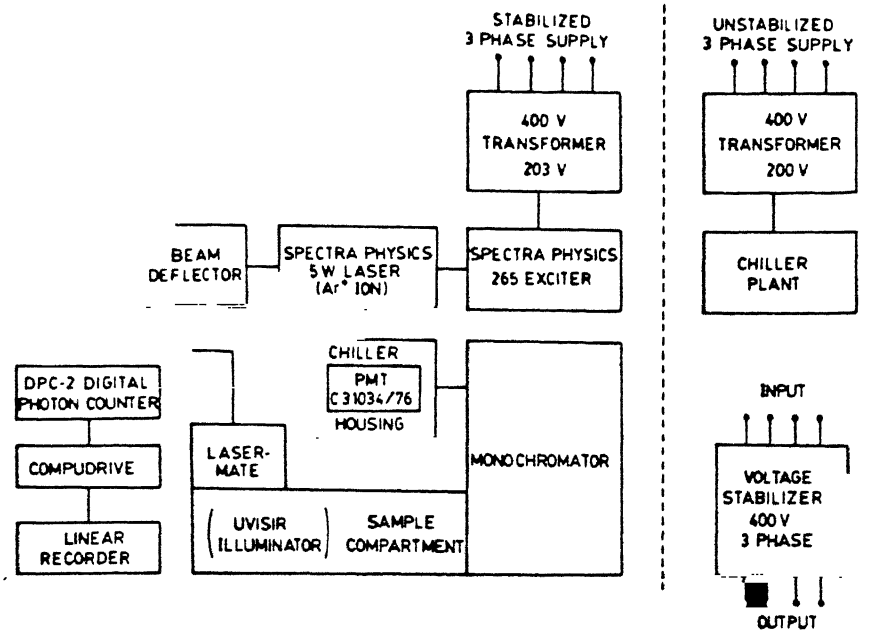

Figure 2.1: The general block diagram of the laser Raman spectrophotometer and other accessories.

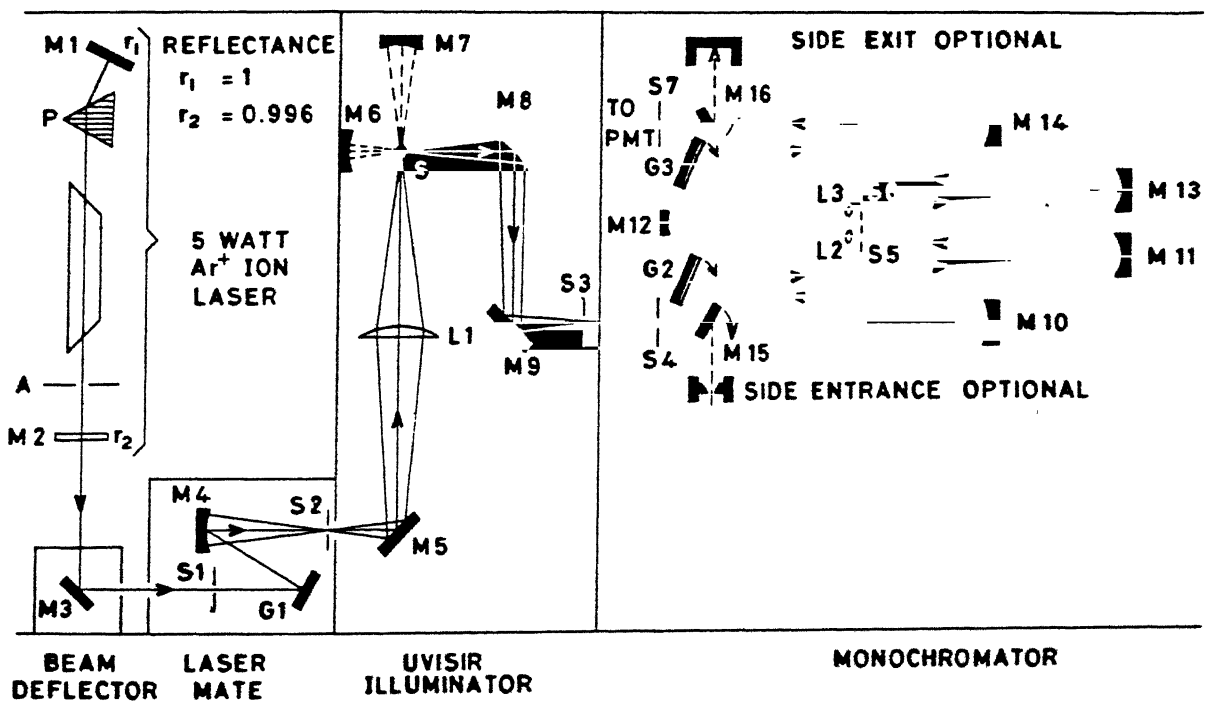

P: Prism; A: Aperture; M1-M3, M5, M9, M15, M16: Plane Mirrors; M4, M6, M7, M10-M14: Concave Mirrors; M8: Elliptical Collector Mirror; S1-S7: Slits; G1-G3: Gratings; L1: Fused Silica Condenser Lens; S: Sample; L2, L3: Optical Filter; PMT: Photomultiplier Tube.

Figure 2.2: The detailed optical diagram of the excitation source, lasermate, collecting optics and the double monochromator.

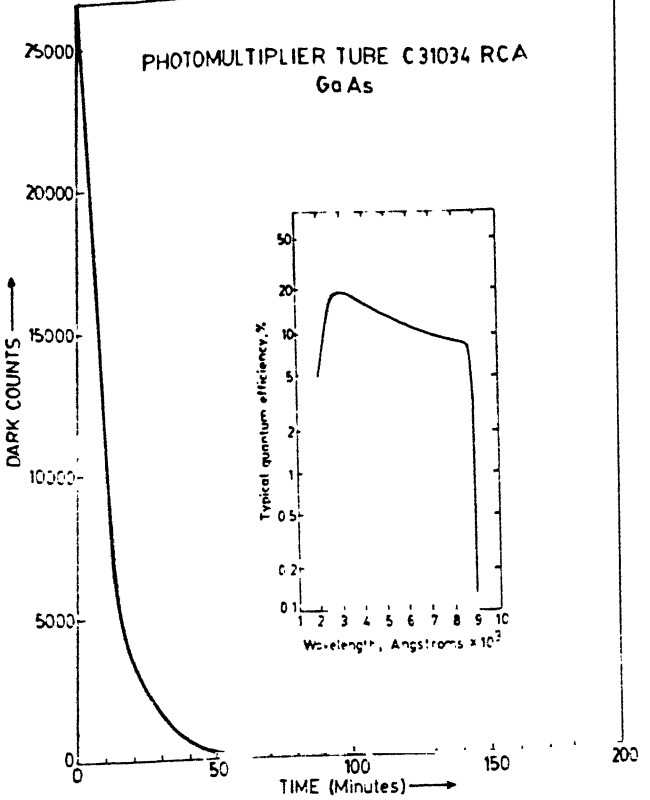

Figure 2.3: Dark count of the PMT (counts/sec) versus cooling time (minutes). Inset shows the (%) quantum efficiency of the PMT as a function of wavelength (Angstroms x 10^3).

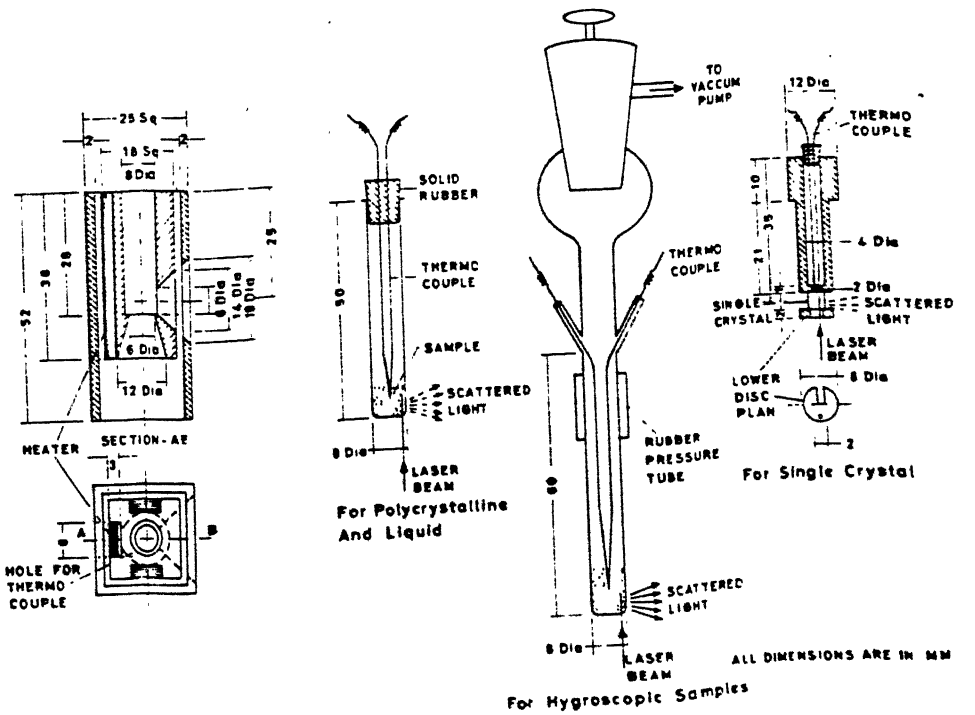

Figure 2.4: The design of a high temperature cell with different types of sample holders used for Raman studies.

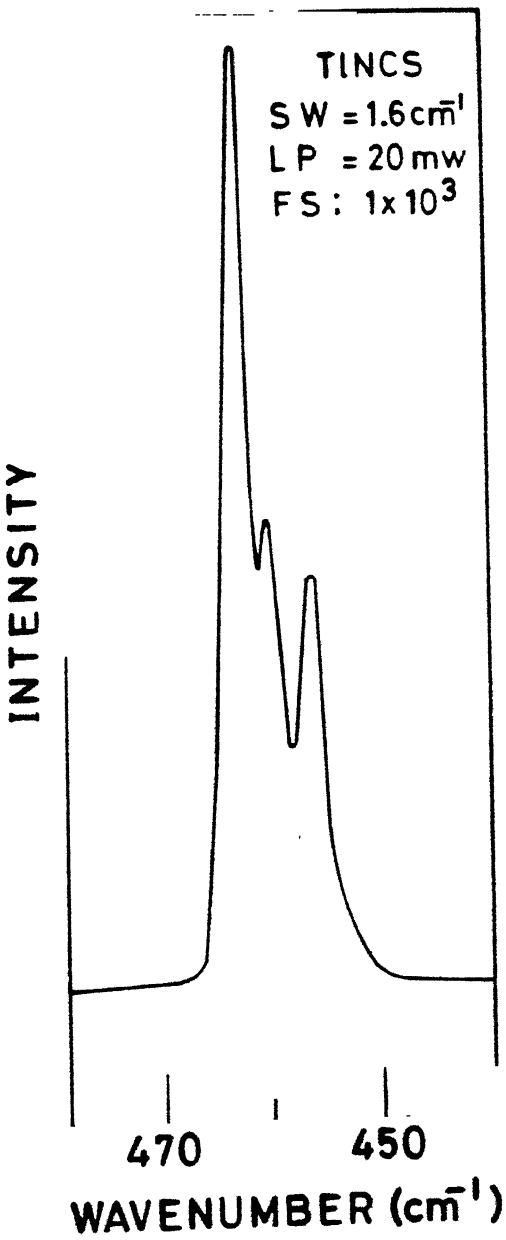

Figure 2.5: Raman spectrum of TlNCS powder in the NCS^- bend. mode region. Power employed for the excitation was 6 mw (514.5 and the slitwidth $\simeq$ 1.6 cm^{-1}.

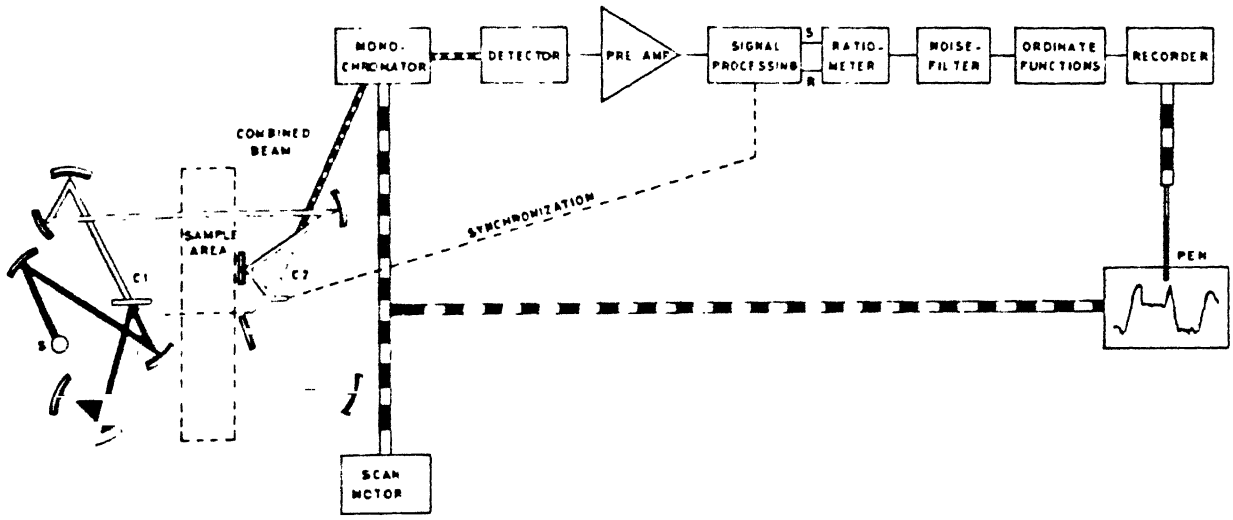

Figure 2.6: Simplified block diagram of the equipment used for recording IR spectra.

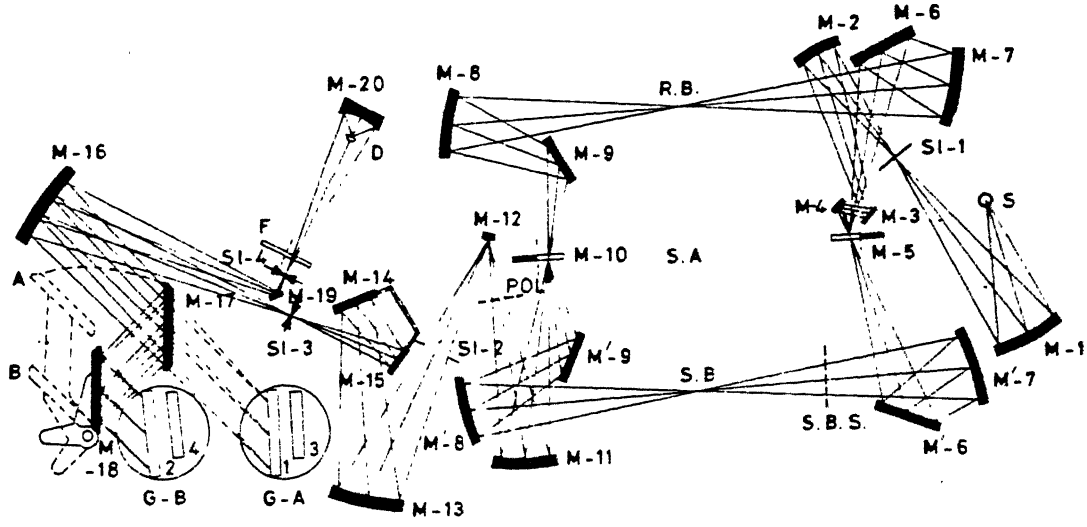

S:Source; M1, M2, M4, M7, M'7, M8, M'8, M11-M13: Toroid Mirrors; M5, M10: Chopper Mirrors; M3, M6, M'6, M9, M'9, M14, M15, M17, M19: Reflection and Scatter Grating Surface Mirrors; M16: Paraboloid Mirror; M20: Elipsoid Mirror; G-A, G-B: Grating Tables; SI-1: Baffle and Secondary Source; SI-2: Pupil Baffle; SI-3: Entrance Slit; SI-4: Exit Slit, POL: Polarizer Accessory; F: Optical Filter; D: Detector; SBS: Sample Beam Shutter; SB: Sample Beam; SA: Sample Area; RB: Reference Beam.

Figure 2.7: The detailed optical diagram of the infrared spectrophotometer.

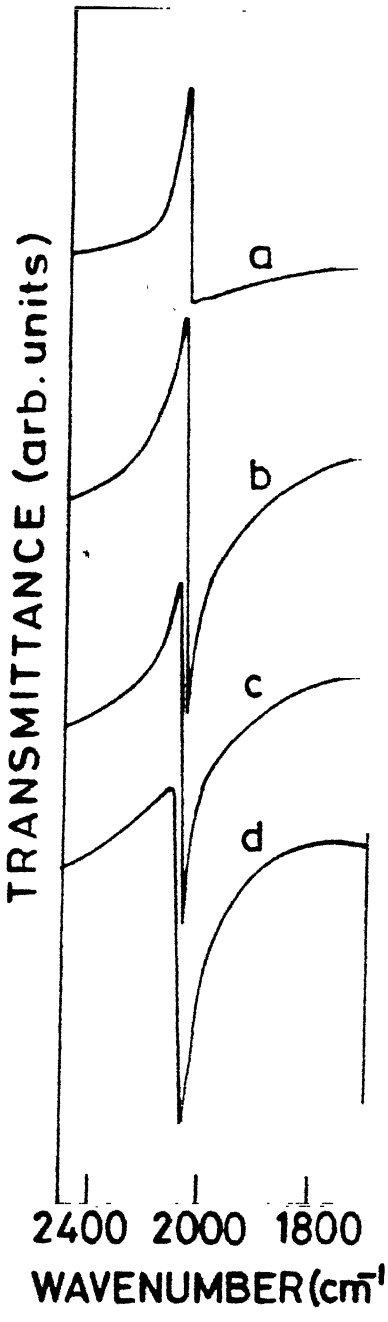

Figure 2.8: The IR transmittance spectra of TlNCS powder in the C-N stretching (ν_{C-N}) region for different particle sizes. Asymmetry in the ν_{C-N} modes for (a) larger, (b) and (c) intermediate particle sizes; and no asymmetry for (d) very small particle ($<\lambda_{min}$) sizes of TlNCS powder can be seen.

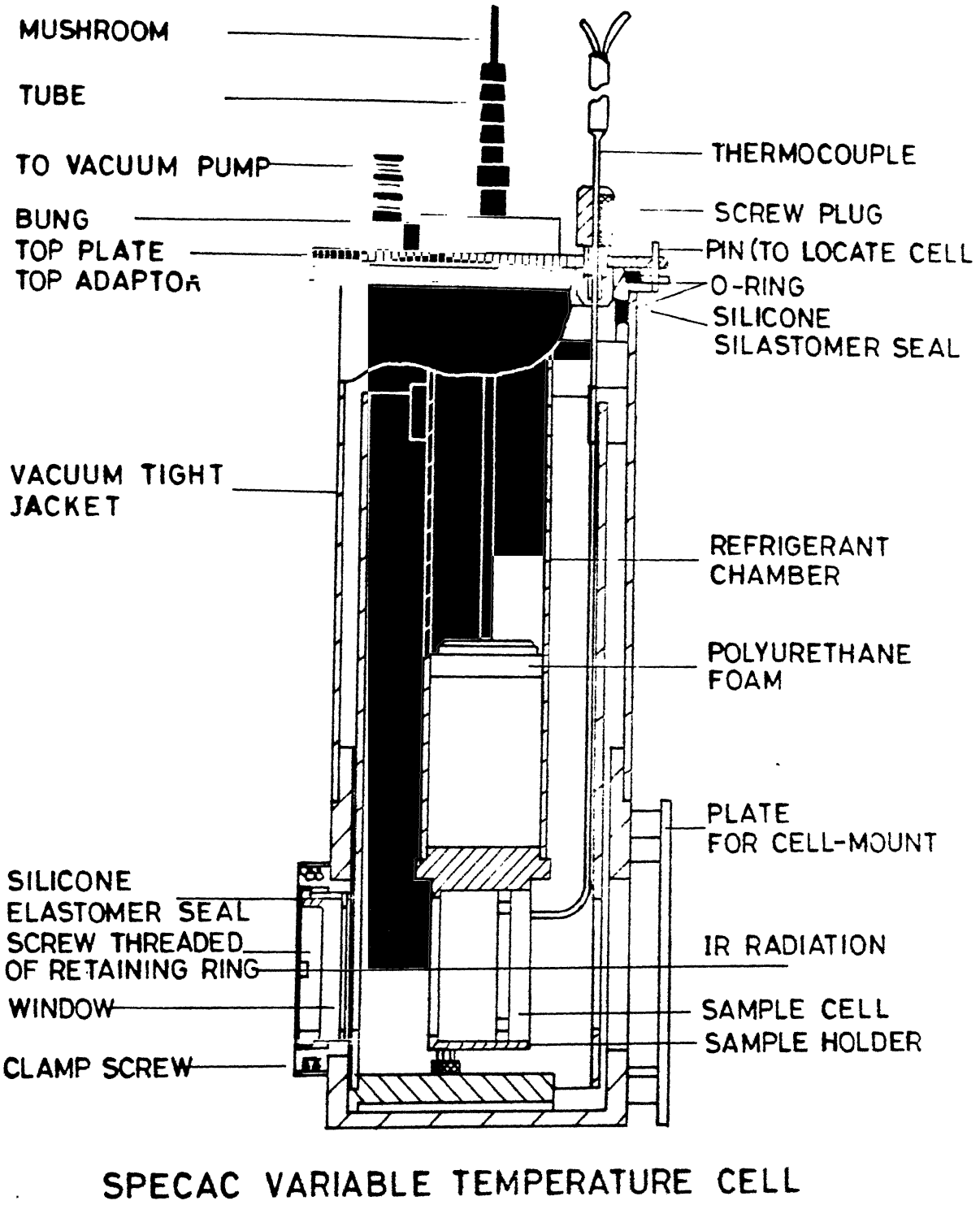

Figure 2.9: The line diagram of the Specac variable temperature cell.

CHAPTER 3

VIBRATIONAL STUDIES OF THE STRUCTURAL PHASE TRANSITION IN CAESIUM THIOCYANATE

Abstract

The room-temperature Raman and infrared (IR) spectra of Caesium thiocyanate (CsNCS) and the temperature (T) dependence (in the 299-475^{o}K range) of various thermo-sensitive bands are presented. On the basis of these detailed experimental studies the orthorhombic to cubic transition in CsNCS at $T_c \simeq 470^{o}K$ has been spectroscopically characterised as an order-disorder transition and to be first order in nature. Typical changes in the integrated intensity I_{C-N} of the $\nu_{C-N} = 2042\ cm^{-1}$ mode in the Raman spectra below T_c are represented as $I_{C-N} \propto (|T-T_c|)^{2\beta}$, with an order-parameter exponent $\beta \simeq 0.35$. These results are discussed in the context of a theory developed by Bruce et al to describe the Raman activity of hard modes near a structural phase transition. A remarkably consistent value of $\beta \simeq 0.35 \pm 0.02$ is obtained by expressing the squares of the frequency shifts of the NCS^- librational mode in the temperature range 300-453^{o}K in terms of $(\nu_R^2 - \nu_0^2) \propto |T - T_c|^{2\beta}$, where $\nu_0 = \nu_R(T_c) = 125\ cm^{-1}$ and ν_R is the frequency of the in-plane librational mode. The anomalous increase in the band widths of many modes in the IR and Raman spectra closer to T_c may be attributed to increased anharmonicities as precursor effects to the transition. Above T_c the Raman spectrum due to the external modes is replaced by a broad-band spectrum and the fine structure ($\nu_{C-N} \pm$ external modes)

in the ν_{C-N} region of the IR spectrum is smeared off. These results have been related to the loss of translational invariance and the emergence of dynamic disorder (near T_c)as both ions (Cs^+, NCS^-) are in motion.

Publications based on the material contained in this chapter are the following:

[A] S. Sathaiah, V.N. Sarin and H.D. Bist, proc. solid st. phys. symp. India, 30 (A), 334 (1987).

[B] S. Sathaiah, V.N. Sarin and H.D. Bist, J. phys. condens. Matter 1, 7829-7841 (1989).

3.1 Introduction

Structural phase transitions (SPT) in crystals between high-symmetry (disordered) and low-symmetry (ordered) phases have attracted the attention of both experimentalists and theoreticians for many years [1]. Raman, infrared (IR) and other vibrational spectroscopic studies provide deeper insight into the microscopic origin of the SPT.

In the Raman technique, light is scattered by fluctuations in the dielectric tensor of a material. Fluctuations of certain physical quantities are coupled to the fluctuations in the dielectric tensor; near phase transitions the fluctuations of some of these quantities are enhanced. This makes Raman scattering an important tool for the study of SPT, especially orientational order-disorder type transitions in ionic crystals [2]. In these substances ions order with a definite orientation below the transition temperature (T_c) and become uncorrelated above T_c. Because of their different orientations from cell to cell, the translational symmetry of the crystal is destroyed. The wavevector **k** need no longer be conserved in a light scattering process and phonons of any **k** that feel the disorder can contribute to the light scattering spectrum. In undergoing this order-disorder transition the crystal may change its structure. Caesium thiocyanate (CsNCS) is a typical ionic crystal that consists of spherical cations and rod shaped anions. In this chapter, the temperature dependence of Raman and IR spectra (in the 300 to 475^{o}K range) and spectroscopic characterisation of the order-disorder SPT in CsNCS are reported for the first time.

3.2 Crystal Structure

At room temperature CsNCS has an ordered orthorhombic structure with space group D_{2h}^{16} (Pnma). The primitive cell contains four formula units (i.e. z = 4) and the lattice parameters are a = 7.978 Å, b = 6.332 Å and c = 8.332 Å. The structure is layered along the b axis. In each unit cell two NCS^- ions lie on planes perpendicular to the b axis at y = 1/4 and y = 3/4; both cations and anions occupying sites of C_s symmetry. The adjacent thiocyanate ions in the same layer are almost perpendicular to one another (Figure 3.1). Between 470°K and the melting point (≃ 480°K) CsNCS crystallises in a cubic structure similar to CsCl, with lattice constant a_o = 4.83 Å, z = 1 and space group O_h^1 (Pm3m). Because of its existence in the very narrow temperature region (≃ 10°K), detailed dynamic information about the cubic phase is slightly difficult to acquire. X-ray, differential scanning calorimetry, differential thermal analysis and neutron diffraction studies identified the transition to be of order-disorder type and it has been characterised as first order on the basis of discontinuous changes in the volume and the latent heat of transformation [3-6]. Several room-temperature studies of vibrational spectra and lattice dynamics have been reported [7-13].

3.3 Experimental Details

The CsNCS sample used for the present studies was an extra-pure sample from K and K Laboratories and it had been further purified by recrystallising three times from saturated

aqueous solutions. The pure sample thus obtained was finely ground and used for the temperature dependence study of Raman spectra. Flat plate-like crystals with well developed (001) planes were obtained by slow evaporation of a saturated aqueous solution. These single crystals were properly polished to make very thin platelets and used for room-temperature and temperature-dependent IR spectral studies.

For the Raman measurements, linearly polarised 514.5 nm radiation from an argon ion laser was used to excite the sample. A Spex 1403 double monochromator coupled with a photon counting system was used to record the spectra. For high-temperature studies a finely powdered CsNCS sample was positioned in the high-temperature cell. A Specac temperature controller with copper-constantan thermocouple touching the sample was used to measure the sample temperature with an accuracy of $\pm$ $1^{o}K$. The average heating rate and the laser power employed at the sample were $1^{o}K\ min^{-1}$ and 50 mW, respectively.

For infrared measurements a thin single-crystal platelet was mounted on a special sample holder and fixed in the pellet holder of the Specac variable-temperature cell. The spectra were recorded using a Perkin-Elmer 580 double-beam grating infrared spectrometer. A Specac temperature controller in conjunction with a copper-constantan thermocouple was used to vary, control and measure the temperature of the sample with an accuracy of $\pm$ $1^{o}K$.

3.4 Results

CsNCS is a typical ionic crystal in which the lattice structure is determined by the forces of at least two different

strengths. The stronger overlap forces bind the N, C and S atoms together to form the rigid NCS^- ion, while the weaker long-range Coulomb forces mixed with some short-range forces bind the Cs^+ and NCS^- ions to form the CsNCS lattice. The lattice dynamics of this system can, to a first approximation, be described in terms of internal modes of intra-ionic NCS^- vibrations and external modes of inter-ionic motions.

3.4.1 Room -temperature Raman Spectrum

The unpolarised Raman spectrum of the CsNCS sample at room temperature is shown in Figure 3.2. The predominant bands in the low-frequency region below 200 cm^{-1} can be attributed to external modes and all other modes above 200 cm^{-1} correspond to internal modes. Peak positions, relative strengths and probable mode assignments for the external and internal modes are listed in Table 3.1. The given symmetry assignments are those from the work of Ti et al [7]. In the external-mode region the band at 143 cm^{-1} (ν_R) is a rotatory mode that involves the hindered rotation of NCS^- about the b axis on the (0 1 0) plane. The band at 129 cm^{-1} is another rotatory mode, which involves the hindered libration out of the (0 1 0) plane. The band at 95 cm^{-1} is probably a two-phonon mode. All other low-frequency modes are translational modes. In the internal-mode region the two strong bands at 2042 and 2053 cm^{-1} are due to correlation field splitting of the C-N stretching mode ν_{C-N}. The band at ν_{C-S} = 750 cm^{-1} is the C-S stretching mode. Whereas δ^{a}_{N-C-S} = 475 and δ^{b}_{N-C-S} = 486 cm^{-1} correspond to in-plane and out-of-plane bending modes of NCS^- ions.

Bands at 950 and 975 cm^{-1} are overtones and the band at 963 cm^{-1} is a combination mode of δ_{N-C-S} fundamentals. The weak feature around 1494 cm^{-1} is an overtone of the ν_{C-S} fundamental. Other weaker features at 742 and 746 (ν'_{C-S}); 2007 and 2027 cm^{-1} (ν'_{C-N}) are C-S and C-N stretching modes of isotopic species. The overtones of NCS^- bending modes have higher peak intensities ($\simeq$ 5 times) compared to their fundamentals, indicating anharmonic effects even at room temperature.

3.4.2 Room-temperature Infrared data

The unpolarised transmission IR spectrum of the CsNCS thin single-crystal platelet is given in Figure 3.3. Peak positions and tentative assignments of all the observed bands are listed in Table 3.2. The dominant bands around 488, 758 and 2050 cm^{-1} are NCS^- bending, C-S stretching and C-N stretching modes, respectively. All other broader and weaker features correspond to multi-phonon processes. The observed complex fine structure in the C-N stretching region , can be attributed to multi-phonon processes involving $\nu_{C-N} \pm$ external modes.

3.4.3 Temperature Dependence of Raman Spectra

Raman spectra in the C-N stretching region of CsNCS powder are shown in Figure 3.4(a), for 10 typical temperatures between 299 and 465°K. On increasing the temperature the peak intensities of (2042, 2053 cm^{-1})ν_{C-N} modes decreased monotonically, with marginal changes in half-widths, but there are no appreciable changes in their peak positions till 440°K. Around 446°K a broad wing appears on the higher-frequency side of the

ν_{C-N} modes. As the temperature increases further, the band widths of ν_{C-N} modes increase exponentially. The higher-frequency wing enhances in intensity at the expense of a decrease in the peak intensities of the main ν_{C-N} modes. Finally around 461^{o}K the complete C-N stretching region is replaced by a single broad ($\simeq$ 7 times broader than ν_{C-N} modes) band peaked around 2059 cm^{-1}. For temperatures higher than 461^{o}K this broad band also starts to decrease in peak intensity. Typical changes in the integrated intensity I_{C-N} and band width γ_{C-N} of the ν_{C-N} (at 2042 cm^{-1}) mode with temperature are plotted in Figure 3.5(a). Integrated intensity decreases continuously in a well defined manner in the temperature range 300-458^{o}K, and by extrapolating the curve it becomes zero around 463^{o}K. Assuming this value as the approximate transition temperature (T_c), a plot of $\log I_{C-N}$ versus $\log|T-T_c|$ (Figure 3.5(b)) for $5 \leq |T-T_c| \leq 95^{o}$K gives a perfect straight line with a slope of 0.69 $\pm$ 0.04. So the strong variation in the integrated intensity with temperature can be represented as $I_{C-N} \propto (|T-T_c|)^{2\beta}$ with an order-parameter exponent $\beta \simeq 0.35 \pm 0.02$. This characteristic behaviour has been verified by repeating the experiment. The β-value obtained in the repeated experiment is $\beta \simeq 0.36 \pm 0.02$. The band width γ_{C-N} increases linearly until 440^{o}K and exponentially near the transition temperature. Peak frequencies of ν_{C-N} modes remained constant throughout the temperature range studied (Figure 3.6(a)).

Figure 3.4(b) shows typical changes in the external-mode (50-200 cm^{-1}) region. Apart from small changes in the peak positions and band widths and a decrease in their peak

intensities, the lattice mode structure does not change appreciably until 446°K. For temperatures above 446°K the continuous broadening of all the bands, and finally around 462°K the replacement of the complete lattice spectrum by a broad-band spectrum with a small hump around 125 cm^{-1}, can be seen. Plots of peak frequencies of the lattice modes ν_i versus temperature are given in Figure 3.6(b). The peak frequencies of all the lattice modes decrease monotonically. The in-plane rotatory mode displays the largest softening of 11% (at 453°K). The out-of-plane rotatory mode softens by 7% and all other translational modes by 6%. It is interesting to note that the squares of the frequency shifts of the in-plane rotatory mode (ν_R) in the temperature range 300-453°K vary as $(\nu_R^2 - \nu_0^2) \propto |T - T_c|^{2\beta}$, with $\beta \simeq 0.35 \pm 0.02$, $\nu_0 = \nu_R(T_c) = 125\ cm^{-1}$ and $T_c \simeq 462°K$. A plot of log $(\nu_R^2 - \nu_0^2)$ versus log$|T-T_c|$ gives an exact straight line (inset in Figure 3.6(c)) with a slope of 0.7 ± 0.04. For the other lattice modes, ν_i^2 do not change linearly with temperature but the product of squares $\pi_i \nu_i^2$ of external modes (includng ν_R^2) follows an exact linear relationship. Figure 3.6(c) is a plot of $\pi_i \nu_i^2$ versus T showing a straight line in the temperature range 300-453°K. This behaviour has been verified by repeating the experiment. Typical changes in the Rayleigh wing (on the anti-Stokes side of the spectrum) with temperature are shown in Figure 3.4(c). As the sample temperature increases, the Rayleigh wing slowly narrows down and finally a sharper wing can be seen around 463°K. All the observed changes in the Raman spectra of polycrystalline CsNCS during the heating cycle are also observable in the cooling cycle

but with a large hysteresis of about 35°K. This large hysteresis ($\simeq$ 35°K) in the transition temperature is consistent with the value of about 45°K reported from x-ray results (Figure 3.2 in [3]) and the value of about 40°K from our IR data.

3.4.4 Temperature Variation of the Infrared Data

As the temperature increases above 300°K the gradual broadening and smearing of fine structure in the C-N stretching region can be clearly seen (Figure 3.7(a)). Finally around 472°K it is completely smeared off and a single broad band can be seen for temperatures above 472°K. This behaviour is consistent with the Raman results, where the low-frequency external-mode region is replaced by a broad-band spectrum for temperatures above 462°K. The IR spectra in the C-S stretching and NCS^- bending (400-1050 cm^{-1}) region are shown in Figure 3.7(b), for four different temperatures below and above the transition temperature. Apart from small changes in the band widths and peak intensities, the spectra do not change much till 463°K. In fact the IR spectrum at 463°K is identical to that at room temperature. For temperatures 5-10°K above 463°K, an anomalous increase in peak intensities and half-widths of the C-S stretching and NCS^- bending modes can be seen. Similarly overtones of NCS^- bending fundamentals merge into a single broader band with stronger peak intensity. Similar broadening is observed for all other multi-phonon modes and some of the weaker multi-phonon bands become too broad to observe. The characteristically different spectrum around 475°K, consisting of very broad bands, indicates the highly disordered nature of the

high-temperature phase I. In the cooling cycle this phase I persisted until 433^{o}K (denoted by the asterisk (*) in Figure 3.7(b)), showing a large hysteresis of 40^{o}K in the transition temperature.

3.5 Discussion

All the changes in the Raman spectra above 463^{o}K, e.g. the replacement of the external-mode region by a broad-band spectrum, the appearance of a very broad band around 2059 cm^{-1} in place of sharp(2042, 2053 cm^{-1})C-N stretching modes and the characteristic changes in the integrated intensity, reveal an order-disorder transition around that temperature. The changes in the IR spectra indicate the transition temperature to be at 472 $\pm$ 1^{o}K, in agreement with the reported $T_c \simeq 470^{o}$K from x-ray, neutron diffraction and thermal investigations [3-6]. The discrepancy in the observed T_c value in our Raman measurements can be attributed to local heating effects, i.e. the laser irradiated spot temperature of the sample is about 7^{o}K higher than the measured one at a slightly different point.

3.5.1 First-order Nature of the Transition

At room temperature the two ν_{C-N} modes (2042 and 2053 cm^{-1}) in the Raman spectrum are due to correlation field splitting. So the replacement of these ν_{C-N} modes by a single broad band (2059 cm^{-1}) can be attributed to the apparent decrease in the anisotropy of the crystal field around the NCS^{-} ion, which probably occurs as a result of the disordering oscillations of the NCS^{-} ion near T_c. Then the simultaneous appearance of both the

broad band at 2059 cm^{-1} (characteristic of disordered phase I) and the 2042 and 2053 cm^{-1} modes (characteristic of low-temperature ordered phase II) in the temperature range 446-462^{o}K indicates the coexistence of both phases in that range. Such coexistence phases are also seen in IR spectral studies during a cooling cycle. In the heating cycle there are marginal changes in the IR spectra (of phase II) until 463^{o}K. However, an increase in the temperature by 5-10^{o}K above 463^{o}K results in a spectrum consisting of anomalously broad and stronger bands characteristic of the highly disordered nature of phase I. In the cooling cycle this phase I persisted upto 433^{o}K as a metastable phase. All these observations, i.e. the coexistence phases, large hysteresis in the T_c value and sudden changes in the spectra within a small temperature range, are characteristic features of a first-order transition.

3.5.2 Spectral Manifestation of Disorder

As mentioned earlier, x-ray studies identified phase I to be cubic and a 24-fold orientational disordered arrangement of the NCS^- ion was postulated in order to fulfil the symmetry requirements of the cubic phase. The spectral manifestations of this highly disordered character of phase I can be seen from our observations above T_c, i.e. the appearance of a broad wing in the lattice-mode region of Raman spectra and smeared-off fine structure in the C-N stretchng region of IR spectra, which could occur due to the breakdown of $k = 0$ selection rules. The absence of discrete Raman lines in the lattice region confirms its cubic structure. Since first-order Raman sacttering in the CsCl-like cubic phase is not allowed by group theory, the broad feature around 125 cm^{-1} may be associated with disorder-allowed phonons.

3.5.3 Generalised Soft-mode-like Behaviour of External Modes

Some of the observations in our Raman studies (e.g. gradual narrowing of Rayleigh wing with temperature, finally becoming sharper above T_c, and the broad-band lattice spectra in phase I) look strikingly similar to that reported by Dultz [14] for the disordered cubic phase of KCN. Assuming some similarity between transitions in KCN and CsNCS, Irving et al [5] concentrated their neutron diffraction studies of CsNCS on acoustic modes in an attempt to find soft modes associated with the transition. But they did not observe any such mode from their studies. Our Raman results also show that all the external modes are temperature-dependent to some extent, but none of them individually show purely soft-mode-like behaviour. Interestingly the product of the squares of these external modes, $\Pi_i \nu_i^2$ varies linearly in the temperature range 300-453^{o}K as shown in Figure 3.6(c).By extrapolating the curve,$\Pi_i \nu_i^2$ becomes zero around 600^{o} K, which is considerably higher than the observed T_c value (i.e. 463^{o}K). A similar type of behaviour had been reported by Iqbal et al [15] for KNCS in which the reported order-disorder transition temperature was 413^{o}K and the extrapolated temperature where $\Pi_i \nu_i^2$ becomes zero was 535^{o}K. For $NaClO_3$ crystal Rao et al [16] reported a similar relation, i.e. $\Pi_i \nu_i^2 \propto (T-T_c)$, with an extrapolated T_c = 593^{o}K (greater than the melting point 537^{o}K) for the first-order transition, and their Raman results were comparable with dielectric measurements. These authors interpreted the linear behaviour of $\Pi_i \nu_i^2$ versus T as the

generalisation of Cochran's soft-mode concept. In this line of thought $\Pi_i \nu_i^2$ not becoming zero at T_c in CsNCS may be due to the highly first-order nature of the transition, the sample might have distorted to another phase before $\Pi_i \nu_i^2$ had a chance to go to zero. To confirm the applicability of this generalised soft-mode concept, one also has to observe a linear increase in $\Pi_i \nu_i^2$ with temperature above T_c. This could not be verified in the present case due to the resulting broad-band lattice spectrum above T_c. Additionally, the T dependences of all the lattice modes, including the weaker modes below 60 cm^{-1}, have to be considered in $\Pi_i \nu_i^2$.

On the other hand, the peculiar variations $\nu_R^2 - \nu_0^2 \propto (|T-T_c|)^{0.7}$ in the librational mode for T (< 453°K) well below T_c may probably be associated with the transition. Although ν_R remains as a weak diffusive structure around 125 cm^{-1} ($=\nu_0$) above T_c, this type of softening may not be unusual for the transition triggered by reorientational fluctuations of the ions.

3.5.4 Calculation of Order-parameter Exponent β and Activation Energy U

It is interesting to note that the integrated intensity I_{C-N} falls of ($I_{C-N} \propto (|T - T_c|)^{2\beta}$ for $T \longrightarrow T_c - 5°K$ from below) like the square of the order parameter (η^2), giving an order-parameter exponent $\beta \simeq 0.35 \pm 0.02$. Recently Bruce et al [17] have developed a general theory for the onset of Raman activity of hard modes (modes that are not directly involved in the phase transition) near a SPT. These hard modes are of interest if, on symmetry grounds, they are Raman-active below T_c

and Raman-inactive above T_c. According to this theory, the total Raman intensity I for such modes can be expressed as

$$I = I^{LR} + I^{CP} + I^{PH} \qquad (3.1)$$

where I^{LR} represents the long-range contribution to the first-order scattering in phase II and is proportional to the square of the order parameter (η^2); I^{CP} is the central peak contribution resulting from the first-order hard-mode scattering induced by short-range order; and I^{PH} represents the contribution from two-phonon processes involving hard and soft-phonon quasi-harmonic interactions and giving rise to second-order Raman scattering. The Expression (3.1) has been used to explain the temperature dependence of Raman intensities of hard modes near the tetragonal to cubic (continuous with first-order components) transitions in $KMnF_3$ and $RbCaF_3$ samples [17]. In CsNCS sample the temperature dependence of the integrated intensity I_{C-N} of the ν_{C-N} mode (for T well below T_c) is remarkably consistent with the dominance of the first term in equation (3.1). So in the low-temperature phase the Raman intensity of the ν_{C-N} mode may solely be controlled by the long-range order. It is difficult to draw any quantitative conclusions for temperatures very close to T_c because of the broad-band spectra and first-order nature of the transition. However, the consistent value of $\beta \simeq 0.35 \pm 0.02$ from librational mode frequency shifts (for T well below T_c) gives additional support to the above results.

Deep in the ordered phase the linear increase in the band width of the ν_{C-N} mode can be understood as cubic anharmonic contributions to its half-width. Whereas, the exponential increase in γ_{C-N} (Figure 3.8(a)) in the vicinity of T_c is due to the dominance of reorientational fluctuations of NCS^- ions. The changes in γ_{C-N} for $425 < T \leq 455^oK$ can be represented as $\gamma_{C-N} \propto e^{-U/K_BT}$ where U is the activation energy for the reorientational motion and K_B is the Boltzmann constant. A plot of $\ln\gamma_{C-N}$ versus 1/T (Figure 3.8(b)) gives a straight line; and $U \simeq 0.46 \pm 0.01$ ev has been extracted from the slope.

3.5.5 Phase Transition Mechanism

Neutron diffraction studies of CsNCS sample [5,6] revealed an anomalous increase in the mean-square displacements of both Cs^+ and NCS^- ions near T_c and that highly anharmonic behaviour was attributed to precursor effects associated with the transition. In the vicinity of the transition the anomalous increase in the band widths of many modes in the IR and Raman spectra may be associated with those strongly enhanced anharmonicities near T_c. The large entropy change associated with the transition, 5.7 eu mol^{-1} (almost twice the melting entropy, 3.0 eu mol^{-1}[3]), and the anomalous broad features in the IR and Raman spectra above T_c, suggest that the high-temperature cubic phase is a classic *"plastic crystalline phase"* [18].

The transition in CsNCS may be compared with that of a KNCS sample, which also has an orthorhombic layer structure (space group Pbcm) at room temperature but transforms at 414.5^oK to a tetragonal structure (space group I4/mcm). The transition in KNCS

has been determined to be second order in character, with a small first-order component. Near the transition temperature NCS^- ions in KNCS are believed to undergo dynamic reorientational fluctuations between two energetically equivalent positions [15, 19-22]. One can expect thermodynamically similar transitions in rubidium, ammonium and thallium thiocyanates whose low-temperature phase II structures are known to be (orthorhombic) isomorphous to that of KNCS. But the transition in CsNCS is found to be completely different. The large entropy change at T_c the first-order character of the transition, the cubic symmetry and the highly disordered nature of phase I are unique features of the CsNCS sample among all the alkali thiocyanates. Although the measured change in entropy, 5.7 eu† mol^{-1}, is close to Rln 24=6.3 eu mol^{-1}, supporting the 24-fold orientational disordered arrangement of NCS^- ions in phase I, the large increase in the band widths of almost all the bands in the IR and Raman spectra near T_c .and the temperature dependence of all the observed lattice modes suggest that the transition may not be solely related to NCS^- ion disorder but probably involves shifts of both (Cs^+, NCS^-) ions. This mechanism for the phase transition involving a cooperative dynamic reorientational disordering near T_c as both ions are in motion is consistent with the previously reported neutron diffraction results.

---

†Entropy unit (cal deg^{-1})

References

[1] J.F. Scott, Rev. Mod. Phys. 46, 83-128 (1974).

[2] C.H. Wang, in "Vibrational Spectroscopy of Phase Transitions". (eds.)Z. Iqbal and F.J. Owens (Academic Press, Orlando, New York ,1984) p. 153.

[3] S. Manolatos, M. Tillinger and B. Post, Solid State Chem. 7, 31-5, (1973).

[4] W. Klement Jr. Bull. Chem. Soc. Japan 49, 2148-53 (1976).

[5] M.A. Irving, M.M. Elcombe and T.F. Smith, Aust. J. Phys. 38, 85-95 (1985).

[6] B.K. Moss, S.L. Mair, C.J. Mcintyre and R.K. McMullan, Acta Crystallogr. B 43, 16-23, (1987).

[7] S.S. Ti, S.F.A. Kettle and Ø. Ra, Spectrochim. Acta. A 33, 111-19 (1977).

[8] Ø. Ra, S.S. Ti and S.F.A. Kettle, J. Chem. Phys. 68, 2638 (1978).

[9] S.S. Ti and Ø. Ra, J. Chem. Phys. 73, 5738-48 (1980).

[10] S.S. Ti and Ø. Ra, J. Chem. Phys. 73, 5749-52 (1980).

[11] M.A. Irving, S. Prawer, T.F. Smith and T.R. Finlayson, Aust. J. Phys. 36, 85-92 (1983).

[12] M.A. Irving, M.M. Elcombe and T.F. Smith, Aust. J. Phys. 37, 287-304 (1984).

[13] G. Hua and F. Ninio, Aust. J. Phys., 39, 309-27 (1986).

[14] W. Dultz, Solid State Commun. 15, 595-8 (1974).

[15] Z. Iqbal, L.H. Sarma and K.D. Moller, J. Chem. Phys., 57, 4728 (1972).

[16] A.D.P. Rao, R.S. Katiyar and S.P.S. Porto, Phys. Rev. Lett., 28, 6658 (1972).

[17] A.D. Bruce, W. Taylor and A.F. Murray, J. Phys. C Solid State Phys. 13, 483-504 (1980).

[18] J.N. Sherwood, The Plastically Crystalline State (Wiley, New York, 1979).

[19] M. Sakiyama, H. Suga and S. Seki, Bull. Chem. Soc. Japan 36, 1025-32 (1963).

[20] Y. Yamada and T. Watanabe, Bull. Chem. Soc. Japan 36, 1032-7 (1963).

[21] F.J. Owens, Solid State Commun. 29, 789-91 (1979).

[22] S.V. Karpov, A.V. Khassan Ali and A.A. Shultin, Sov. Phys. Solid State 24, 39-41 (1982).

Table 3.1 : Vibrational frequencies, relative strengths, mode assignments and symmetry species of Raman active modes in CsNCS at 300°K†.

(a) External and Internal Modes

	Vibrational fequency (cm^{-1})	Relative strength	Mode assignment	Symmetry species ††
External Modes	38	s	T	A_g
	45	s	T	(A_g, B_g)
	55	m	T	B_g
	73	vs	T	B_g
	95	s	Two Phonon	?
	130	ms	R	B_g
	143	ms	R	(A_g,B_g)
Internal Modes	475	vw	δ^a_{N-C-S}	(A_g,B_g)
	486	vw	δ^b_{N-C-S}	(A_g,B_g)
	750	s	ν_{C-S}	(A_g,B_g)
	2042	vs	ν_{C-N}	(A_g)
	2053	ms	ν_{C-N}	(A_g)

(b) **Multi-phonon modes and Internal modes of isotopic species**

	Vibrational fequency (cm^{-1})	Relative strength	Mode assignment
Multi-phonon Modes	951	w	$2\delta^{a}_{N-C-S}$
	963	vw	$(\delta^{a}_{N-C-S} + \delta^{b}_{N-C-S})$
	975	mw	$2\delta^{b}_{N-C-S}$
	1494	vw	$2\nu_{C-S}$
Internal Modes of Isotopic Species	742	m	$N-^{13}C-S$ $\quad \nu'_{C-S}$
	746	m	$^{15}N-C-S$ $\quad \nu'_{C-S}$
	2002	w	$N-^{13}C-^{34}S$ $\quad \nu'_{C-N}$
	2007	m	$N-^{13}C-S$ $\quad \nu'_{C-N}$
	2022	w	$^{15}N-C-^{34}S$ $\quad \nu'_{C-N}$
	2027	m	$^{15}N-C-S$ $\quad \nu'_{C-N}$

† The abbreviations v,s,m,w and sh stand for very, strong, medium, weak and shoulder; R and T stand for rotational and translational modes. ν_{C-N}, ν_{C-S}, δ^{a}_{N-C-S} and δ^{b}_{N-C-S} denote C-N & C-S stretching, in-plane and out-of plane bending modes of NCS^{-} ions, respectively. ν'_{C-N} and ν'_{C-S} are C-N and C-S stretching modes of isotopic species.

†† Inferred from [7]

3.2 Vibrational frequencies and tentative assignments of IR active internal and multi-phonon modes

	Vibrational frequency (cm^{-1})	Mode assignment	Critical point frequency (L_{cp})	Observed k=0 external mode frequency (cm^{-1})
Internal Modes	488	δ_{N-C-S}		
	758	ν_{C-S}		
	750	$^{13}C\ \nu'_{C-S}$		
	2050	ν_{C-N}		
Multi-phonon Modes †	957 980	$\delta_{N-C-S}+\delta_{N-C-S}$		
	1500	$2\nu_{C-S}$		
	1927	$\nu_{C-N}-L_{cp}$	123	130
	1982	$\nu_{C-N}-L_{cp}$	68	73
	2092	$\nu_{C-N}+L_{cp}$	42	45
	2128	$\nu_{C-N}+L_{cp}$	78	73
	2180	$\nu_{C-N}+L_{cp}$	130	130

† Very broadbands at 1428, 1680, 1768, 2865, 3100 and 3210 cm^{-1}; and the spectral features at 830, 893, 1025, 1095, 1198, 1238 and 2550 cm^{-1} also correspond to multi-phonon modes.

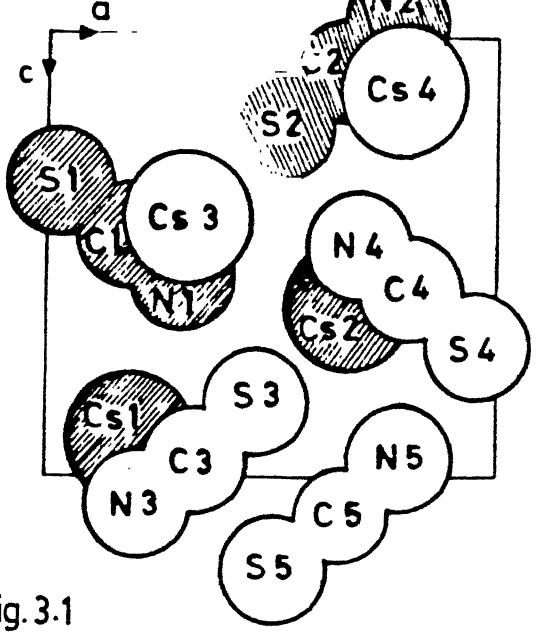

Fig.3.1

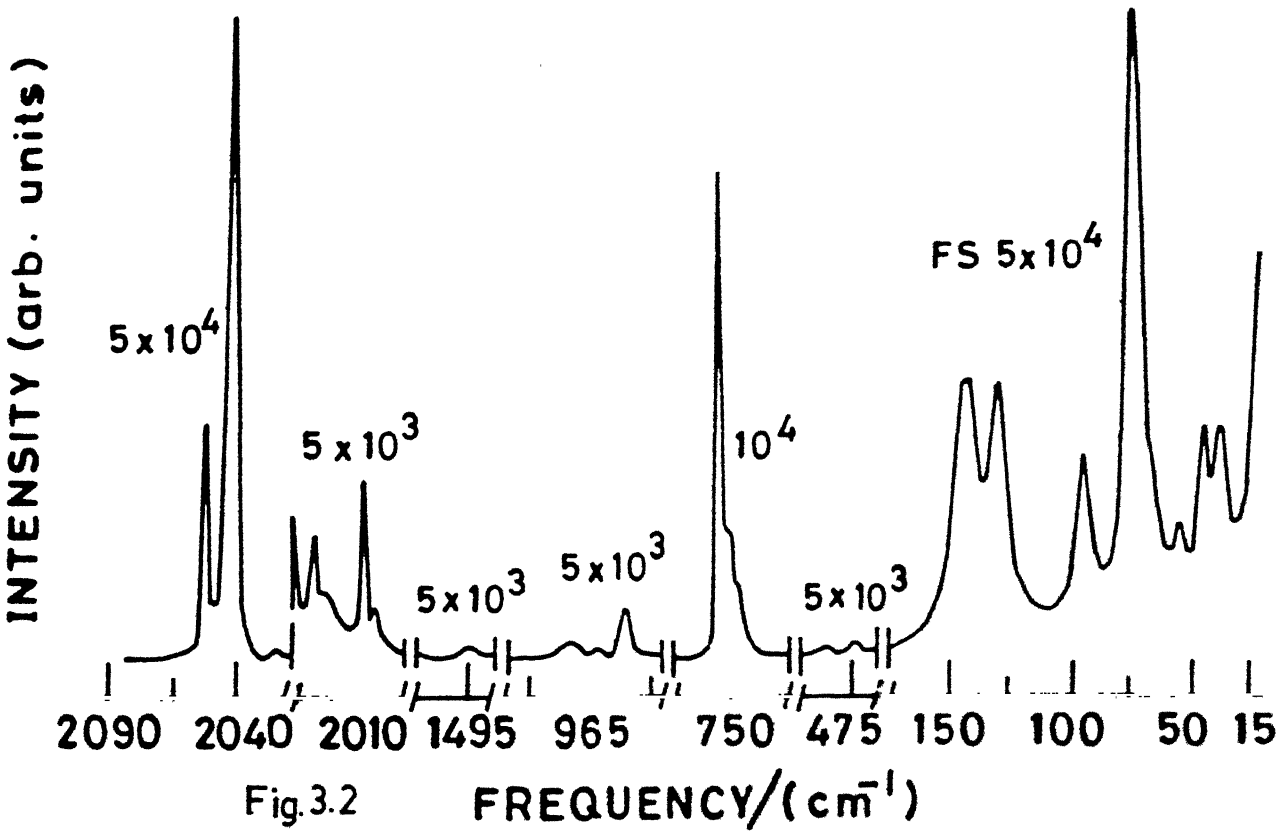

Fig.3.2

Figure 3.1: Arrangement of atoms in the orthorhombic unit cell. Shaded and unshaded atoms are at y = 1/4 and y = 3/4, respectively.

Figure 3.2: Unpolarised Raman spectrum of CsNCS single crystal at room temperature. FS $5x10^4$, $5x10^3$ and $1x10^4$ are recording sensitivities (photon counts per second).

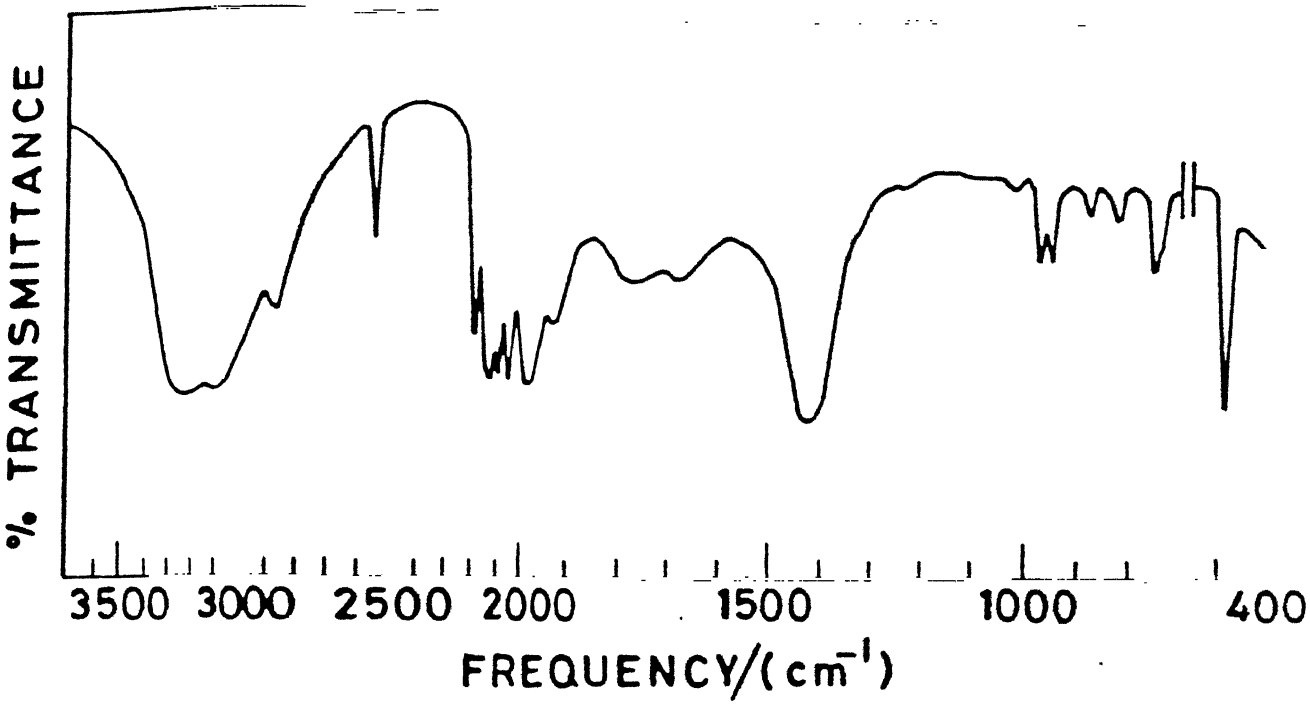

Figure 3.3: Unpolarised transmission IR spectrum of CsNCS single-crystal platelet at room temperature.

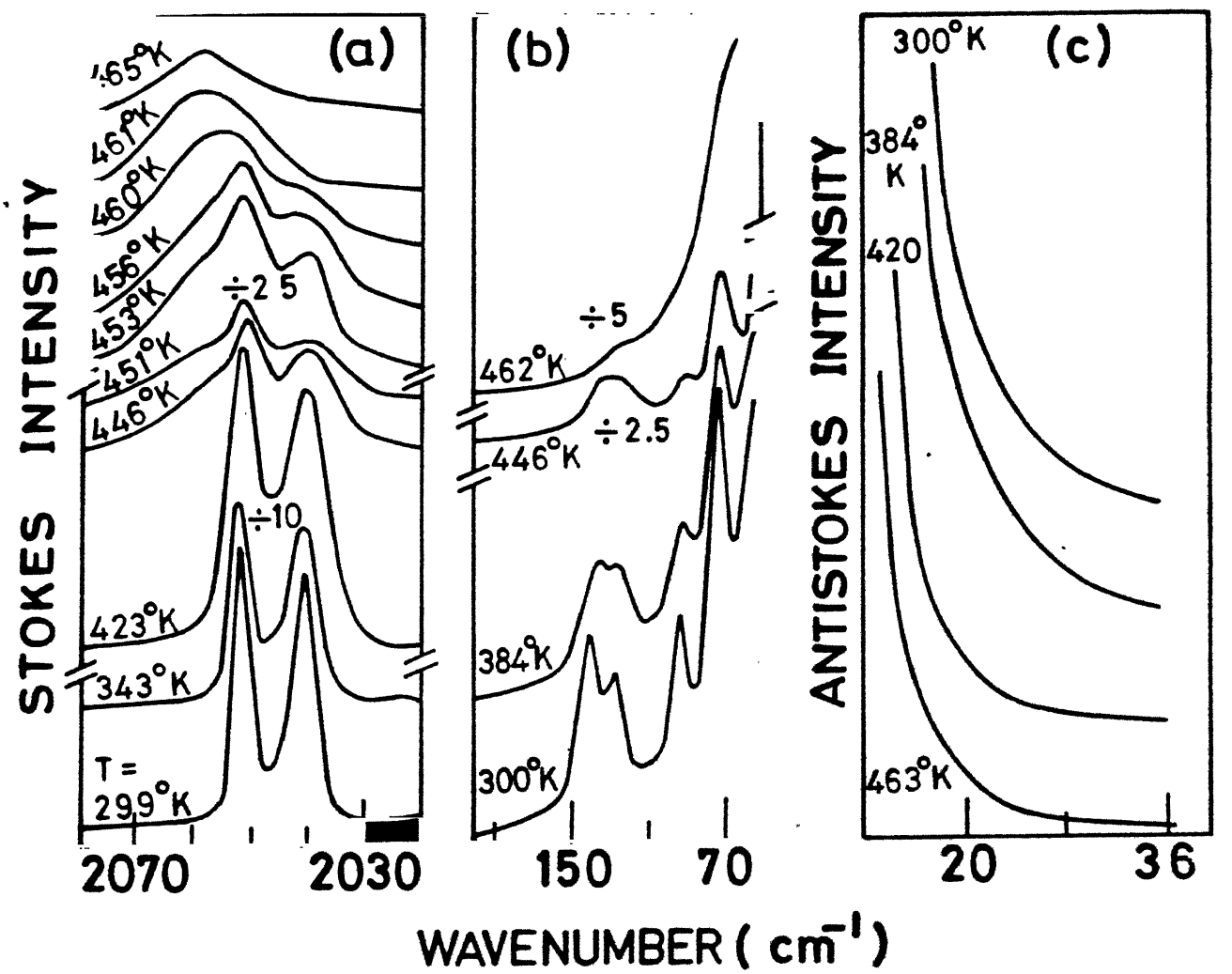

Figure 3.4: Thermo-sensitive mode regions in the Raman spectrum of CsNCS polycrystalline sample. Temperature dependence of Raman spectra in (a) C-N stretching region, (b) lattice-mode region and (c) Rayleigh wing (on the anti-Stokes side of the Raman spectrum).

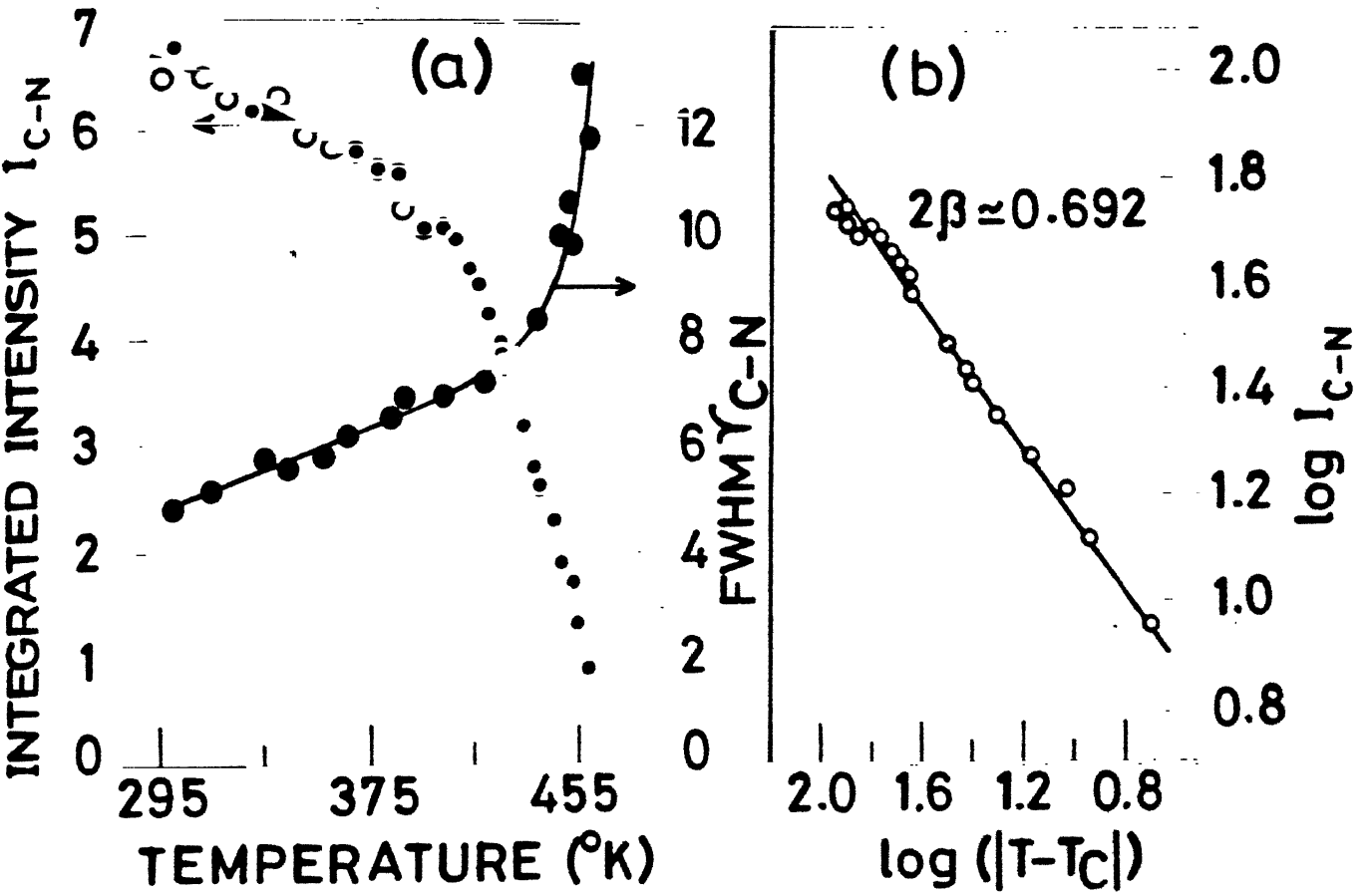

Figure 3.5: (a) Variations in the integrated intensity I_{C-N} and FWHM $\gamma_{C-N}(cm^{-1})$ (O) of C-N stretching mode with temperature. (b) Plot of log I_{C-N} versus log$|T-T_c|$ for $5 \leq |T-T_c| \leq 95^{\circ}K$.

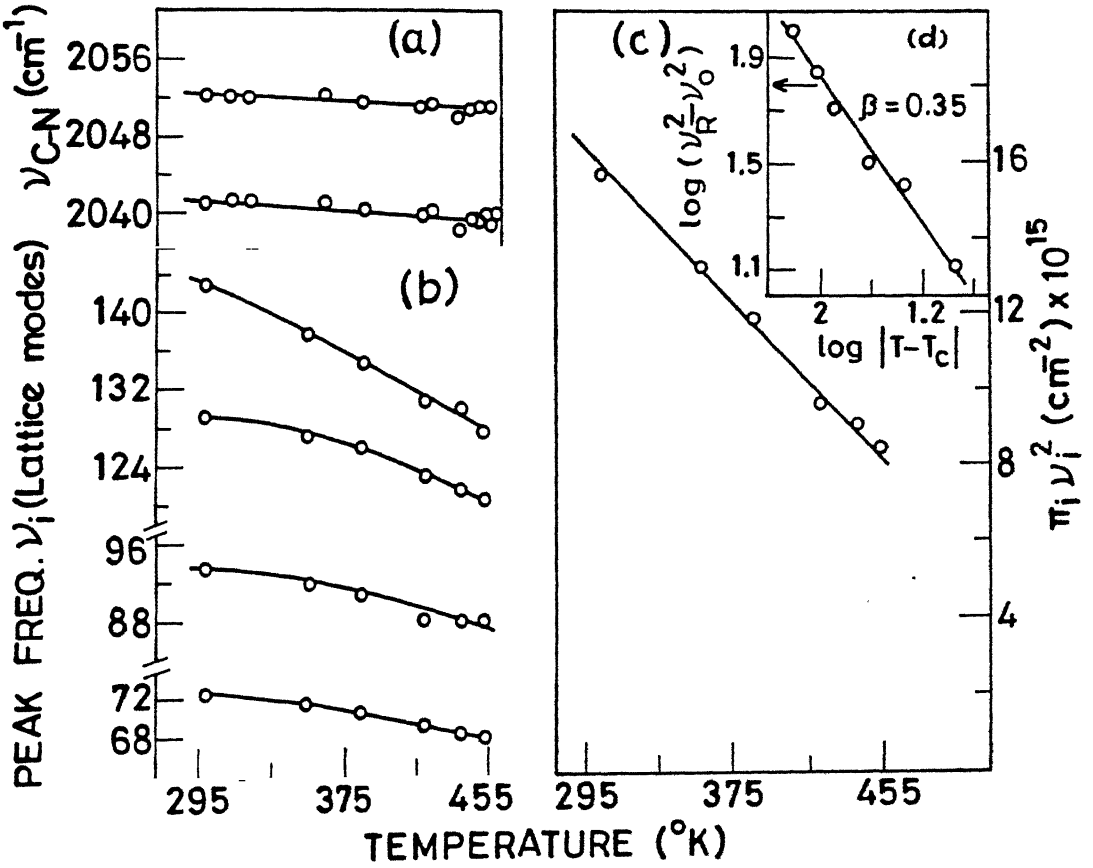

Figure 3.6: Changes in the peak frequencies with temperature: (a) ν_{C-N} modes versus temperature; (b) lattice modes ν_i versus temperature; (c) product of squares of frequencies $\pi_i \nu_i^2$ for four lattice modes (ν_i) versus temperature. The inset shows a plot of $\log(\nu_R^2 - \nu_o^2)$ versus $\log(|T - T_c|)$ in the T range 300-453°K for a librational mode (ν_R).

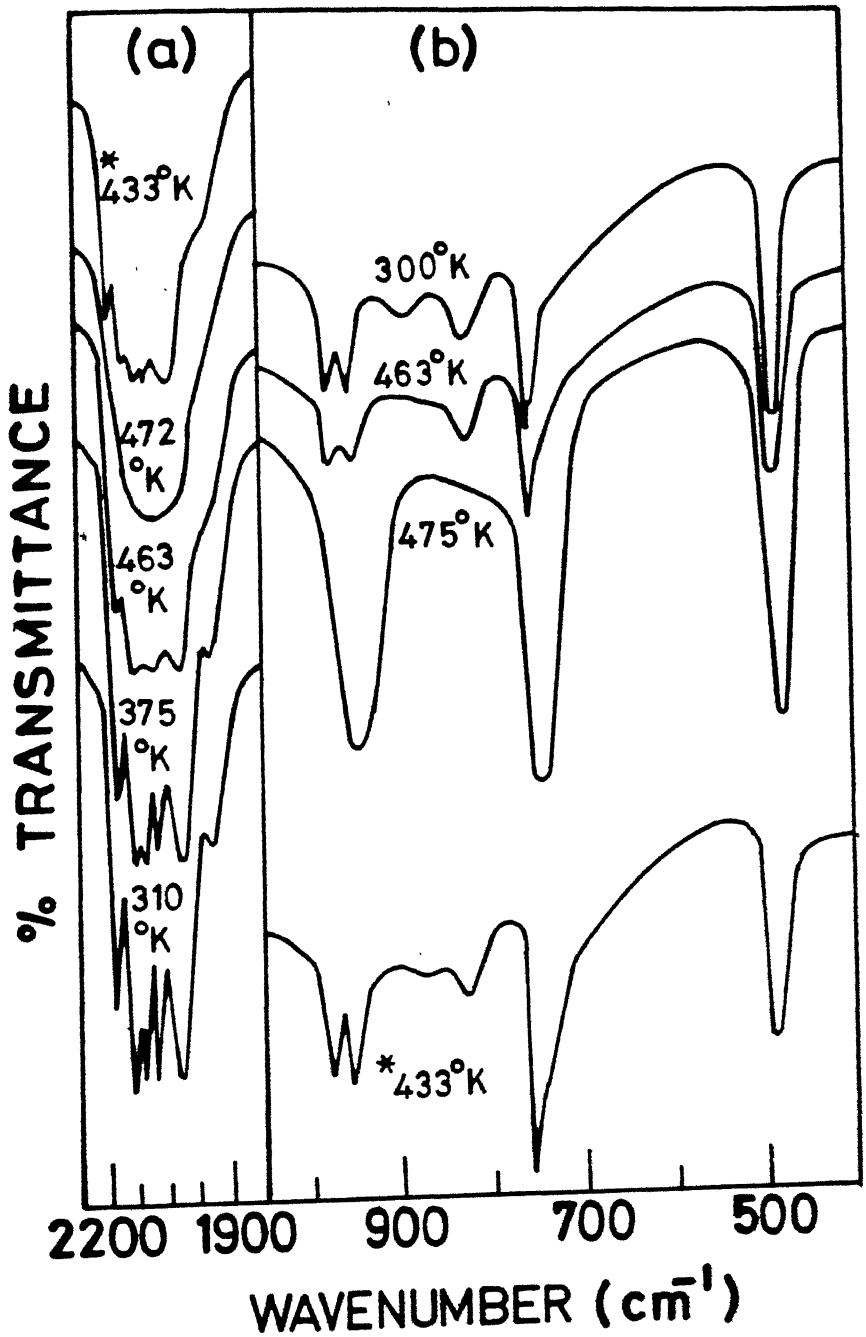

Figure 3.7: Temperature dependence of IR spectra in (a) C-N stretching (1850-2300 cm^{-1}) region and (b) 400-1050 cm^{-1} region. The spectra at 433°K (marked with an asterisk(*)) correspond to the data obtained during the cooling cycle.

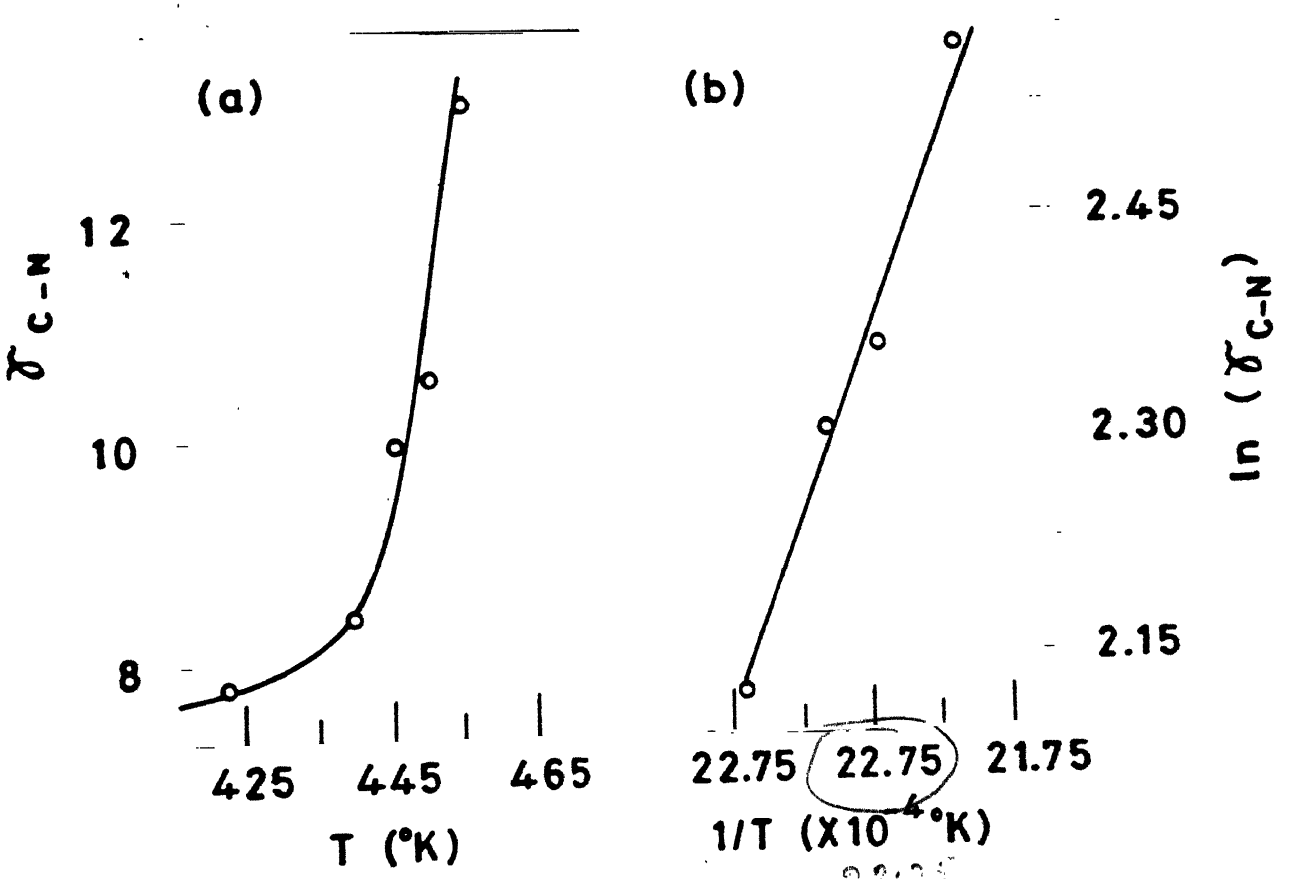

Figure 3.8: Exponential increase in the bandwidth (γ_{C-N}) of ν_{C-N} = 2040 cm^{-1} (Raman) mode. (a) γ_{C-N} versus T and (b) ln (γ_{C-N}) versus 1/T for 425 < to T ≤ 455°K.

CHAPTER 4

TEMPORAL OSCILLATIONS IN THE SCATTERED LIGHT IN CsNCS SINGLE CRYSTAL NEAR THE STRUCTURAL PHASE TRANSITION TEMPERATURE

Abstract :

Temporal oscillations and cascade of period doublings in the oscillatory scattered light were observed as a function of time, when CsNCS crystals were kept stable near the structural phase transition (SPT)* temperatures and irradiated by focussed beams of constant laser powers. From the striking similarities between the observed phenomena and period doubling bifurcations, different oscillatory regions in CsNCS crystal have been related to successive instabilities, as some internal parameter of the system changes with time in a self controlled manner. Considering thermal and photo-induced changes as the major sources, probable nonlinear interaction mechanisms for the observed phenomena have been proposed.

Publications based on the material contained in this chapter are the following :

[A] S Sathaiah, V.N. Sarin and H.D. Bist, Phys Lett. A 140 (6), 348-354(1989)

[B] H.D. Bist, S. Sathaiah and V.N. Sarin, in "Recent trends in Raman spectroscopy" eds.S.B. Banerjee and S.S. Jha (World Scientific, Singapore, 1989) p 340-361

4.1. Introduction

The chaotic behaviour of nonlinear systems has attracted considerable attention in recent years [1-3]. The term chaotic, in the modern literature, represents non-periodic behaviour that arises from the nonlinear nature of the deterministic systems [4]. Recently, experiments on various physical, chemical and biological systems have shown the existence and similarities of the patterns in their chaotic behaviour (i.e. organization of chaos in universal ways) [5]. One thoroughly analysed universal pattern is known as the period doubling route to chaos. Experimentally, diverse nonlinear systems have been found to exhibit the charecteristic behaviour associated with this route [6]. There are striking analogies between pattern formations in the nonlinear systems (far from thermal equilibrium) and phase transitions of systems in thermal equilibrium [7]. In addition there exist a few examples of pattern formations near phase transitions e.g. ,dendritic growth, during liquid to solid transition [8], phase locking and period doubling bifurcations in driven nonlinear crystal oscillators (Rochelle salt [9] , KDP [10]) near their ferroelectric to paralelectric phase transition points. On the other hand recently there has been a great interest in the light induced structural transitions and oscillatory instabilities [11-14]. The present chapter reports on the experimental observation of temporal oscillatory instabilities in the intensity of the light scattered from caesium thiocyanate (CsNCS) single crystal for constant incident laser intensities near the structural phase transition

temperature (T_c) . This oscillatory behaviour looks strikingly similar to the above mentioned, period doubling route to chaos which occurs in many nonlinear systems as some parameter involved is varied. On the basis of experimental results probable mechanisms for the observed phenomena have been proposed.

CsNCS is a typical ionic crystal which has an ordered orthorhombic structure at room temperature (RT). Between 470°K and melting point (≃ 480°K) it crystallizes in a CsCl like cubic structure [15]. As described in the previous chapter the temperature dependence of Raman and Infrared spectra of CsNCS sample revealed the order-disorder and first order nature of the (orthorhombic-cubic) equilibrium SPT [16]. In the course of those studies no temporal oscillations were observed. The present chapter reports on the occurrence of oscillatory scattering in CsNCS single crystal under special experimental conditions. The comparision of the Raman spectral changes in the single crystal with the data on the polycrystalline samples for temperatures above RT is also presented.

4.2. Experimental

Extra pure CsNCS sample from K and K laboratories had been further purified by recrystallizing thrice from its saturated aqueous solutions. On slow evaporation of saturated aqueous solution flat plate like transparent crystals with well developed (001) planes were obtained. For high temperature measurements, CsNCS single crystal was positioned

in the high temperature cell. A linearly polarised 514.5 nm radiation from Argon ion laser was focussed normal to the (001) planes of the crystal. The Raman scattered light was collected in the usual 90° geometry. Spex Ramalog system consisting of a lasermate (to get rid of the plasma lines), a UVISIR sample compartment, a 1403 double monochromator, a thermoelectrically chilled photomultiplier (C-31034) and a photon counting system in conjunction with a compudrive and a linear chart recorder provided automatic recording of the Raman spectra. Specac temperature controller and a copper-constantan thermocouple in touch with the crystal were used to measure the sample temperatures with an accuracy of $\pm 1^{\circ}K$. The details of the instrument are same as described in chapter 2.

4.3. Results and Discussion

Unpolarized Raman spectra of CsNCS single crystal were recorded at various sample temperatures between 300-435°K. The average heating rate and the laser power employed at the sample were $0.25^{\circ}K\ min^{-1}$ and 100 mW, respectively. Typical changes in the lattice mode region of CsNCS single crystal are given in Figure 4.1(b). For comparison, temperature variations in the Raman spectra of polycrystalline sample (data obtained with an average heating rate of $0.4^{\circ}K\ min^{-1}$ and incident power 70 mW), which found to be consistent with order-disorder transition, are given in Figure 4.1(a). It can be seen that until 430°K all the spectral changes in CsNCS single crystal are consistent with data on polycrystalline sample. By maintaining the crystal at constant temperature 431°K and irradiating it continuously for two

hours the complete lattice mode region was replaced by a large number of regularly spaced oscillations as shown in Figure 4.2. These oscillations persisted for about 55 mts. At slightly higher ($\simeq 2^{o}K$) sample temperatures the regular oscillations became irregular, finally a broad band noise like spectrum (well above the instrumental noise) was seen. The experiment was repeated with another fresh CsNCS crystal with reduced incident laser power (45 mW) and the average heating rate ($0.23^{o}K\ min^{-1}$), keeping all other conditions same as in the first experiment. Results obtained were also exactly similar to the first experiment except that the oscillations started at $454^{o}K$ instead of $431^{o}K$. The recorded oscillations near C-N stretching region ($2000\ cm^{-1}$) around the temperature $454^{o}K$ are shown in Figure 4.3.

Typical changes in the C-N stretching modes (ν_{C-N}) with temperature in polycrystalline and single crystal samples are summarized in Figure 4.4 (a) and (b) respectively, for the purpose of comparison. In both the single crystal studies, peak intensities of C-N stretching modes dropped discontinuously to zero at the temperatures where the oscillatory scattering first appeared. Figure 4. 5(b) and (c) show the typical changes in the peak intensities of $\nu_{C-N} \simeq 2042\ cm^{-1}$ modes near the temperatures of oscillatory scattering. These can be compared with CsNCS polycrystalline data (Figure 4. 5(a)) in the vicinity of order-disorder transition where the peak intensity of $\nu_{C-N} \simeq 2042\ cm^{-1}$ mode decreased continuously to zero, finally a new broad band $2059\ cm^{-1}$ (Figure 4.4(a)) characteristic of high temperature disordered cubic phase

appeared. Variations in the background intensities with temperature are plotted in Figure 4.6, for all the polycrystalline (I,II & III) and single crystal (IV & V) Raman measurements.

4.3.1 Period Doubling Behaviour

By changing the recording (chart) speeds, proportional variations in linewidths (Figure 4.7 (a)) and peak to peak separations of the oscillatory modes were noticed. It's well known that the bandwidths and peak seperations of Raman modes (in general, any spectral line) don't vary with scanning speeds as along as the modes are time independent (Figure 4.7(b)). Peak seperations were also observed to vary by repeated scanning of a fixed wave number region at different instants of time. One should not have observed such variations, if the recorded spectra really had oscillations in the frequency domain. Additionally oscillations in the intensity were observed to persist even by turning off the spectrometer at any wave number. Figure 4.8 shows the typical temporal oscillations recorded at $T = 437^{o}K$, by turning off the spectrometer drive at $\nu \simeq 2000\ cm^{-1}$, in the third experiment (with an average heating rate $0.3^{o}K\ min^{-1}$ and incident power 45 mW). Although this experiment gave direct evidence for the temporal behaviour, different periodic oscillatory regions were not seen due to poor temperature control at $T = 437^{o}K$. So, the only better experimental results (Figure 4.2) among all the data have been analysed here. Since the oscillatory modes (in Figures 4.2 & 4.3) have been identified to be real time oscillations in the scattered intensity, the recorded scale had been converted to the intesity versus time scale using the following conversion relation :

$$\text{Time-chart scale (sec/cm)} = \frac{\text{wave number chart scale } (cm^{-1}/cm).}{\text{chart speed } (cm^{-1}/sec)}$$

In Figure 4.2, the converted time scale (in 10^2 sec, scale on the top) versus the intensity of scattered light in the lattice mode region is shown. One expects a flat broad band spectra as in polycrystalline data Figure 4.1(a) characteristic of disordering of the lattice, near T_c. Instead, time dependent intensity oscillations superimposed on the flat Rayleigh wing can be clearly seen at $T = 431^{\circ}K$. Let $t = 0$ be the initial time at which periodic oscillations with an average period $\tau_1 = 20 \pm 4$ sec ($\pm\sigma$ sec is the standard deviation) first appeared. A very striking feature was that the observed oscillations with initial period τ_1 were stable only upto $t = 4\times10^2$ sec. For $t \geq 4\times10^2$ sec another series of oscillations with a modulated period of $\tau_2 = 49\pm4$ sec ($\simeq 2\ \tau_1$) appeared. The period τ_2 remained constant for some time and at $t = 14\times10^2$ sec it got doubled again i.e. oscillations with period $\tau_3 = 101\pm5$ sec ($\simeq 2\ \tau_2$) appeared. These τ_3 periodic oscillations became unstable at $t = 20\times10^2$ sec and gave rise to another series of oscillations with $\tau_4 = 20\pm3$ sec ($\simeq \tau_1$). Again these remained stable for some more time, finally for $t \geq 29\times10^2$ sec broad band noise like irregular temporal oscillations were seen. In Figure 4.2 only a small portion of the observed irregular oscillatory region is shown. Additionally, period doubling was observed to produce higher

period modulation of the original period. This may not clearly be seen in Figure 4.2 due to merging of original periodic oscillations in the wings of higher period modulations and limited observable resolution in the final reproduction of the data. The cascade of period doublings (within experimental accuracies) and coming back to initial period of oscillatory scattered light with respect to time are summarized in Figure 4.9(b). Similar temporal oscillations were found in the second experiment but evidently due to their appearance at higher sample temperatures (viz. more thermal fluctuations; also the sample temperature was not maintained stable for longer durations as in the first experiment), the complete cascade was not seen (Figure 4.9(a) and Figure4.3).

Spurious oscillatory phenomena such as incident laser oscillations, oscillations due to switching devices and photomultiplier instabilities have been ruled out by doing same experiments under similar experimental conditions on other crystalline materials which do not exhibit this oscillatory behaviour. For the better understanding of the phenomena, the following experiments were performed. Once the oscillatory behaviour was set in, we shifted the irradiation spot to some other point on the crystal, then the oscillations were not seen, instead we were able to record the Raman spectrum which was consistent with the corresponding spectrum of CsNCS polycrystalline sample at that temperature (456^{o}K in {Figure 44(a) and (b)}. This implies that some changes (probably photoinduced) had taken place in the crystal and gave rise to

some sort of instabilities localized at the irradiated spot. The occurrence of these instabilities above a particular temperature depends on the total time of irradiation and laser power employed at the sample. However keeping CsNCS crystal at room temperature and irradiating it for longer times upto 14 hrs (more than the effective irradiation times of the two earlier high temperature experiments), oscillatory behaviour was not found. In fact the scattered intensity was observed to remain constant as shown in Figure 4.10 even after such a long time irradiation of the crystal. By irradiating the sample with larger power $\geq$ 140 mW, the crystal got burnt but there were no oscillations in the scattered light. Figure 4.11 gives the details of the rates of heatings in different experiments on polycrystalline {Figure 4.11(a)} and single crystal {Figure 4.11(b)and (c)}samples. It is very clear that to observe oscillatory instabilities, the sample has to be kept at stable temperature well below T_c, then very slow rates of heating {Figure 4.11(c)} are needed to obtain a clear cascade. All these observations indicate that the oscillatory phenomena is due to the combined effects of photoinduced and thermal changes occurring at the irradiated spot of the crystal.

The well organised temporal oscillations in the intensity of the scattered light for constant incident laser powers, tempted us to conclude that these periodic oscillatory regions may probably be associated with successive instabilities as some internal parameter of the system changes with time in a

self-controlled manner. This looks strikingly similar to the period doubling route to chaos [5] which occurs in diverse nonlinear physical, chemical and biological systems as some parameter involved is varied. To explain the oscillatory instabilities one has to consider the possible nonlinear interaction mechanisms between the laser field and CsNCS single crystal. Here we suggest that there are two types of such mechanisms that may be important sources of the observed phenomena.

4.3.1.a Instabilities associated with Structural and Photothermal Changes

Recent neutron diffraction studies on CsNCS crystal [17,18] revealed anomalous large increase in the mean square displacements of both Cs^+ and NCS^- ions for temperatures above 440^oK and less than T_c (Figure 4.12). Due to these large displacements of the ions the restoring forces may become strongly nonlinear. In turn, the optical response of the CsNCS system may also become nonlinear. In other words, optical constants like refractive index (n) may become nonlinear function of T, near T_c. In fact there are a few systems known to exhibit optical nonlinearities near their phase transition temperatures [11,19-21]. Additionally, there are reports on the observations of phase locking and period doubling bifurcations which characterise the low frequency nonlinear responses of the driven crystal oscillators e.g. Rochelle Salt [9] , KDP [10] near their ferroelectric phase transition temperatures. The observed oscillatory phenomena in CsNCS

crystal may be related to the instabilities associated with enhanced optical nonlinearities near its structural phase transition temperature. We believe structural changes including local photothermal changes in the irradiated spot play a dominant role in the observed phenomena. As described in the previous section to observe oscillatory instabilities sample should be kept at stable temperature well below T_c for longer durations ($\simeq$ 2 hrs) and very slow rates of heating are needed to observe the clear cascade. This could be achieved by local heating due to focussed beam of $\simeq$ 100 mW laser power and can be understood in the following way. As CsNCS crystal is poor thermal conductor, the laser beam produces a significant local temperature rise in the illuminated spot. As a result the complex refractive index n, in particular, the absorption coefficient α (i.e. imaginary part of complex n) may increase and enhance the dissipation of laser field in the sample. Thus local temperature rises further and the continuation of this process may result in local temperature distribution which becomes strongly T dependent near T_c. This temperature profile gives rise to refractive index (real n) gradient which can defocus the laser beam. As a result local heating in the spot reduces and spot temperature decreases slowly with time until uniform T is achieved. When the laser beam attains its original convergence, the local temperature rises again, and this may continue as a cyclic process under appropriate conditions of heat dissipation and conduction which govern the time dependence of the spot temperature. Once

crystal may be related to the instabilities associated with enhanced optical nonlinearities near its structural phase transition temperature. We believe structural changes including local photothermal changes in the irradiated spot play a dominant role in the observed phenomena. As described in the previous section to observe oscillatory instabilities sample should be kept at stable temperature well below T_c for longer durations ($\simeq$ 2 hrs) and very slow rates of heating are needed to observe the clear cascade. This could be achieved by local heating due to focussed beam of $\simeq$ 100 mW laser power and can be understood in the following way. As CsNCS crystal is poor thermal conductor, the laser beam produces a significant local temperature rise in the illuminated spot. As a result the complex refractive index n, in particular, the absorption coefficient α (i.e. imaginary part of complex n) may increase and enhance the dissipation of laser field in the sample. Thus local temperature rises further and the continuation of this process may result in local temperature distribution which becomes strongly T dependent near T_c. This temperature profile gives rise to refractive index (real n) gradient which can defocus the laser beam. As a result local heating in the spot reduces and spot temperature decreases slowly with time until uniform T is achieved. When the laser beam attains its original convergence, the local temperature rises again, and this may continue as a cyclic process under appropriate conditions of heat dissipation and conduction which govern the time dependence of the spot temperature. Once

there is a nonlinear optical response which probably occurs due to large displacements of ions near T_c, the above mentioned feed back mechanism between T dependence of optical constants and the enhancement of local temperature can give rise to a highly nonlinear behaviour of the optical characteristics of CsNCS crystal and may produce oscillatory instabilities in the scattered light intensity in a controlled way. More detailed observations of nonlinear dynamical responses in CsNCS near T_c, may provide deeper insight into the correlation between nonlinearity and phase transition dynamics.

4.3.1.b Photo Chemical Instabilities

Another possible mechanism for the observed phenomena may be related to instabilities in solid state photochemical reactions. Probably, some photo-reactions might have taken place in the illuminated region above a particular temperature (near SPT) depending on the laser power and time of irradiation. By keeping the sample stable at this temperature, varying the spot temperature very slowly with the help of focussed laser beam, successive instabilities in the photochemical reactions might have occurred and exhibited temporal oscillations and bifurcation sequence in colour (or fluorescence). In fact there are many oscillatory chemical reactions (liquid phase) known to exist [22]. Interestingly some of these chemical reactions show period doubling bifurcations, B.Z reaction [23] is the one thoroughly studied among these. Additionally, there are reports on oscillatory reactions between thiocyanates and H_2O_2 [24],

bromate and thiocyanates [25] showing different types of bistabilities and bifurcation sequence. On these lines one can qualitatively say that oscillatory photochemical reactions (solid state) exhibiting temporal oscillations in colour (or fluorescence), may be responsible for the oscillatory scattering in CsNCS crystal. One of the possibilities is that the photoreactions may produce sulfer S_8, and then the polymerization of S_8 at $T=433^{o}$ K [26] into different allotropes may be responsible for the observed oscillatory scattering. But this posibility has been ruled out by performing temperature dependent Raman scattering measurements on the polymerization of S_8 crystal [27].

More experiments are needed to understand clearly the mechanisms involved and to find out the parameters which control the stability of the periodic oscillations in the present system. Further work is planned to obtain well controlled experimental time series data for quantitative analysis(e.g. to construct phase portraits, Poincare sections and return maps; to calculate the largest Layapunov exponents, universal numbers and so on.)

Finally, it should be emphasized that the observed temporal oscillatory scattering near SPT in CsNCS is first of its kind. In order to explain all the observations quantitatively, a theoretical model is needed which takes into account the combined effects of structural and photoinduced changes on the optical characteristics of CsNCS crystal.Additionally,the changes in the Raman scattered intensity with incident power (Figure 4.13) indicate the importance of photo-induced effects (in CsNCS crystal)even at room temperature.

References

[1] F. Heslot, B. Castaing and A. Libchaber, Phys. Rev. A. 36 5870 (1987).

[2] See for example for the following collections of articles: "Quantum measurement and chaos", eds. E.R. Pike and Sarben Sarker, NATO ASI Series B 161 (Plenum, New York 1987); Physica 23D, 1-482 (1987); "Optical chaos", eds. J. Chrostowski and N.B. Abraham, Proc. SPIE 667 (1986)

[3] F. Argoul, A. Arneodo, P. Richetti, J.C. Roux and H.L. Swinney, Acc. Chem. Res. 20, 436 (1987) and ref. therein.

[4] H.G. Schuster, "Deterministic Chaos", (Physik-Verlag, Weinheim, 1984); P. Berge, Y. Pomeau and C. Vidal, "Order within chaos", (Wiley, New York, 1986).

[5] P. Cvitanovic, ed. Universality in chaos (Hilger, Bristol, 1984); H. Haken, "Advanced Synergetics" (Springer-Verlag, Berlin, 1983).

[6] P. Cvitanovic, in: "Optical instabilities", eds. R.W. Boyd, M.G. Raymer and L.M. Narducci (Cambridge University Press, England, 1986) p. 151.

[7] J.F. Scott, in "Frontiers of Nonequilibrium statistical physics", eds. G.T. Moore and M.O. Scully, NATO ASI Series B135 (Plenum New York, 1986) p. 465.

[8] J.S. Langer 309-336; J.H. Bilgram 443-369, in: Nonlinear phenomerna at phase transitions and instabilities, ed. T. Riste,NATO ASI Series B 77 (Plenum, New York, 1982).

[9] J. Jefferies, Phys. Lett. A90(6), 316 (1982).

[10] Jung-Yun Huang and Jong-Jean Kim, Phys. Rev. B34(11),8122 (1986) .

[11] J. Hajto and I. Janossy, Phil. Mag. B47(4), 347 (1983).

[12] S.M. Arakelian and Yu. S. Chillingarian, "Nonlinear Optics of Liquid Crystals" (Nauka, Moscow, 1984).

[13] I. Janossy, M.R., Toglizadch and E. Abraham, in: "Optical Bistability III", eds. H.M. Gibbs, P. Mandel, N.Peyghambarain and S.D. Smith (Springer-Verlag, Berlin Heidelberg, 1986) p. 160.

[14] I. Abdulhalim, R. Beserman and Yu.L.Khait, Euro. Phys. Lett.4(12),1371 (1987) : I. Abdulhalim and R. Beserman, Solid State Commun. 64(6), 951 (1987) and ref. therein.

[15] S. Manolatos, M. Tillinger and B. Post, J. Solid State Chem. 7, 31 (1973) .

[16] S. Sathaiah, V.N. Sarin and H.D. Bist, J. Phys: Cond. Matt., 1,7829-41 (1989).

[17] M.A. Irving, M.M. Elcombe and T.F. Smith, Aust.J. Phys. 38,85 (1985).

[18] B.K. Moss, S.L. Mair, C.J. Meintyre and R.K. Mcmullan, Acta. Cryst. B43,16 (1987).

[19] G.K.L. Wong and Y.R. Shen, Phys. Rev. A19, 1757 (1979).

[20] S.Kh. Esyan, A.V. Kityik and V.V. Lemanov, Sov. Phys. Solid. State 29(5),891 (1987).

[21] K. Uchinokura, T. Inushima, E. Matsuura and A.Okamato, Ferroelectrics, 38,901 (1981).

[22] R.J. Field, M. Burger, eds. Oscillations and Travelling waves in Chemical Systems (Wiley, New York, 1985).

[23] H.L. Swinney, J.C. Roux, in: "Non-equilibrium Dynamics in Chemical Systems", eds. C. Vidal, A. Pacault (Springer-Verlag, Berlin, 1984), pp. 124-140.

[24] M. Orban, J. Am. Chem. Soc.108,6893 (1986).

[25] R.H. Simoyi, J. Phys. Chem.91(6),1557 (1987).

[26] R. Steudel, S.P. Stephan and G. Holdt, Z. Anorg. allg. chem. 517,7-42(1984).

[27] S Sathaiah and H.D. Bist, "Raman Scattering studies of structural phase transition and polymerization in S_8" (to be communicated).

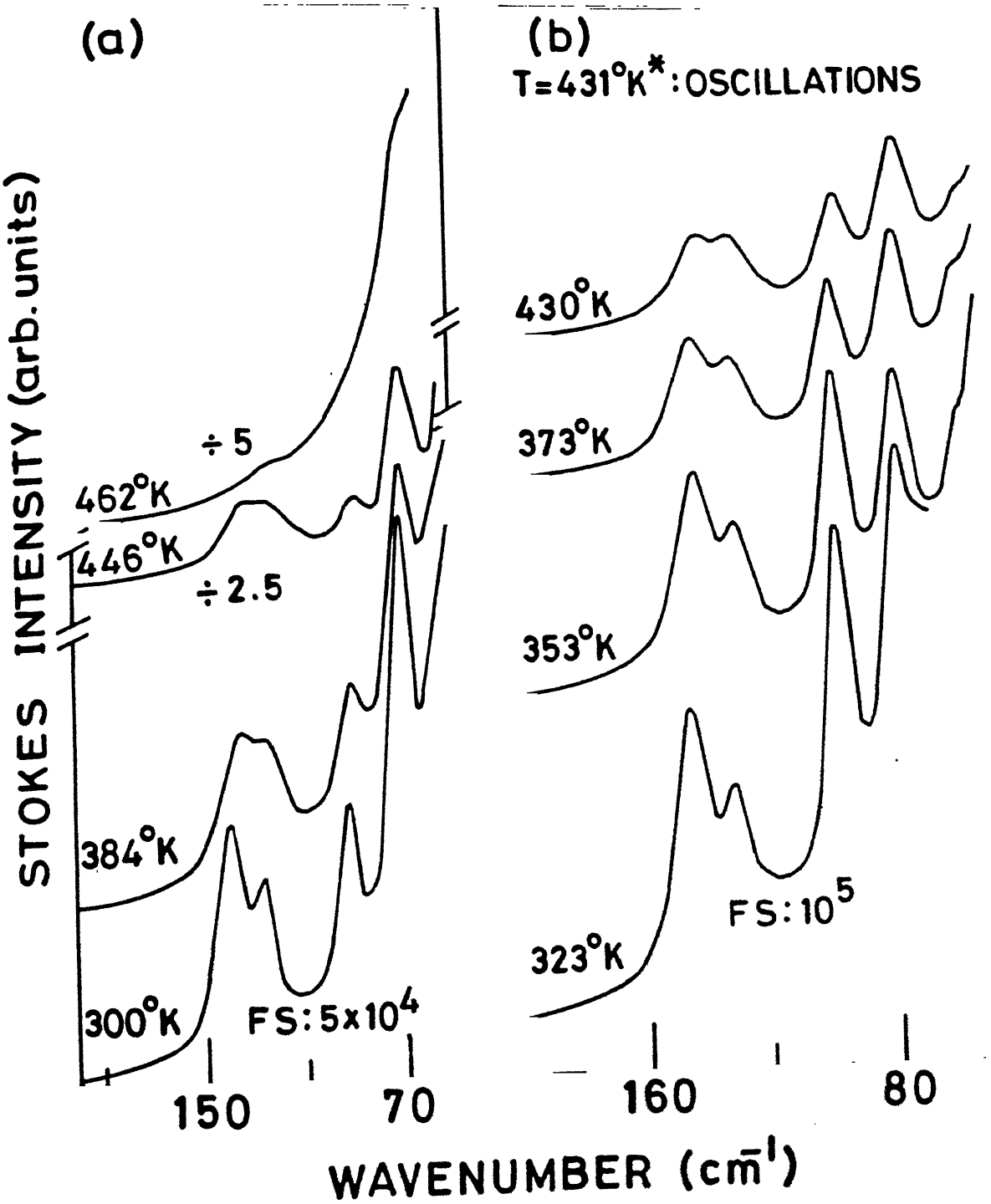

Figure 4.1: Temperature dependence of lattice modes in the depolarized Raman spectra of CsNCS (a) polycrystalline and (b)single crystal samples.[Note that the variations in the lattice modes are consistent with (a), upto 430°K.] * denotes the occurrence of oscillatory scattering (see Figure 4.2) at431°K.

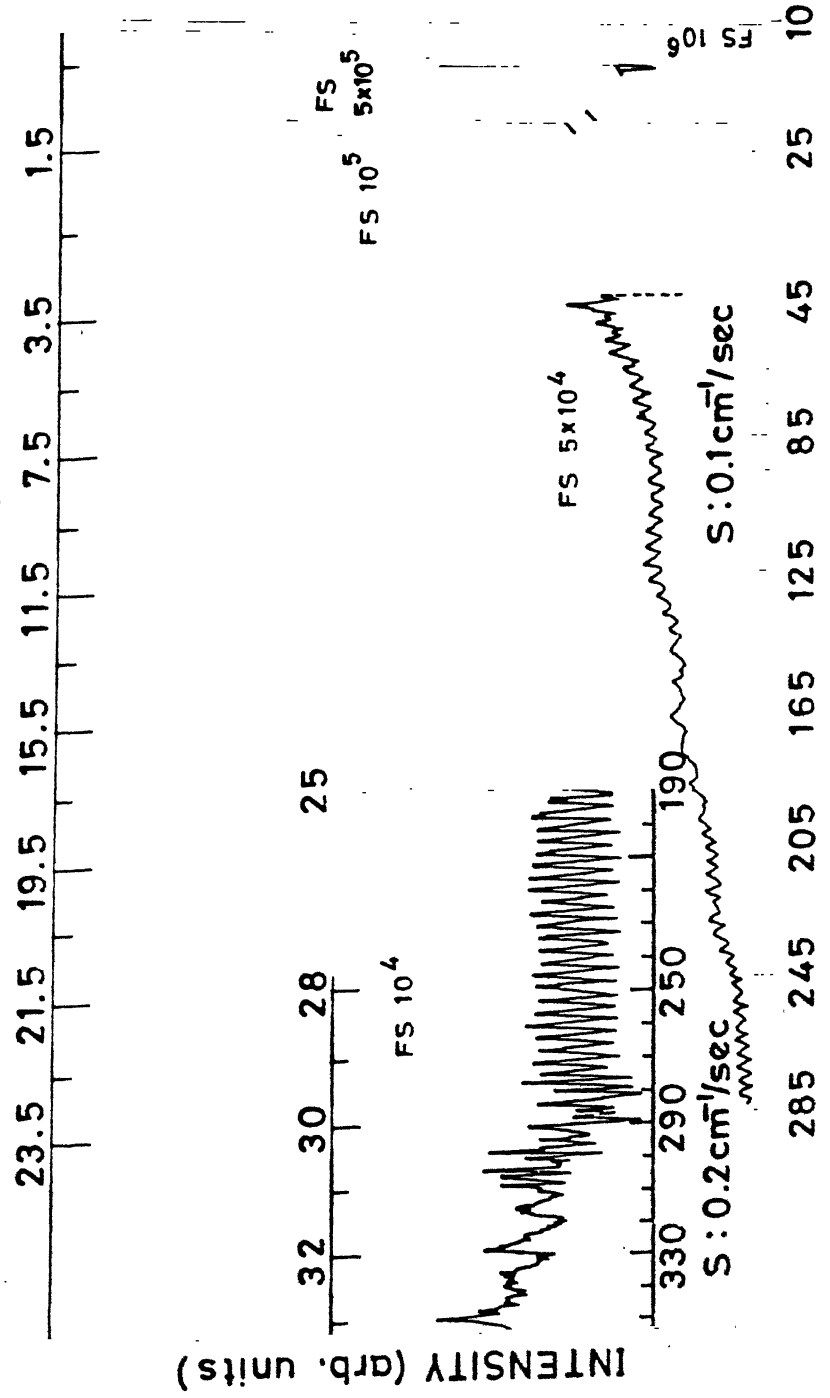

Figure 4.2: Recorded oscillatory scattering in the lattice region, at 431°K. Upper scale corresponds to the real time in seconds. The inset shows the repeated scan of 190-330 cm^{-1} region for $t > 25x10^2$ sec. Notice, the change in the separation between the maxima of two consecutive oscillations (190-205 cm^{-1}) recorded at different times.

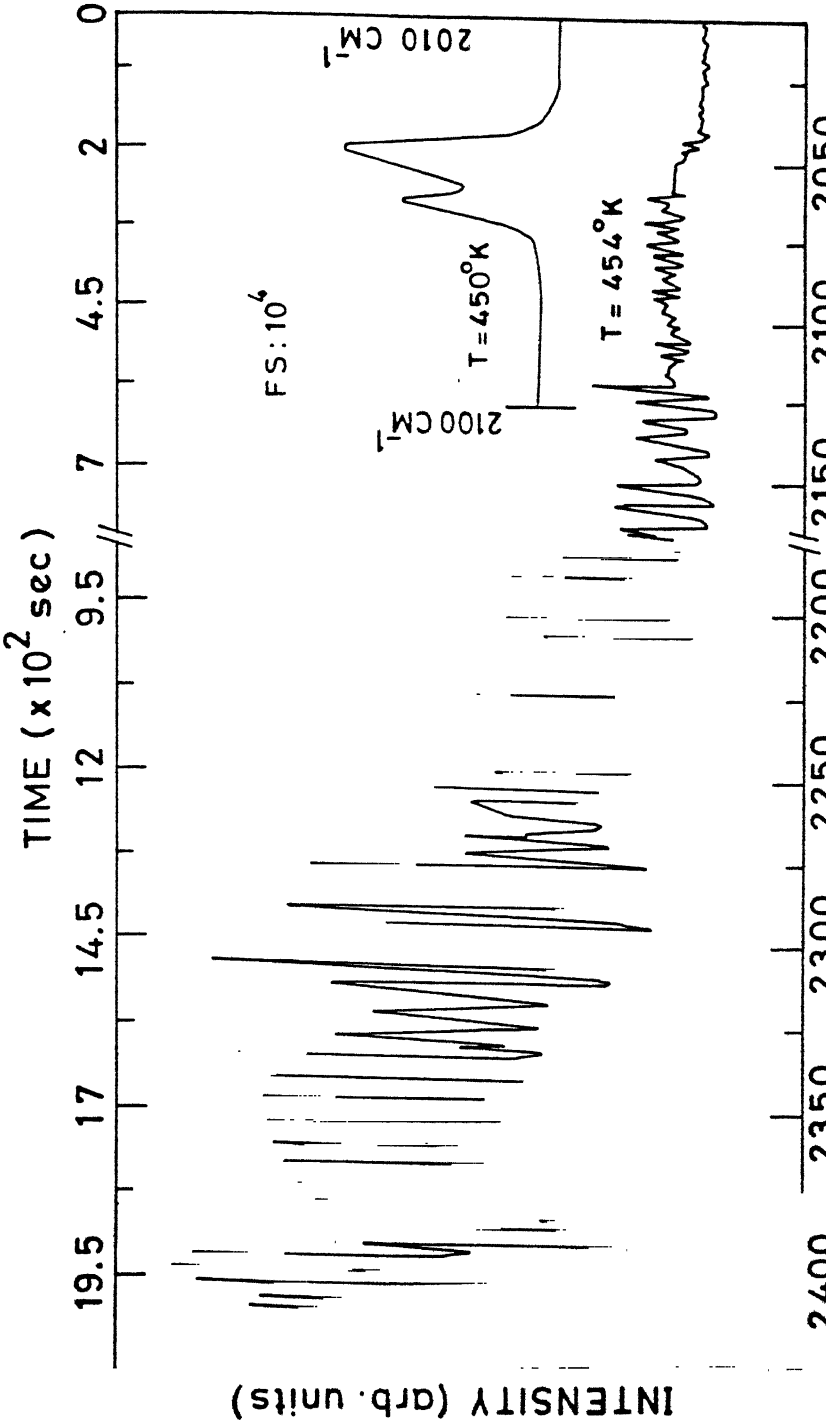

Figure 4.3: Recorded temporal oscillations in the C-N stretching region at temperature T = 454°K. Upper scale corresponds to real time in seconds. In the inset one can clearly see C-N stretching modes (2042, 2053 cm^{-1}), at 450°K.

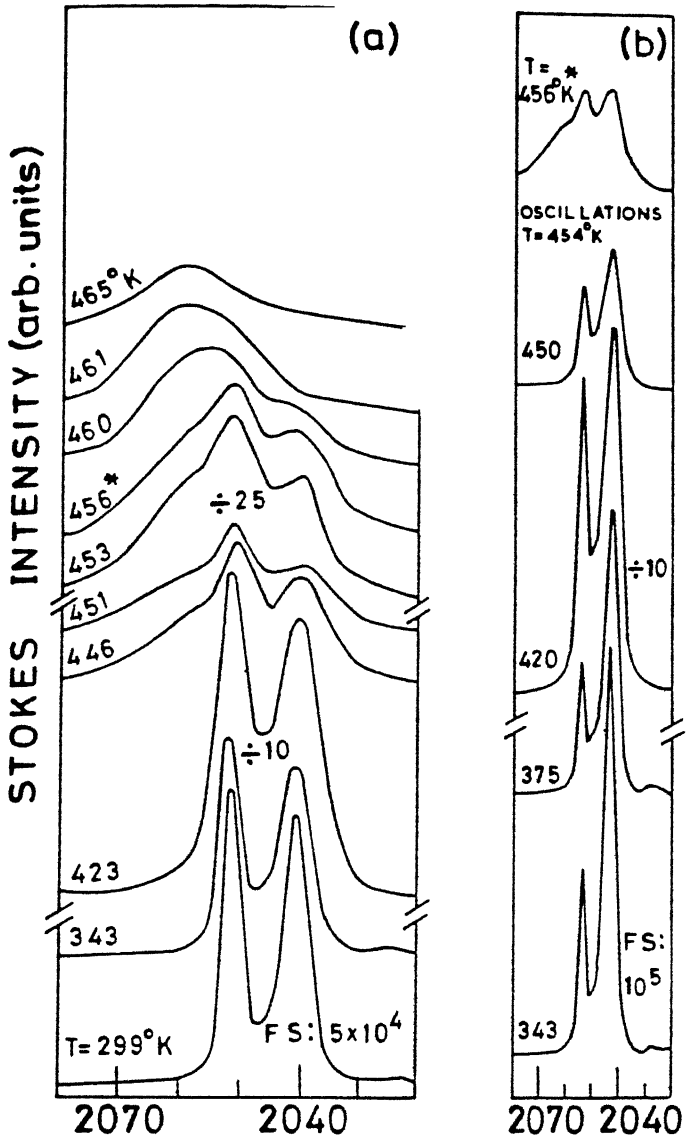

Fig. 4.4

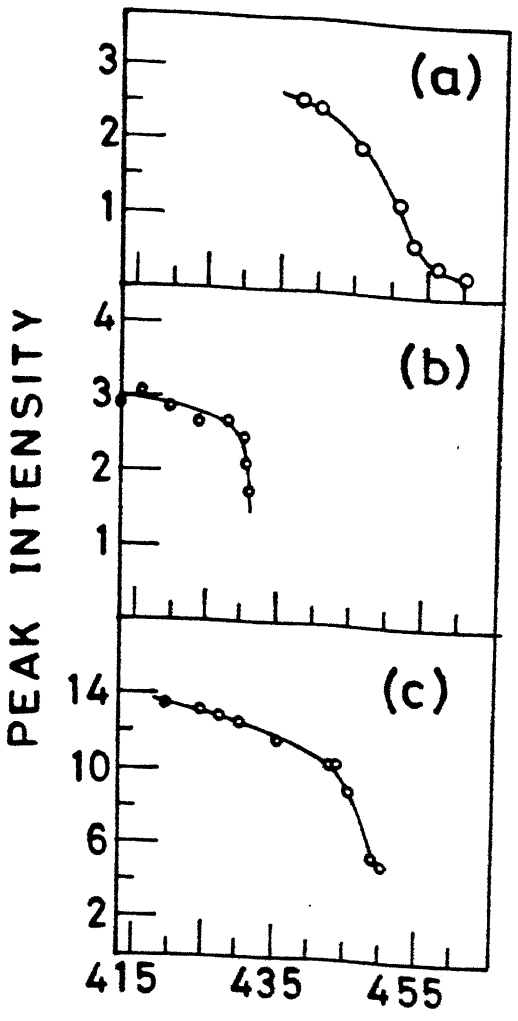

Fig. 4.5

Figure 4.4: Temperature (T) variations of Raman spectra in the C-N stretching region of CsNCS (a) polycrystalline and (b) single crystal: * denotes the spectrum obtained at 456°K by shifting the irradiation spot to some other point in the crystal. It can be compared with the corresponding spectrum denoted by * in (a).

Figure 4.5: Typical changes in the peak intensity of the C-N stretching mode (C-N = 2042 cm^{-1}) of (a) CsNCS polycrystalline sample near the SPT, (b) and (c) CsNCS single crystal in the vicinity of oscillatory scattering temperatures, $T \leq 431^{\circ}K$ and $T \leq 454^{\circ}K$, respectively.

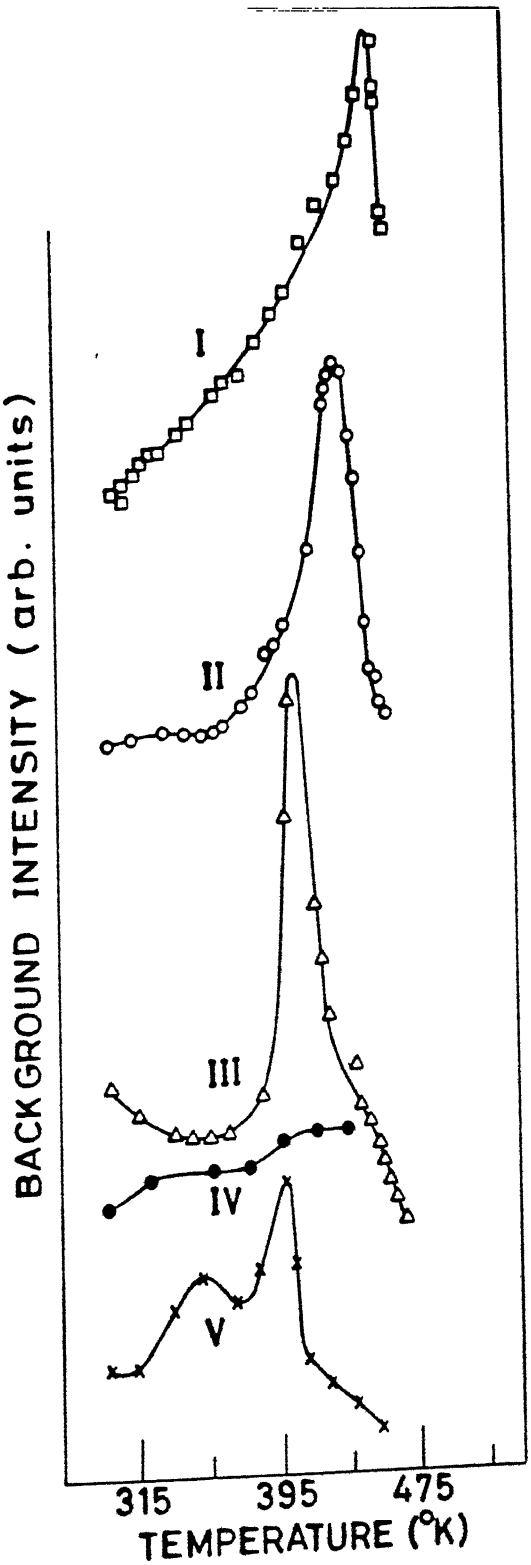

Figure 4.6: Variations in the background scattering ($\nu \simeq 2000$ cm^{-1}) intensities with temperature. Data on the polycrystalline (I, II and III) and single crystal (IV & V) samples with different incident powers, heating rates: (I) 67 mw, 1.5 $^{o}K\ min^{-1}$; (II) 70 mw, $1^{o}K\ min^{-1}$; (III) 70 mw, $0.4^{o}K\ min^{-1}$; (IV) 100 mw, $0.25^{o}K\ min^{-1}$; , and (V) 45 mw, $0.23^{o}K\ min^{-1}$.

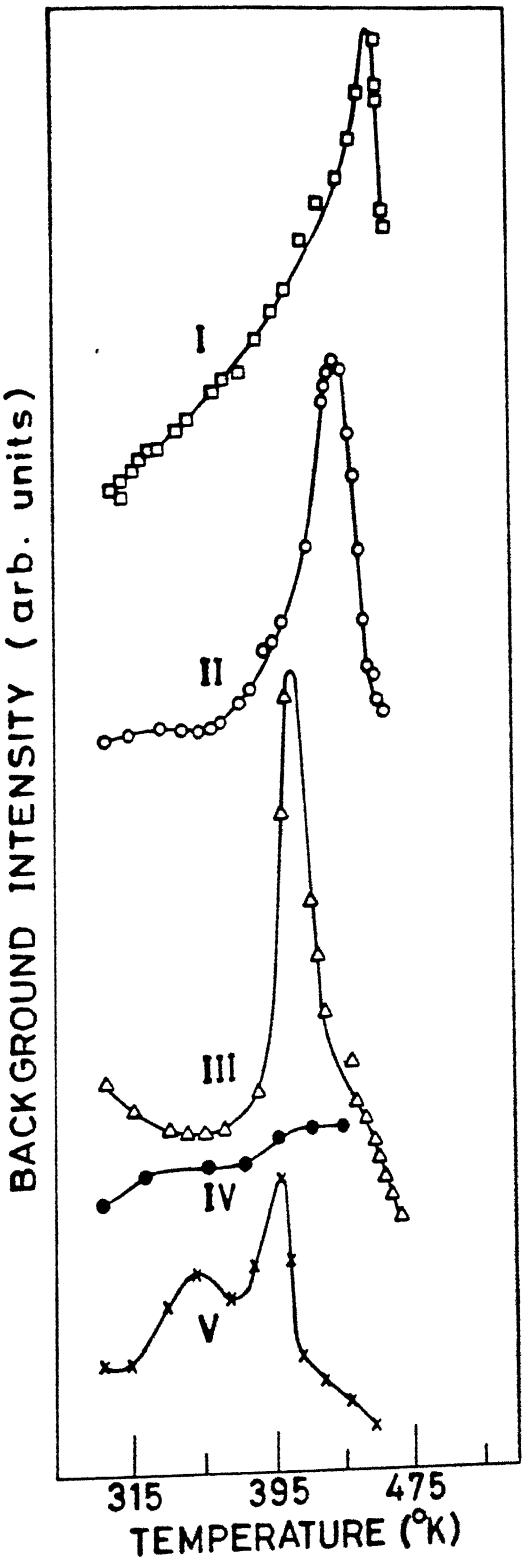

Figure 4.6: Variations in the background scattering ($\nu \simeq 2000$ cm^{-1}) intensities with temperature. Data on the polycrystalline (I,II and III) and single crystal (IV & V) samples with different incident powers, heating rates: (I) 67 mw, 1.5 $^{o}K\ min^{-1}$; (II) 70 mw, $1\ ^{o}K\ min^{-1}$; (III) 70 mw, $0.4\ ^{o}K\ min^{-1}$; (IV) 100 mw, $0.25\ ^{o}K\ min^{-1}$; , and (V) 45 mw, $0.23\ ^{o}K\ min^{-1}$.

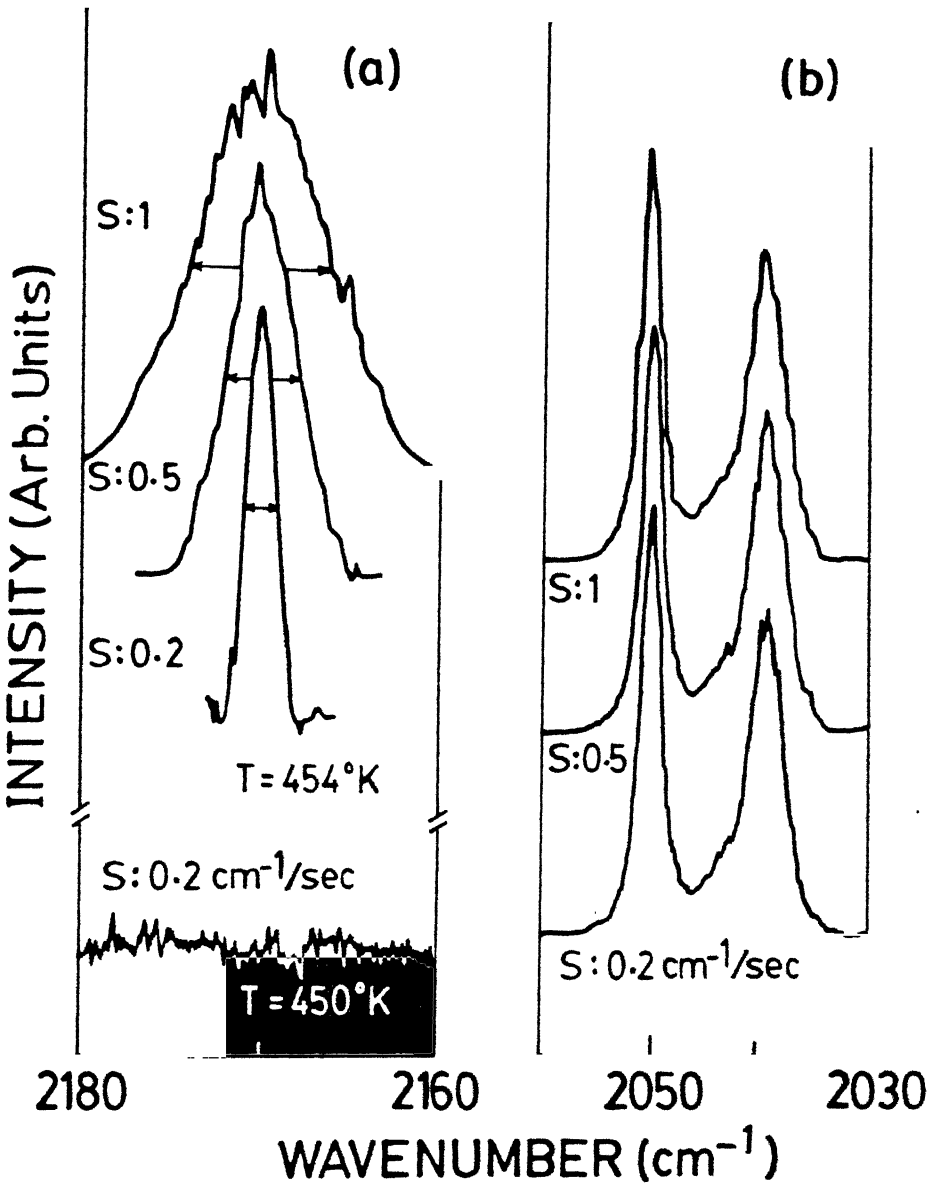

Figure 4.7:(a) Demonstration of temporal behaviour of the oscillatory scattering (at $T=454^{\circ}K$) through the observed variations in linewidths with different scanning speeds: 0.2, 0.5 and $1 cm^{-1}$/sec. Note that in the chosen wavenumber (2160-2180 cm^{-1} region there is only a flat background till $T = 450^{\circ}K$. (b) Raman spectra of CsNCS crystal at $300^{\circ}K$ showing the independence of spectra for different scanning speeds (same as in (a))

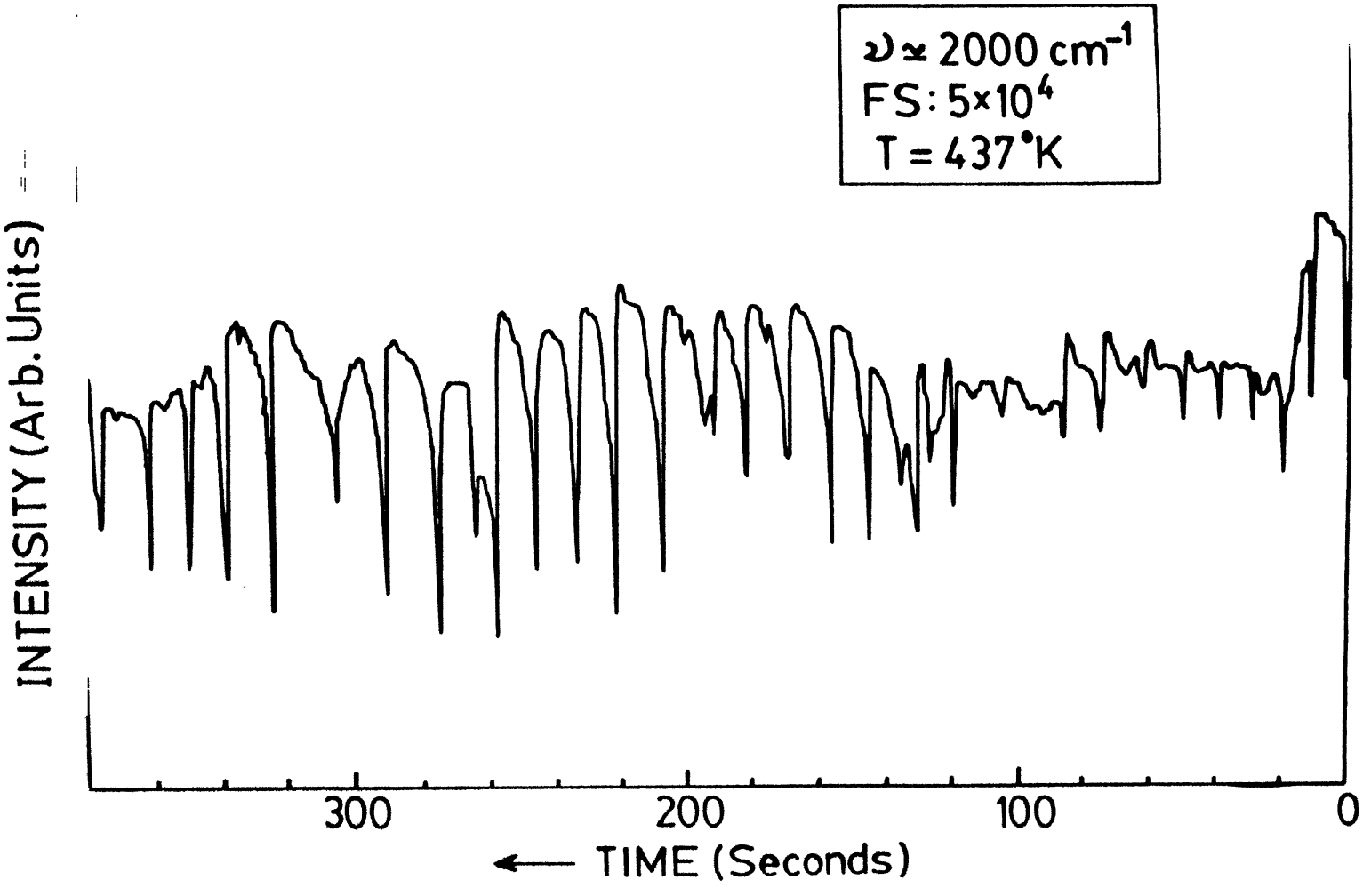

Figure 4.8: Temporal oscillatory scattering recorded (at T= 437°K, in an experiment with the average heating rate 0.3°K min^{-1} and incident power 45mw) by fixing the spectrometer at 17435 cm^{-1} (i.e 2000 cm^{-1} away from the excitation frequency).

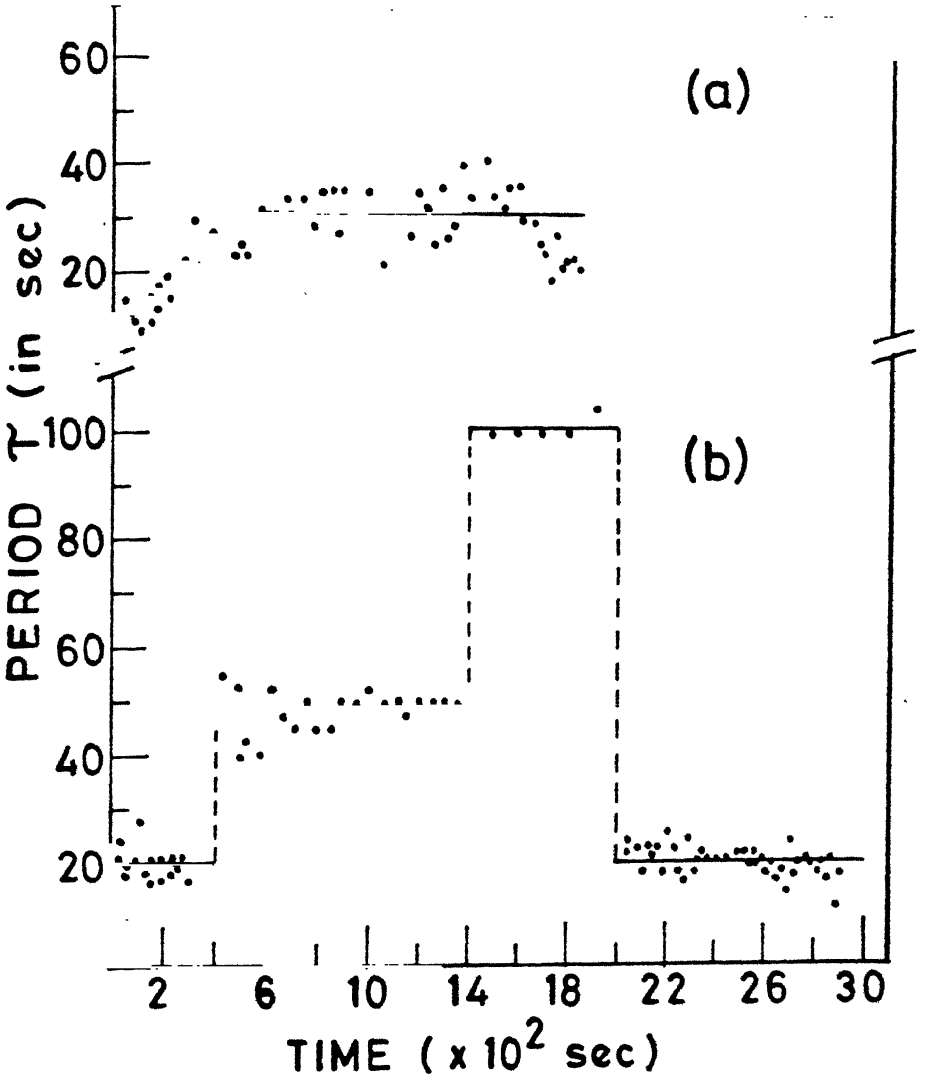

Figure 4.9: Variations in the period (τ) with respect to time for the observed oscillations at different temperatures (a) 454°K and (b) 431°K (see text).

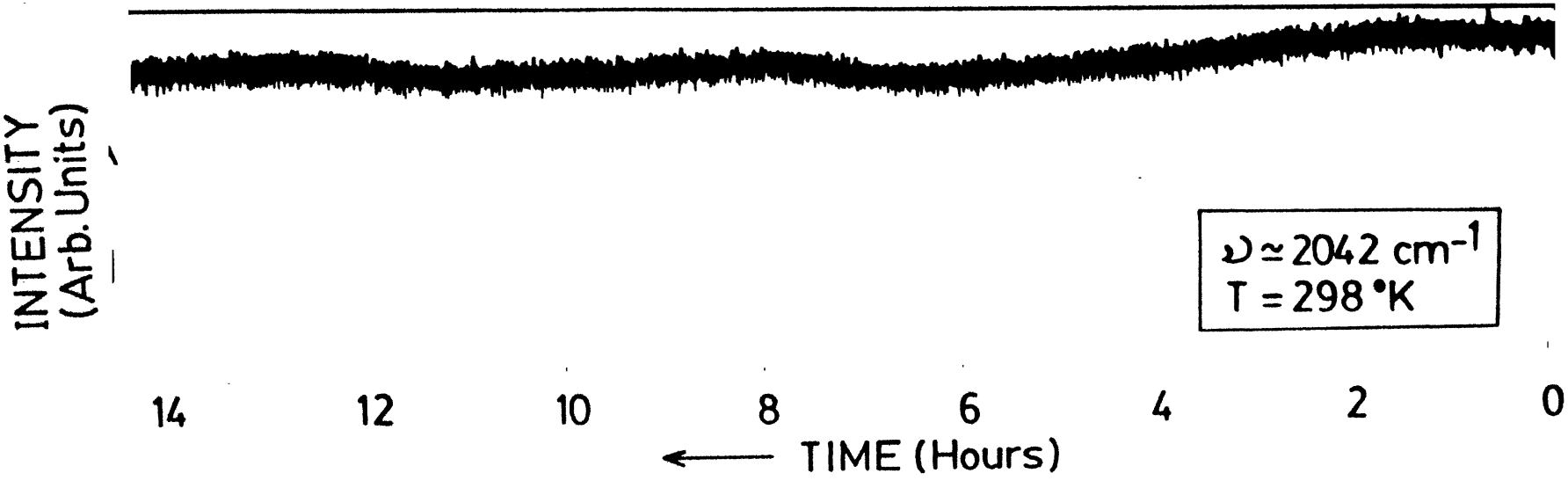

Figure 4.10: Time independence of Raman Scattering ($\nu \simeq 2042 cm^{-1}$) intensity of CsNCS crystal at room temperature.

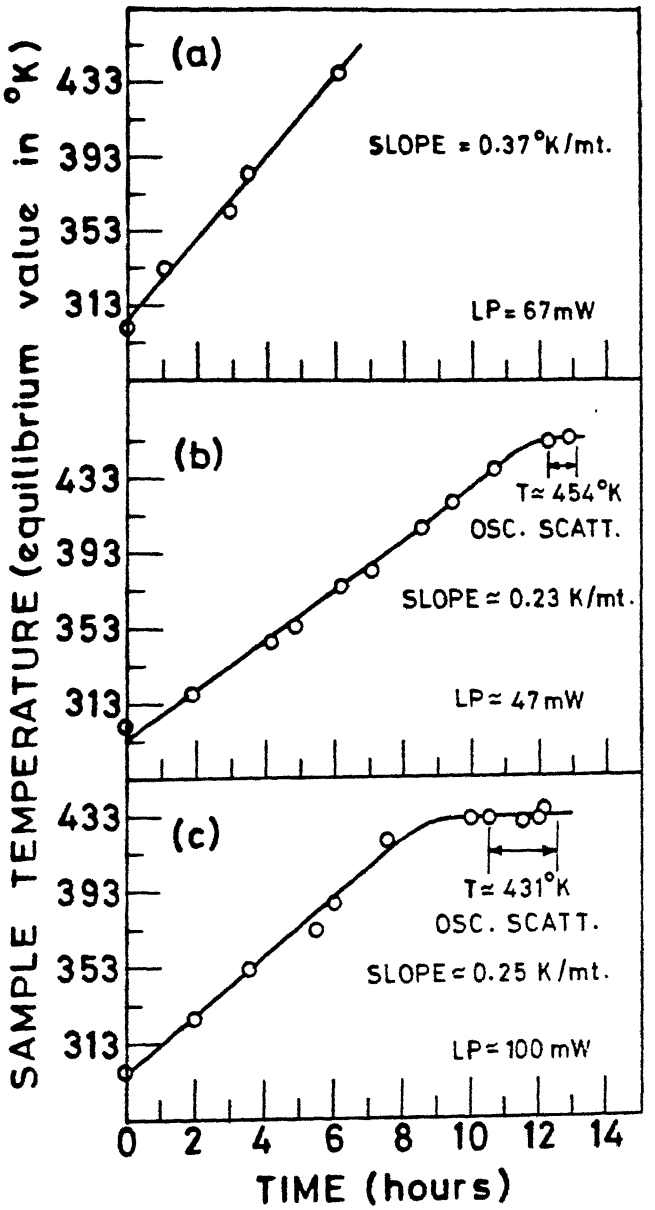

Figure 4.11: Sample temperature (equilibrium value) versus the time taken to attain that value in different scattering experiments on (a) polycrystalline , (b) and (c) single crystal samples. The slopes of curves : 0.37, 0.23 and 0.25°K min^{-1} represent the average heating rates; LP = 67, 47 & 100 mw are the powers employed at the sample.

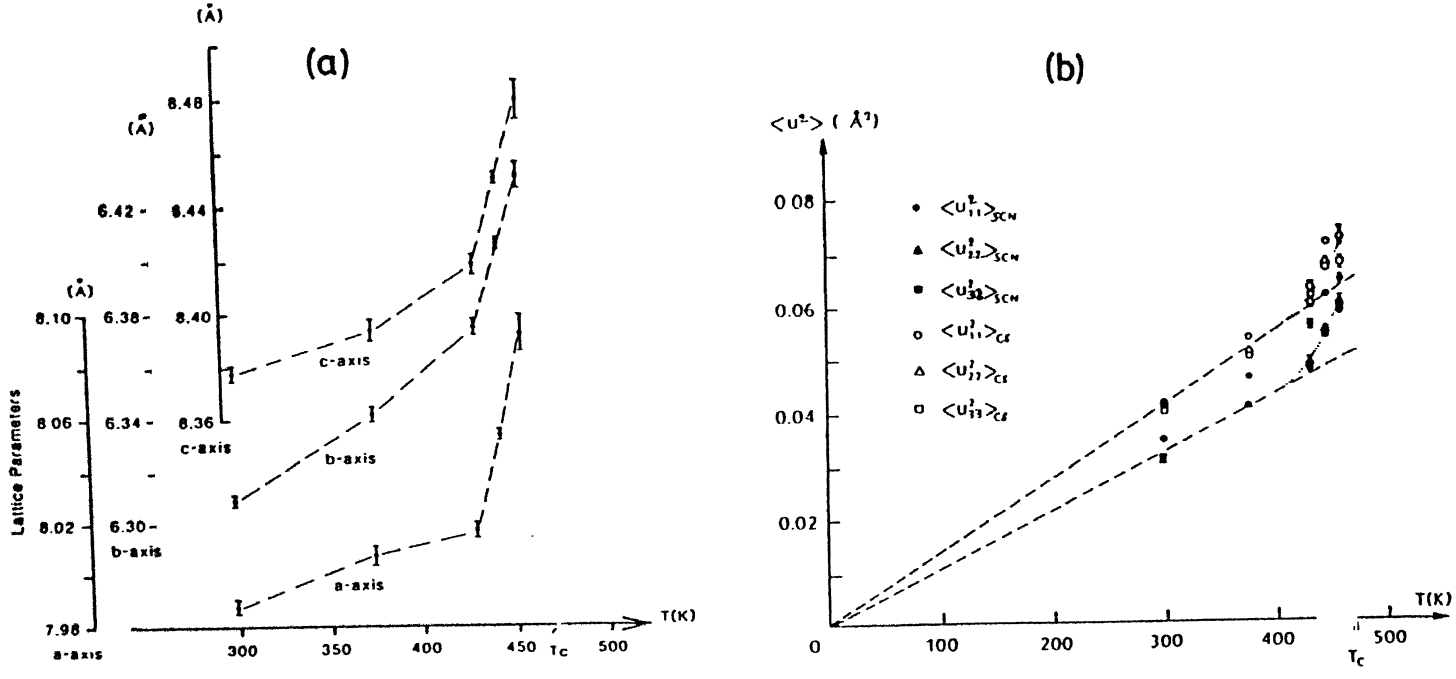

Figure 4.12:(a) The temperature dependence of the lattice parameters and(b) the temperature dependence of the mean square displacements for the Cs^{+} ion, and the rigid body translations of the NCS^{-1} ion. Taken from [18].

CHAPTER 5

STRUCTURAL PHASE TRANSITION AND INTERNAL FIELDS IN RUBIDIUM THIOCYANATE PROBED THROUGH VIBRATIONAL SPECTROSCOPY

Abstract

In this chapter, comprehensive Raman and IR studies of structural phase transition in Rubidium thiocyanate (RbNCS) are presented. Thermal behaviour of many vibrational modes, in the 298-448^{o}K range, indicates that the orthorhombic to tetragonal transition at $T_c \simeq 440^{o}K$ is of order-disorder type and it exhibits purely second order characteristics. The peculiar linear fall in the relative Raman intensity (I_{C-N}) of C-N stretching (ν_{C-N}) mode can be related to the progressive re-orientational disordering of NCS^- ions as T approaches T_c. An order-parameter exponent $\beta \simeq 0.45 \pm 0.04$ has been obtained by expressing: $I_{C-N} \propto (|T-T_c|)^{2\beta}$. Similarly, a consistent value of β ($\simeq 0.45$) has been obtained from the linear decrease in the IR intensity of the in-plane bending mode. In the Raman spectra, the appearance of sidebands in ν_{C-N} and ν_{C-S} regions can be related to splittings due to an internal electric field in the ordered orthorhombic phase. The continuous growth in their relative intensities and the decrease in splitting energies reveal the gradual diminution of internal field as T approaches T_c. Further the C-N and C-S oscillators were found to be affected by the field in an opposite way. These results have been discussed in the context of an anharmonic oscillator model developed to describe some of the spectral manifestations of an

order-disorder SPT in KCN system. The resultant broad band spectra in the external and internal mode regions, for $T > T_c$, can be attributed to the rapid head to tail fluctuations of NCS^- ions. An activation energy (U) for the reorientational motion of NCS^- ions, $U \simeq 0.29 \pm 0.02$ ev, has been calculated from large changes in the bandwidth (γ_{C-N}) near T_c.

Publications based on the material contained in this chapter are the following:

[A] S. Sathaiah, V.N. Sarin and H.D. Bist, Proc. ICORS XII, USA, 496 (1990).

[B] S Sathaiah and H.D. Bist, J . Chem. Phys. (Submitted)

5.1 Introduction

The thermal behaviour of the vibrational modes of solids in the vicinity of a structural phase transition contains information on the nature of the transition [1-3]. In some cases, variations in the band profiles of the thermosensitive internal modes may give more insight and they can be used as the internal probes for the study of various structural phase transitions and local environmental changes occurring in the crystals [3-8]. With these points in view, the detailed temperature dependence study (in the range 298 to 448^{o}K) of Raman and IR spectra of Rubidium thiocyanate (RbNCS) has been carried out.

5.2 Crystal Structure

At room temperature (RT), RbNCS has an ordered orthorhombic structure (Phase II), which can be assumed to be isostructural with that of Potassuim thiocyanate (KNCS) system [9]. The symmetry of the structure belongs to the space group Pbcm (D_{2h}^{11}), with four formula units in the primitive cell. The unit cell of the orthorhombic structure of the RbNCS system projected on to the (001) plane is shown in Figure 5.1. The NCS^{-} ions occupy the site of C_s symmetry on the (001) planes and they are oriented along the face diagonal [110] of the unit cell. The cations are sandwitched between NCS^{-} layers and occupy sites of C_2 symmetry. Differential thermal analysis and structural studies revealed a SPT around $T_c \simeq 439 \pm 3^{o}$K. Between T_c and melting point (457 ± 3^{o}K), RbNCS is believed to crystallize in a disordered

tetragonal structure (Phase I) isomorphous to that of Phase I in KNCS [10]. The room temperature vibrational spectra and mode assignments have already been reported [9,11]. The temperature dependence of vibrational spectra and the detailed analysis of the spectroscopic manifestations of disorder in RbNCS are presented here for the first time.

5.3 Experimental

For Raman spectral measurements 514.5nm radiation from an Argon ion laser was used to excite the sample and a Spex Ramalog system to record the spectra. IR spectra were recorded using Perkin Elmer 580 double beam spectrometer. The details of the experimental set up are same as given in chapter 2. The average heating rates in Raman and IR measurements are 0.3 and $0.5^{o}K\ min^{-1}$, respectively.

5.4 Results

5.4.1 Raman Spectrum at RT

The unpolarized Raman spectrum of RbNCS powder recorded at RT($298^{o}K$) is shown in Figure 5.2. The dominant bands below 150 cm^{-1} correspond to lattice modes and all other modes above 150 cm^{-1} are internal and multi-phonon modes. Peak frequencies (cm^{-1}), relative strengths and probable mode assignments of all the modes are listed in Table 5.1. Given symmetry assignments are inferred from the earlier reports [9,11]. Among the lattice modes, the band at 118 cm^{-1} is a rotatory mode of A_g symmetry and

it involves the hindered rotation of NCS^- about the C-axis on the (001) plane. The weak shoulder around 72 cm^{-1} may be due to the two-phonon processes involving difference bands. All other lattice modes correspond to translatory modes. In the internal mode region, strong bands at ν_{C-N} = 2051 cm^{-1} and ν_{C-S} = 747 cm^{-1} are C-N and C-S stretching modes. Whereas, the weak bands at δ^{a}_{N-C-S} = 481 cm^{-1} and δ^{b}_{N-C-S} = 475 cm^{-1} are in plane and out-of-plane bending modes of NCS^- ions, respectively. Bands at 963 and 953 cm^{-1} correspond to $2\delta^{a}_{N-C-S}$ and $2\delta^{b}_{N-C-S}$ respectively. The weak band around 1487 cm^{-1} (Table 5.1) is an overtone of ν_{C-S} fundamental. Small satellite bands at ν'_{C-S} = 742 and 738; ν'_{C-N} = 2006 and 2026 cm^{-1} are C-S and C-N stretching modes of $N-^{13}C-S$ and $^{15}N-C-S$ isotopic species. The weak spectral features around 2001 and 2074 cm^{-1} have been attributed to multiphonon processes, involving $\nu_{C-N} \pm L_{CP}$ (L_{CP} represents critical point frequencies of external modes). Like all other MNCS (M = K, Cs,Na and NH_4) systems, peak intensities of the overtones of NCS^- bending modes in RbNCS are 3.5 times stronger than that of their fundamentals indicating significant anharmonic effects even at RT.

5.4.2 IR Data at RT

IR spetrum recorded at RT(298^0K) can be seen from Figure 5.3. The predominant bands at 2050, 748 and 483 and 470 cm^{-1} are C-N stretching (ν_{C-N}), C-S stretching (ν_{C-S}) and NCS^- bending (δ^{a}_{N-C-S} and δ^{b}_{N-C-S}) modes, respectively. The spectral features around 960 and 951 cm^{-1} are overtones and combination modes of

NCS^- bending modes. Bands at 2005 and 740 cm^{-1} are ν_{C-N} and ν_{C-S} modes of $N-^{13}C-S$ isotopic species, respectively. The shoulder around 2070 cm^{-1} may be due to multiphonon processes involving $\nu_{C-N} \pm L_{CP}$ external modes. Peak frequencies, relative strengths and mode assignments of all the observed IR bands are summarized in Table 5.2.

5.4.3 Thermosensitive Raman Spectral Regions

The evolution of Raman Spectra, in the C-N stretching region with rising temperature is shown in Figure 5.4(a), for typical seven temperatures between 301 and 446°K. As the temperature increases peak intensity of the ν_{C-N} mode decreases monotonically with a slight linear increment in its bandwidth (γ_{C-N}), whereas the peak position of (ν_{C-N}) remains constant till 395°K and increases abruptly for T>395°K. A small hump appears on higher frequency side of the ν_{C-N} mode around 368°K. As T increases further, the hump grows in its intensity at the expense of decrease in the peak intensity of the main ν_{C-N} mode. Typical changes in the normalized peak intensity of ν_{C-N} mode (I_{C-N}) with T are shown in Figure 5.5(a). It is interesting to note that I_{C-N} decreases linearly with T in the temperature range 391-436°K. For T>436°K, it becomes infinitely small with a slight deviation from its linear behaviour. However, by extrapolating the linear behaviour, I_{C-N} curve intersects the horizontal axis around 439°K. Considering $T \simeq 439^{\circ}K$ as an approximate transition temperature (T_c), a plot of log I_{C-N} versus log ($|T-T_c|$) for $3 \leq |T-T_c| \leq 48^{\circ}K$

gives an exact straight line with a slope of 0.902±0.08 (Figure 5.5(b)). So the characteristic changes in I_{C-N} with T can be expressed as $I_{C-N} \propto (|T-T_c|)^{2\beta}$ with an order parameter exponent $\beta \simeq 0.45 \pm 0.04$. This behaviour has been verified by repeating the experiment. The value of β obtained in the repeated experiment is $\beta = 0.48 \pm 0.04$. As mentioned earlier, γ_{C-N} and ν_{C-N} remain almost constant for T well below T_c. But as T approaches T_c (i.e. $395 < T < T_c$) both γ_{C-N} and ν_{C-N} increase anomalously (Figure 5.6(a) and (b)) and once again become constant for $T > T_c$.

Raman Spectra in the C-S stretching region, recorded at five different temperatures above and below T_c are given in Figure 5.4(b). As T increases peak intensity of ν_{C-S} mode decreases monotonically with gradual broadening in its band width. Whereas the spectral features in the low frequency side of ν_{C-S} mode enhance in their intensity with T and become part of the wing to the main ν_{C-S} mode. For $T \geq 448^{o}K$, a broad and weaker ν_{C-S} mode with a large asymmetrical wing in its lower frequency side, can be seen. Like the ν_{C-N} mode, peak frequency ν_{C-S} also remains constant for T well below T_c. It is interesting to note that as T approaches T_c, ν_{C-S} decreases (Figure 5.6(c)) in an exactly opposite manner to ν_{C-N} and once again becomes constant for $T > T_c$.

The temperature dependence of Raman spectra in the external mode region is presented in Figure 5.4(c). On increasing the temperature, peak positions and relative strengths of all the lattice modes decrease continuously with a gradual increase in their band widths. Finally for $T > 430^{o}K$, the lattice

structure completely smears off and a broad band spectrum with a small hump around 99 cm^{-1} results in the external mode region. Typical variations in the peak frequencies of the lattice modes with T are plotted in Figure 5.7. Peak frequencies of all the modes decrease gradually with T. Traslatory modes at 47, 65 cm^{-1} and a rotatory mode at 118 cm^{-1} (RT) show significant softening (i.e. 15% at 430°K) with T. Whereas the peak frequencies of other lattice modes do not change appreciably.

5.4.4 Thermal Behaviour of IR Modes

IR spectra recorded at three different temperatures namely at 298°K (RT), 423°K (below T_c) and 448°K (above T_c) are shown in Figure 5.3. On increasing the sample temperature gradual changes in the spectra can be seen. The most characteristic change is the apparent transformation of a doublet into a singlet in the NCS^- bending mode (δ_{N-C-S}) region. Similarly, the doublet in the overtone region of δ_{N-C-S} mode almost merges into a single band. The detailed IR spectra in the δ_{N-C-S} mode region were recorded in the absorbance mode and the typical spectra are shown in Figure 5.8 for five different temperatures below and above T_c. As T increases, peak position and intensity of δ^a_{N-C-S} mode decrease gradually. Whereas, the peak position and relative intensities of δ^b_{N-C-S} mode remain constant with T. The variations in the peak frequencies and peak intensities of δ_{N-C-S} modes with T are summarized in Figure 5.9. As mentioned earlier, the peak position - δ^a_{N-C-S} decreases continuously until 433°K; further increase in T causes an abrupt fall and finally becomes constant for T > 441°K (Figure 5.9(a)). There is only a marginal decrease

5.12(a)}. Whereas ν_{C-S} decreases continuously with temperature and becomes constant for $T>T_c$ {Figure 5.12(c)}. Characteristic changes in these ν_{C-N} & ν_{C-S} frequencies with T are consistent with the Raman results. Peak intensity of ν_{C-N} mode remains constant for $T < T_c$ and shows a small jump around T_c {Figure 5.12(b)}. Whereas, the peak intensity of ν_{C-S} mode decreases continuously with T {Figure 5.12 (d)}.

5.5 Discussion

Since the structures of the low (II) RbNCS and KNCS phases are known to be isomorphous, it may be reasonable to assume that the structures of the high (I) phases are also isomorphous [10]. Hence, the transitions in both the materials can expected to be thermodynamically similar. The transition in KNCS has been interpreted as order-disorder type with regard to the orientations of NCS^- ions [12,13]. Further, it has been identified as second order transition with a first order component [10].

All the observed changes in the Raman spectra of RbNCS, namely, (i) the gradual broadening and replacement of the external mode region by a broad band spectrum, (ii) the characteristic linear fall in the peak intensity of the C-N stretching mode, (iii) the appearance and continuous growth in the relative intensities of sidebands in the ν_{C-N} and ν_{C-S} regions, and (iv) the anomalous changes in peak frequencies and band widths of the main ν_{C-N} and ν_{C-S} modes, reveal an order-disorder transition around $439\pm2^{o}K$. Similarly, the changes in the IR spectra reveal the transition at $441\pm3^{o}K$. The T_c values inferred from the

present studies are in good agreement with the reported ($439\pm3^{o}K$) value [10]. The observed reversible changes in the Raman and IR spectra without any hysteresis in the T_c value, indicate a purely second order nature of the transition.

5.5.1 Antiferroelectric - like Ordering and Calculation of Order-Parameter Exponent

At room temperature the doublet in the δ_{N-C-S} region of IR spectrum is due to anisotropy of the crystalline field which is brought about by the layer structure of the RbNCS system. So, the gradual reduction in the peak separation between δ^{a}_{N-C-S} and δ^{b}_{N-C-S} as T approaches T_c can be attributed to apparent decrease in the anisotropy which probably occurs as a result of disordered oscillations of NCS^{-} ions. Additionally, the profound frequency shifts and the characteristic changes in the peak intensities of in plane bending modes (δ^{a}_{N-C-S}), and the absence of such tendencies in the out-of-plane bending δ^{b}_{N-C-S} modes suggest that the crystal field parallel to (001) plane is much influenced during the phase transition.

In the NCS^{-} group, the N atoms are more electro-negative than the S atoms on the Pauling scale. So, one can expect a net dipole moment; like in the case of KNCS [14], the orthorhombic structure of RbNCS can be considered as analogous to an antiferroelectric with an ordered antiparallel arrangement of the net dipoles along [100] direction. Along these lines, the peculiar linear fall in the relative intensities, (I_{C-N} and I_a), of ν_{C-N} (Raman) and δ^{a}_{N-C-S} (IR) modes with T (i.e. I_{C-N} and I_a $\propto$

$|T-T_c|^{2\beta}$ with $\beta \simeq 0.45 \pm 0.04$), like square of the orderparameter (η^2), symbolizes the progressive (head to tail) reorientational disordering of NCS^- ions which leads to a paraelectric like phase above T_c. In other words, deep in the ordered phase the relative intensities, I_{C-N} and I_a, are solely controlled by a long-range (antiferroelectric like) order. The consistent mean field type order parameter exponent ($\beta \simeq 0.45$) obtained from two independent (Raman and IR) measurements suggests that thermally activated disordering processes in the vicinity of transition (i.e. $390 \leq T < 440^oK$) can be described in the frame work of Landau theory of structural phase transitions [15,16]. To explain the saturation of the orderparameter observed at lower temperatures an Ising type free energy may be more appropriate [16].

5.5.2 Raman Evidence of Internal Field

According to the Curie principle [17], the centre of symmetry must always be preserved at an antiferroelectric phase transition if it is there in either of the phases. Although, dielectric measurements on RbNCS are not available, the retained centre of inversion symmetry during the (tetragonal to orthorhombic) transition supports the *"antiferroelectric"* - like picture of RbNCS. Moreover, the anomalous changes observed in the ν_{C-N} and ν_{C-S} regions (especially in the Raman spectra) of RbNCS near T_c, look strikingly similar to those (changes in the ν_{C-N} modes) reported by Durand et al [8] for KCN and NaCN near the antiferroelectric (ordered orthorhombic) to paraelectric transitions.

Durand et al [8] have proposed an anharmonic oscillator model in which the influence of an intense electric field building up with decreasing T has been considered to explain thermal behaviour of ν_{C-N} modes in the antiferroelectric phases of KCN and NaCN systems. According to their model, the nth harmonic stretching mode (ν_n) under the influence of an internal electric field ($E_\uparrow$) splits into two components related to aligned ($E_\uparrow$)and counter aligned ($E^\downarrow$) CN^- dipole configurations. The splitting energy difference is given by

$$\Delta\left[h\nu_n(E_\uparrow^\downarrow)\right] = h\nu_n(E_\uparrow) - h\nu_n(E^\downarrow)$$

$$= \frac{h\nu_n(o)}{K_e r_e}(3a_1-\rho)\,p'(o)E_\uparrow \qquad (5.1)$$

Whereas, the relative shift in $\nu_n(E_\uparrow)$ with respect to the zero field unsplit $\{\nu_n(o)\}$ is given by

$$\nu_n(E_\uparrow) - \nu_n(o) = \nu_n(o)\,\frac{E_\uparrow}{2K_e r_e}\left[(3a_1-\rho)p'(o) + \frac{1}{2}(3a_1-A)\alpha_e' E_\uparrow\right] \qquad (5.2)$$

where K_e = force constant; r_e = equilibrium position; p'= dipole moment gradient $\frac{dp}{dr}$; $\rho=\left(\frac{d^2p}{dr^2}\right)/\left(\frac{dp}{dr}\right)$; α_e'= polarizability gradient $\frac{d\alpha_e}{dr}$; $A=\left(r_e\frac{d^2\alpha}{dr^2}\right)/\left(\frac{d\alpha}{dr}\right)$;and a_1 = anharmonic potential parameter.

Along the similar lines, the observed Raman spectral changes in the ν_{C-N} and ν_{C-S} regions of RbNCS sample can be

explained by considering an internal electric field which is probably produced due to the cationic (Rb^+) displacements in the ordered orthorhombic phase. Indeed, such cationic displacements have been observed [18] in (an isomorphous) KNCS system; moreover the thermal variations of cationic (K^+) displacements were found to correlate with the temperature dependence of the order parameter (η) of NCS^- groups in the orthorhombic phase. So, the appearance of sideband on the higher frequency side of the main ν_{C-N} mode (of RbNCS) is probably due to the splitting of ν_{C-N} mode under an internal electric-field (E). The stronger ν_{C-N} band in the orthorhombic phase can be attributed to the Raman transitions from those NCS^- groups which form an aligned ($E_\uparrow$) dipole configuration with respect to the field ($E_\uparrow$). Whereas, the sideband is related to the transitions from the NCS^- groups which form a counter aligned ($E^\downarrow$) dipole configuration. The gradual growth in the relative intensity of sideband reveals an increase in the population of the counter aligned ($E^\downarrow$) dipoles while the main electric field ($E_\uparrow$) decreases as T approaches T_c, from below. The characteristic linear fall in the peak intensity (I_{C-N}) of the main ν_{C-N} mode, (as T approaches T_c) symbolizes the gradual diminution of internal field ($E_\uparrow$) and the progressive disordering in the antiferroelectric arrangements. Additionally, the anomalous increase in the peak frequency of ν_{C-N} ($E_\uparrow$) mode and the gradual merging of the main and side bands into a broad singlet as T approaches T_c are in accordance with Equations (5.1) and (5.2). They can also be regarded as spectral manifestations of internal field diminution by considering a positive sign for the

co-efficient $\{(3a_1-\rho)P'(o)\}$ and a negative sign for $\{(3a_1-\rho)P'(o)+\frac{1}{2}(3a_1-A)\alpha_e'E_\uparrow\}$ in Equations (5.1) and (5.2).

Similar arguments can be put forth to explain the frequency shifts and intensity variations of the ν_{C-S} mode and its sideband. Unlike the ν_{C-N} case, the stronger ν_{C-S} mode at higher frequency side is related to the aligned ($E_\uparrow$) dipole configuration and the satellite at lower frequency corresponds to the counter aligned ($E^\downarrow$) component. The gradual decrease in the peak frequency of the main ν_{C-S} mode with T is also in opposite to the temperature variations of ν_{C-N} mode. These results can be understood in the following way:

From Equation (5.1), the appearance of the main $\nu_n(E_\uparrow)$ band at higher or lower frequency with respect to the sideband $\nu_n(E^\downarrow)$ depends on the plus or minus sign of $\{(3a_1-\rho)P'(o)\}$. Similarly, a minus or plus sign of the coefficient $\{(3a_1-\rho)P'(o)+\frac{1}{2}(3a_1-A)\alpha_e'E_\uparrow\}$ in Equation (5.2) determines whether the main $\nu_n(E_\uparrow)$ mode increases or decreases as the internal field decreases on approaching T_c. A more general theoretical model is needed for the quantitative analysis. However, the thermal behaviours of ν_{C-N} and ν_{C-S} mode suggest that an internal field in the orthorhombic phase of RbNCS influences C-N & C-S oscillators in an opposite way.

5.5.3 Band Width Variation and Activation Energy

As described earlier, all the external modes are temperature dependent to some extent but none of them individually show soft mode-like behaviour. Generally, in order-disorder transitions, the soft mode is likely to be a diffusive large amplitude motion which may be too low in frequency to be observed

by Raman spectroscopy [19,20]. However, an indirect manifestation of the relaxation motion may be observed in the large changes of the band widths of vibrational modes [21]. The anomalous increase in the band widths of many modes, in particular γ_{C-N} (Figure 5.13(a)) of ν_{C-N} modes, can be related to the rapid head to tail fluctuations in the orientations of $NC\bar{S}$ ions as T approaches T_c. An activation energy, $U \simeq 0.29 \pm 0.01$ev for the reorientational motion of NCS^- ion has been calculated by expressing the changes in γ_{C-N} in terms of $\ln\gamma_{C-N} \propto \left(\frac{-U}{K_B T}\right)$ (Figure 5.13(b)).

The replacement of Raman Spectrum in the external mode region by a broad band spectrum and all other characteristic spectral changes described in the previous section reveal the loss of translational invariance and the emergence of dynamic disorder in phase I as both the (NCS^- and Rb^+) ions are in motion.

REFERENCES

[1] Z.Iqbal and F.J. Owens, "Vibrational Spectroscopy of Phase Transitions", (Academic Press Inc., Orlando, 1984).

[2] J.M. Loveluck and J.B. Sokoloff, J.Phys. Chem. Solids. 34, 869 (1973).

[3] J. Petzelt and V. Dvorak, J. Phys. C 9, 1587 (1976).

[4] M.H. Brooker, J. Chem. Phys. 68, 67 (1978)

[5] S.V. Karpov, A.V. Khassan Ali and A.A. Shultin, Sov. Phys. Solid St. 24, 39 (1982).

[6] V. Winterfeldt, G. Schaack and A. Klopperpieper, Ferroelectrics 15, 21 (1977).

[7] C.W. Garland and N.E. Schumaker, J. Phys. Chem. Solids 28, 799 (1967).

[8] D. Durand, L.C. Scavarda do Carmo and F. Luty, Phys. Rev. B39, 6096 (1989).

[9] S.S. Ti, S.F.A. Kettle and Ø. Ra,Spectrochimica Acta 32A, 1603-13 (1976).

[10] W. Klement Jr. and C.W.F.T. Pistorius, Bull. Chem. Soc. Japan 49, 2148 (1976).

[11] M.J. Joyce and F. Ninio, Aust. J. Phys. 42, 389-99 (1989).

[12] M. Sakiyama, H. Suga and S. Seki, Bull. Chem. Soc. Japan 36, 1025, (1963).

[13] Y. Yamada and T. Watanabe, Bull. Chem. Soc. Japan, 36, 1032 (1963).

[14] Z. Iqbal, L.H. Sarma and K.D. Moller, J. Chem. Phys. 57, 4728 (1972).

[15] J. Petzelt and V Dvorak, J. Phys. C. 9, 1571 (1976).

[16] W. Schranz, H. Warhanek and P. Zielinski, J. Phys. Condens. Matter 1, 1141 (1989).

[17] R. Blinc and B.Zeks, in "Soft modes in ferroelectrics and antiferroelectrics", (North-Holland, Amsterdam, 1974) p. 72.

[18] S. Yamamoto, M.Sakuno and Y. Shinnaka, J. Phys. Soc. Jpn. 56(12), 4393 (1987).

[19] J.F. Scott, Rev. Mod. Phys. 46, 83-128 (1974).

[20] F.J. Owens, Solid State Communications 29, 789-91 (1979).

[21] Z. Iqbal and C.W. Christoe, J. Chem. Phys. 62, 3246 (1975).

able 5.1 : Vibrational frequencies, relative strengths, mode assignments and symmetry species of Raman active modes in RbNCS at 298°K

(a) External and Internal Modes

	Vibration frequency (cm^{-1})	Relative strength	Mode assignment	Symmetry species †
	47	vs	T	(A_g, B_g)
	53	vs	T	B_g
	65	s	T	(A_g, B_g)
:xternal	72	sh	?	B_g
lodes	99	ms	T	B_g
	118	vs	R	A_g
	131	sh	T	A_g
	475	vvw	δ^b_{N-C-S}	B_g
	481	vvw	δ^a_{N-C-S}	(A_g, B_g)
Internal lode	747	ms	ν_{C-S}	(A_g, B_g)
	2051	vs	ν_{C-N}	(A_g, B_g)

(b) **Multi-phonon modes and Internal modes of isotopic species**

	Vibrational frequency (cm^{-1})	Relative strength	Mode assignment	Symmetry species †
Multi-phonon Modes	953	vvw	$2\delta^{b}_{N-C-S}$	(A_g, B_g)
	963	w	$2\delta^{a}_{N-C-S}$	(A_g, B_g)
	1487	vvw	$2\nu_{C-S}$	(A_g, B_g)
	2001	w	$\nu_{C-N}-L_{cp}$ ($L_{cp} \simeq 50$)	(A_g, B_g)
	2074	w	$\nu_{C-N}+L_{cp}-L'_{cp}$, (three phonon ?)	(A_g, B_g)
Internal Modes of Isotopic Species	738	m	$^{15}N\ \nu'_{C-S}$	(A_g, B_g)
	742	m	$^{13}C\ \nu'_{C-S}$	(A_g, B_g)
	2006	m	$^{13}C\ \nu'_{C-N}$	(A_g, B_g)
	2026	w	$^{15}N\ \nu'_{C-N}$	(A_g, B_g)

† Inferred from [9,11]

Table 5.2 : IR active internal and multi-phonon modes of RbNCS at room temperature

Vibrational fequency (cm^{-1})	Relative strength	Mode assignment
470	m	δ^{b}_{N-C-S}
484	s	δ^{a}_{N-C-S}
739	sh	$^{13}C\ \nu'_{C-S}$
746	s	ν_{C-S}
951	w	$\delta^{a}_{N-C-S}+\delta^{b}_{N-C-S}$
966	m	$2\delta^{a}_{N-C-S}$
2005	m	$^{13}C\ \nu'_{C-N}$
2050	s	ν_{C-N}
2070	sh	$\nu_{C-N}+L_{cp}$ ($L_{cp}=20$)

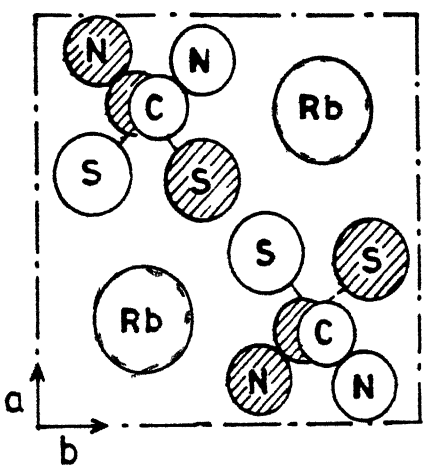

Figure 5.1: Orthorhombic structure of RbNCS projected onto the (001) plane. The shaded and unshaded NCS^- ions lie at Z = 1/4 and Z = 3/4, respectively. While the dashed Rb^+ ions lie in the Z= 1/2 plane.

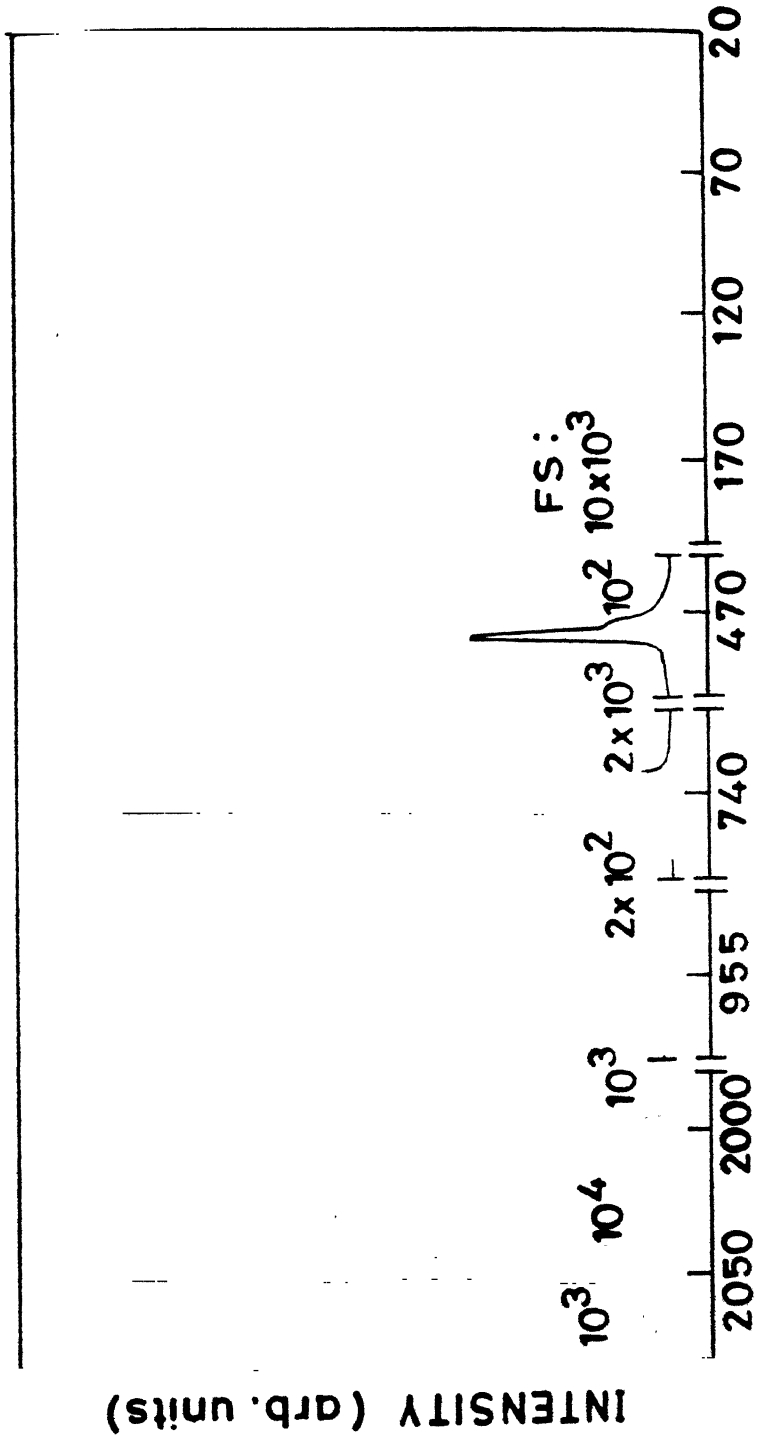

Figure 5.2: Unpolarized Raman spectrum of RbNCS powder at room temperature (i.e. 298°K). FS : $10x10^3$, $2x10^3$ etc. were the recording sensitivities.

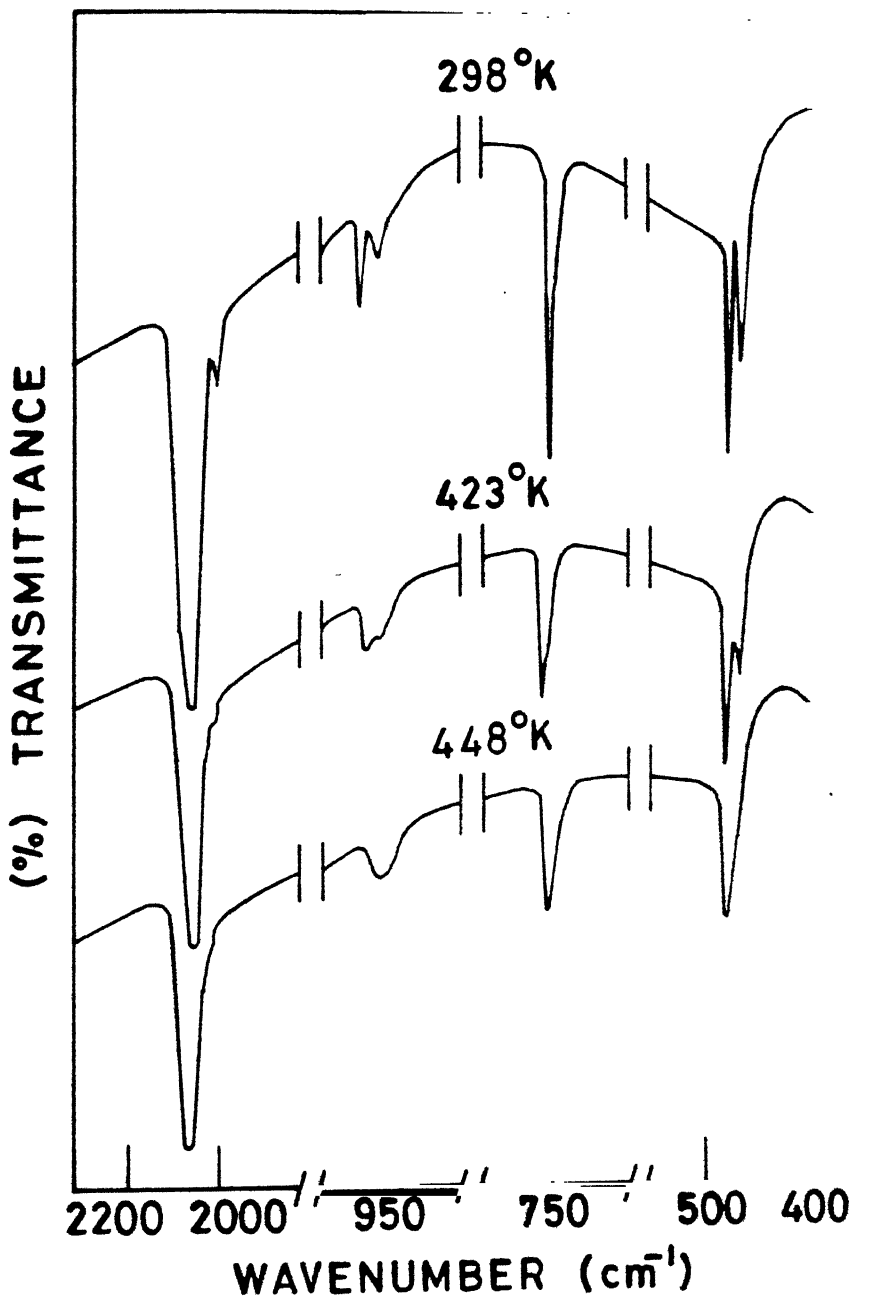

Figure 5.3: Infrared spectra of RbNCS recorded in the transmittance mode at 298 (RT), 423 and 448°K.

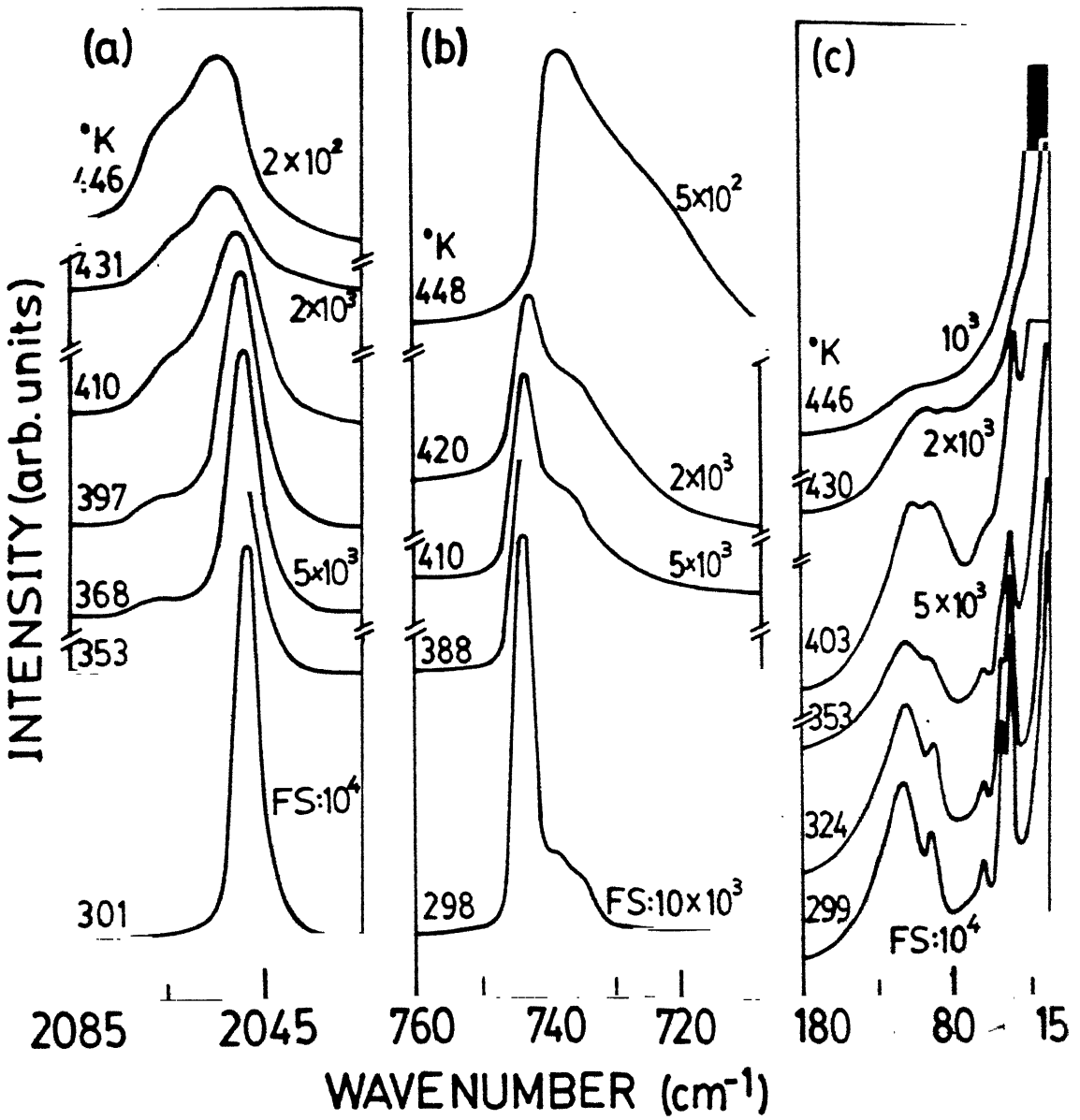

Figure 5.4: Temperature evolution of Raman spectra in the (a) C-N stretching, (b) C-S stretching and (c) lattice modes regions. FS : represents the recording sensitivity (photon counts/seconds).

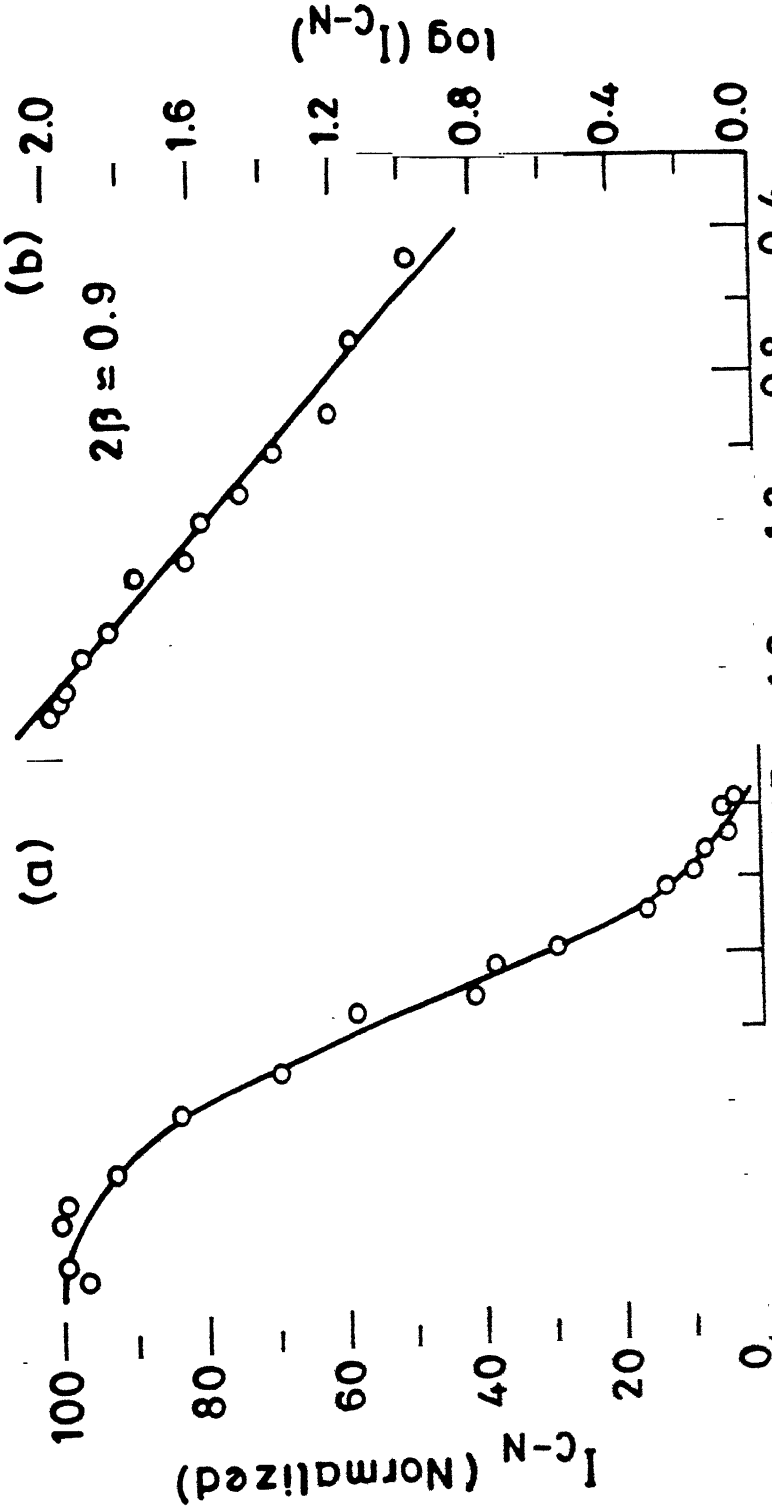

Figure 5.5: Variations in the peak intensity (I_{C-N}) of the ν_{C-N} (Raman) mode with temperature (T), (a) (I_{C-N})(normalized) versus T and (b) log (I_{C-N}) versus log ($|T-T_c|$), for $391 \leq T \leq 436^{o}K$.

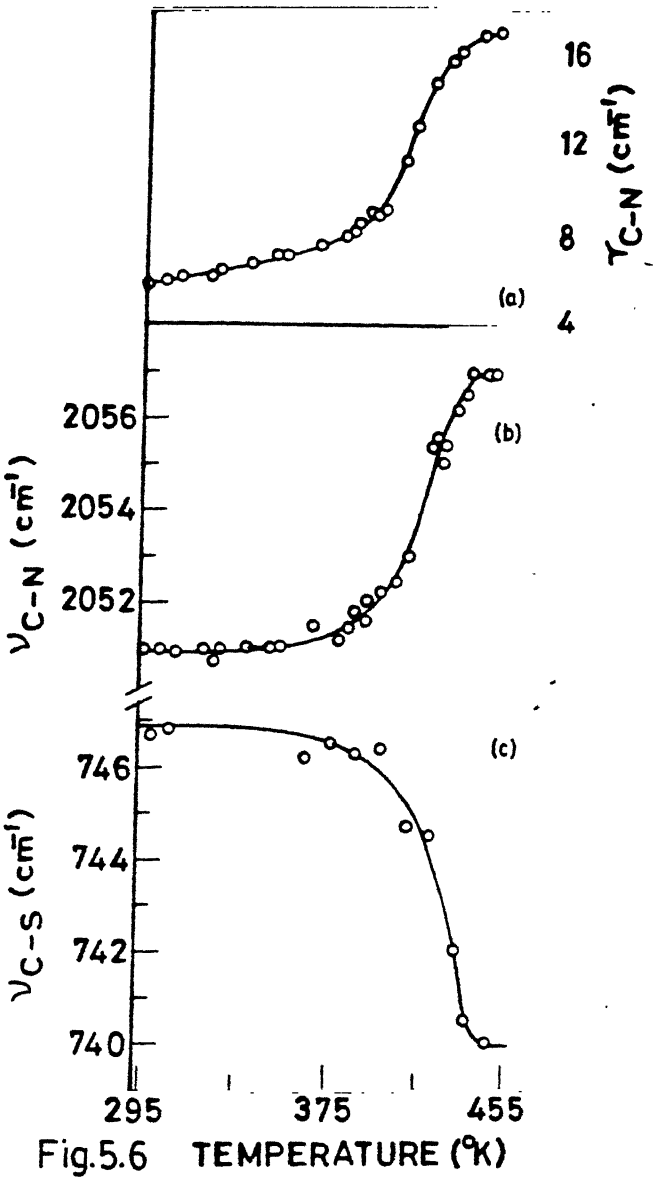

Fig.5.6

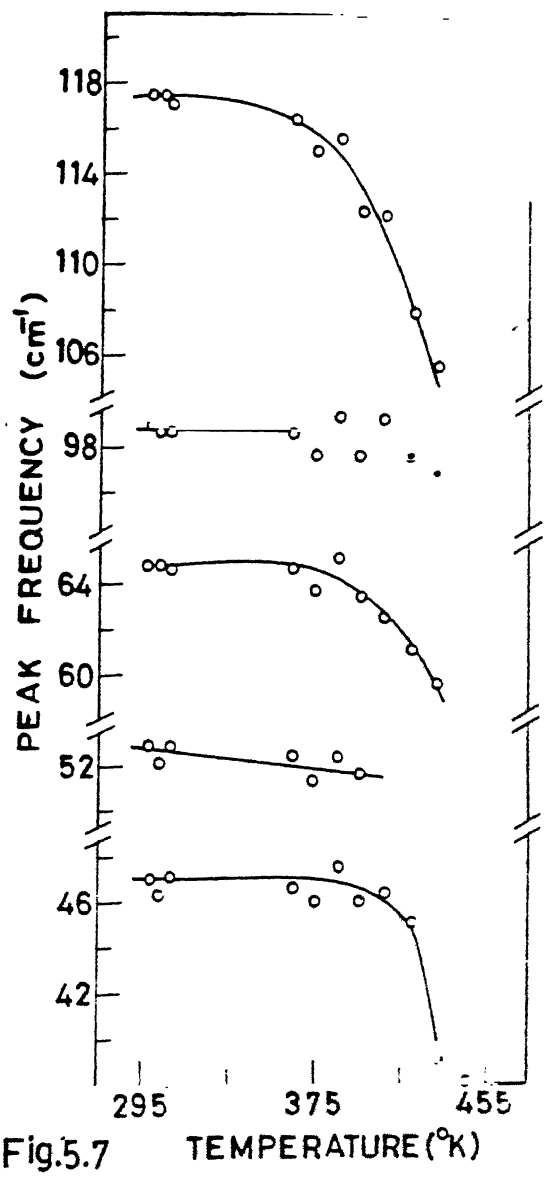

Fig.5.7

Figure 5.6: Typical changes in the (a) bandwidth γ_{C-N}, peak positions, (b) ν_{C-N} and (c) ν_{C-S} of Raman modes with temperature.

Figure 5.7: Peak frequencies (cm^{-1}) of the lattice (Raman) modes (ν_i) as a function of temperature.

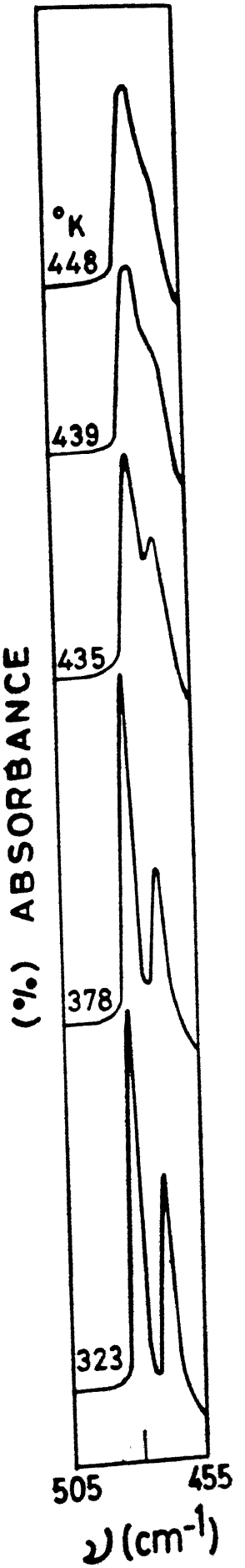

Figure5.8: Thermosensitive NCS^- bending mode (455-505 cm^{-1}) region of IR spectra (recorded in the absorbance mode) for the typical five different temperatures below and above T_c.

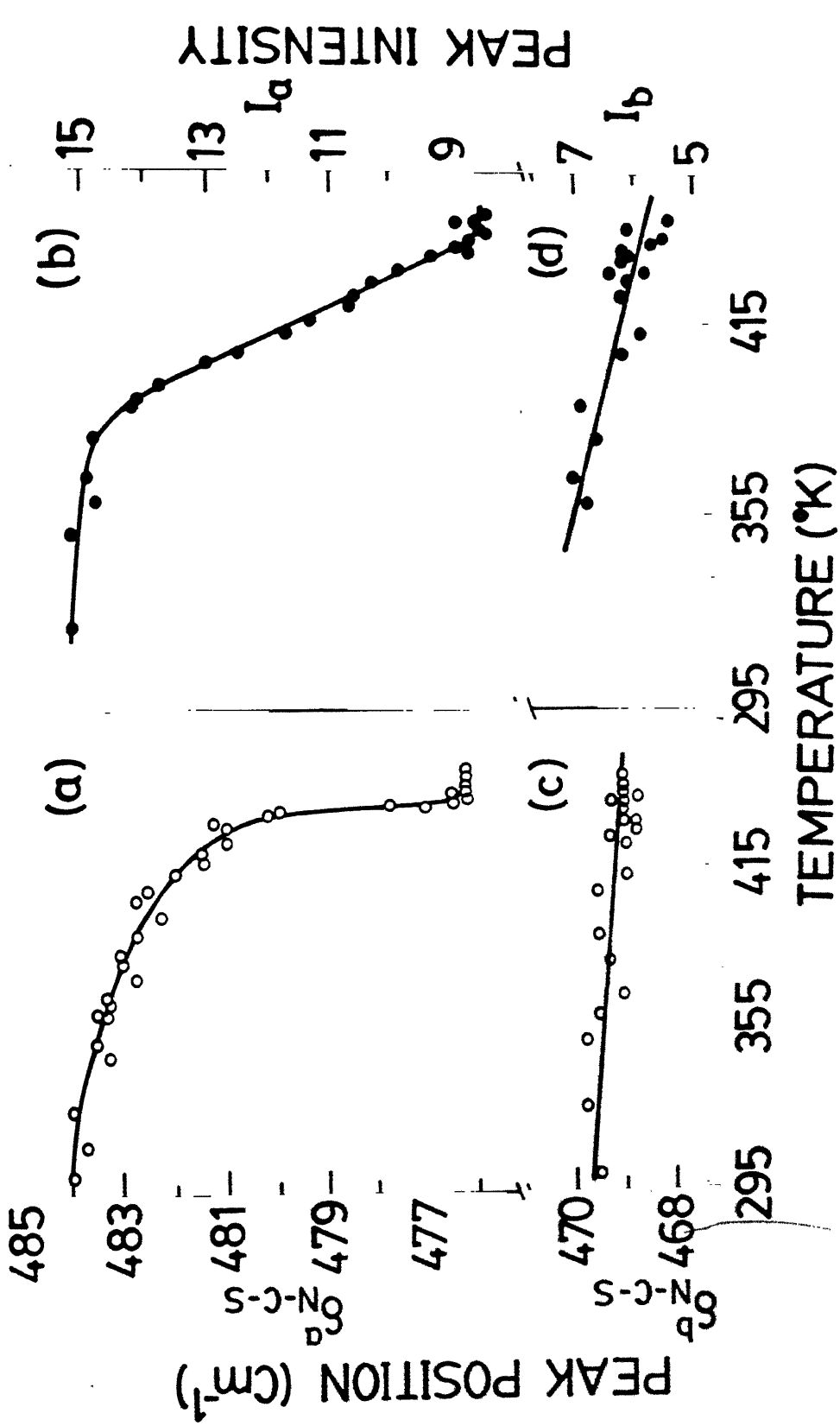

Figure 5.9: Temperature dependence of the peak positions and peak intensities of δ_{N-C-S}(IR) modes (a) δ^a_{N-C-S} vs T. (b) I_a vs T, (c) δ^b_{N-C-S} vs T and (d) I_b vs T.

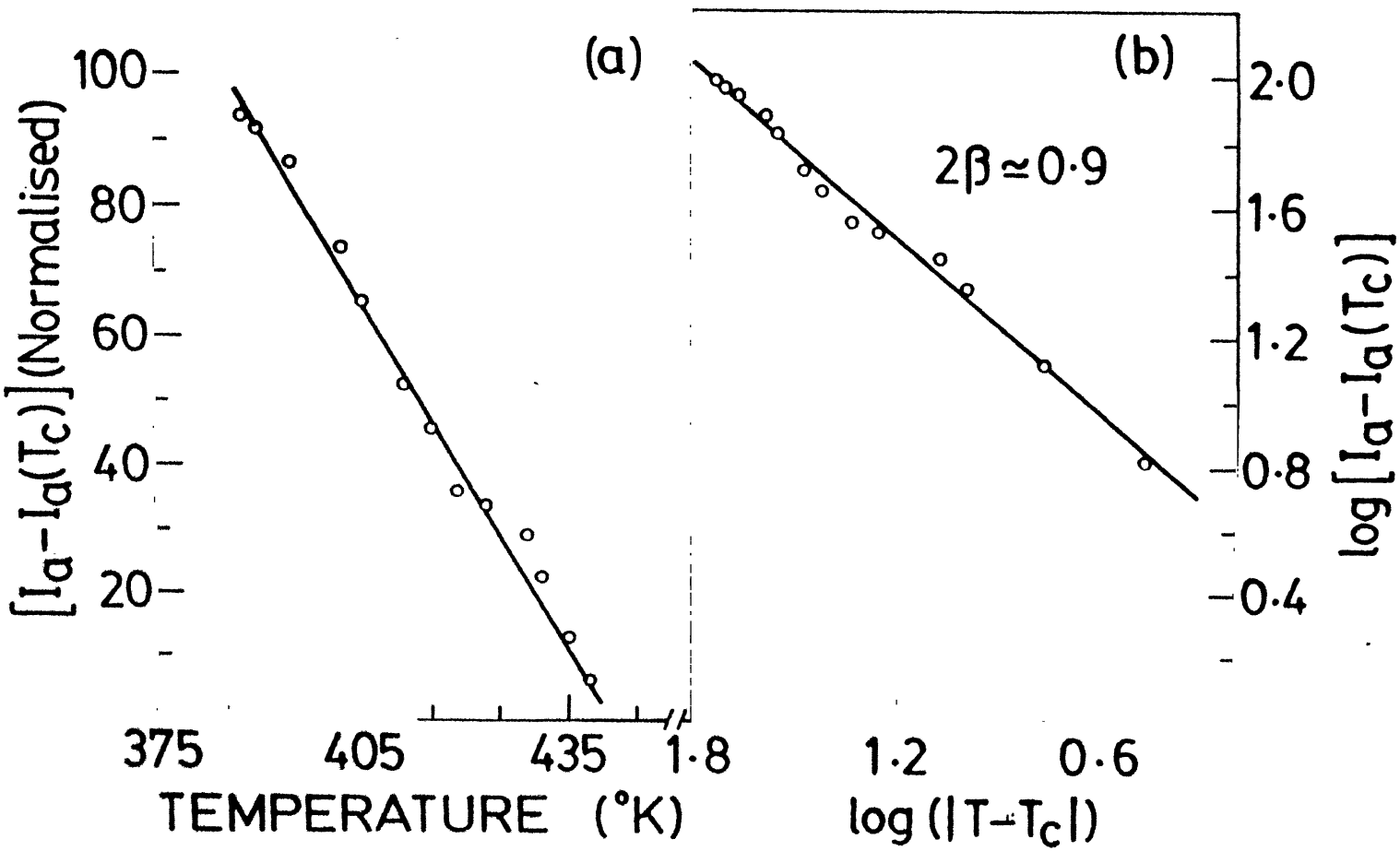

Figure 5.10: The linear variation in the normalized intensity of $\delta^{(a)}_{N-C-S}$ (IR) mode with T, (a) $[I_a-I_a(T_c)]$ vs T and (b) log $[I_a-I_a(T_c)]$ versus log $(|T-T_c|)$, for $388 < T < 441^{\circ}K$.

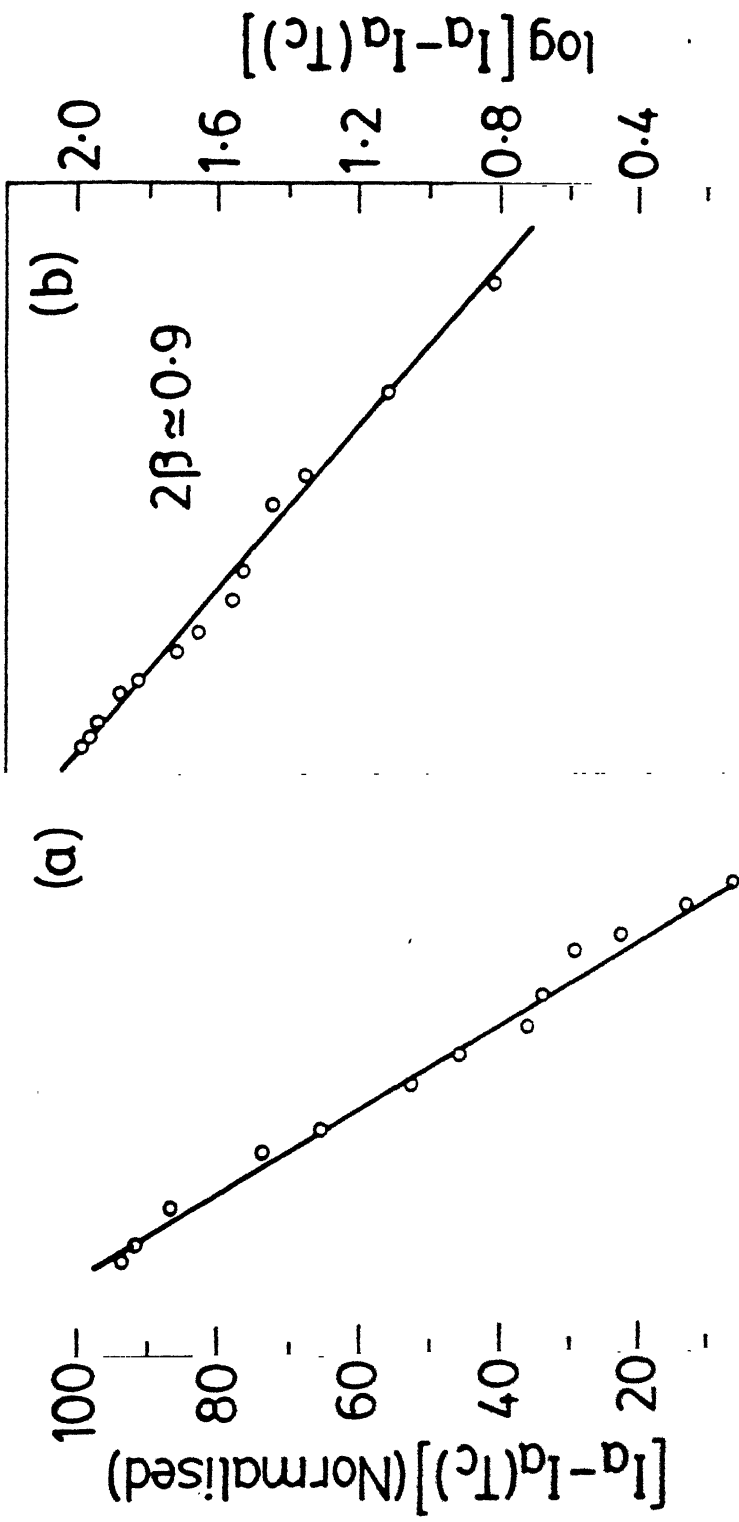

Figure 5.10: The linear variation in the normalized intensity of $\delta^{(a)}_{N-C-S}$ (IR) mode with T, (a) $[I_a - I_a(T_c)]$ vs T and (b) log $[I_a - I_a(T_c)]$ versus log ($|T - T_c|$), for 388 < T < 441°K.

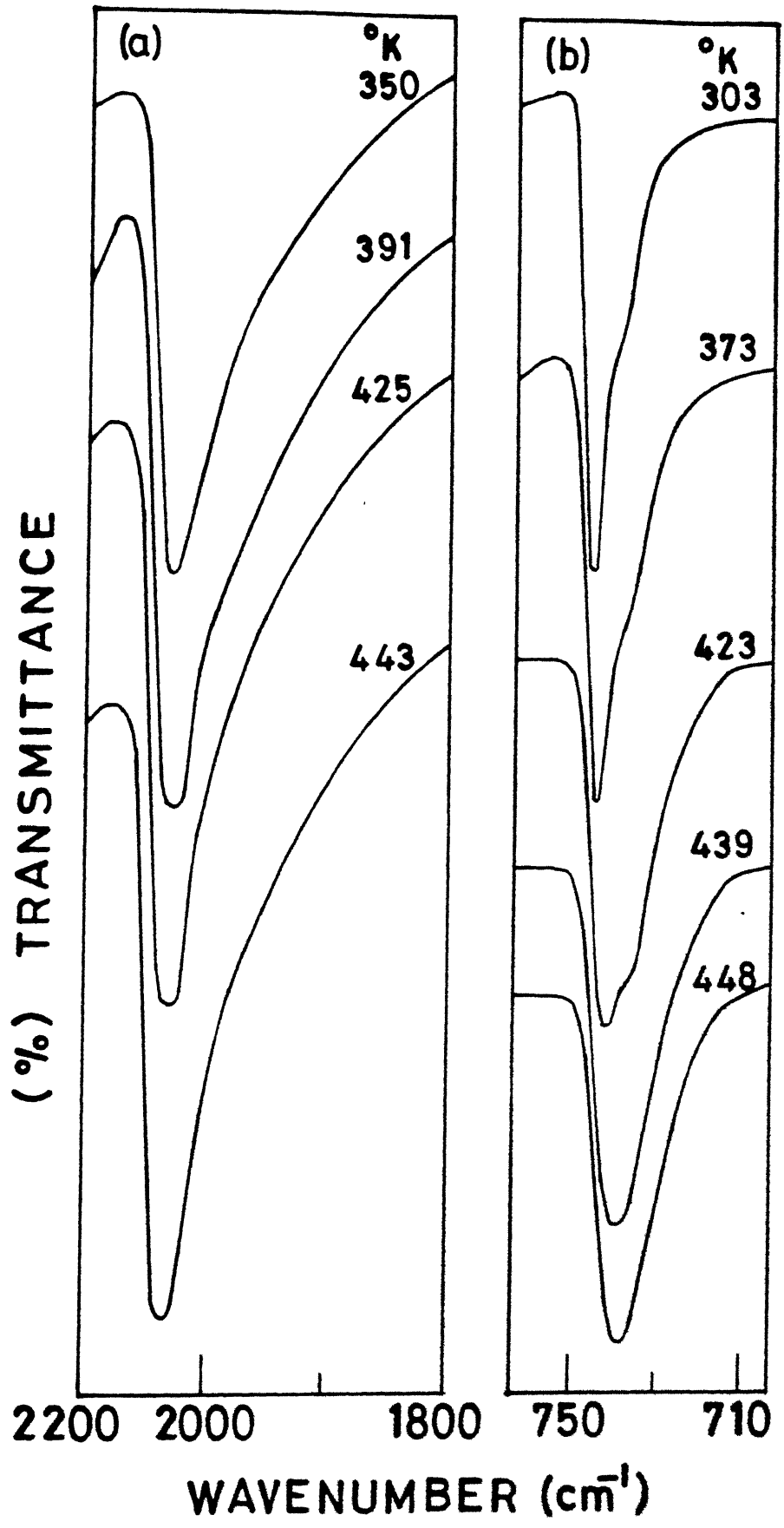

Figure 5.11: IR transmittance spectra in (a) ν_{C-N} and (b) ν_{C-S} regions at various temperatures below and above T_c.

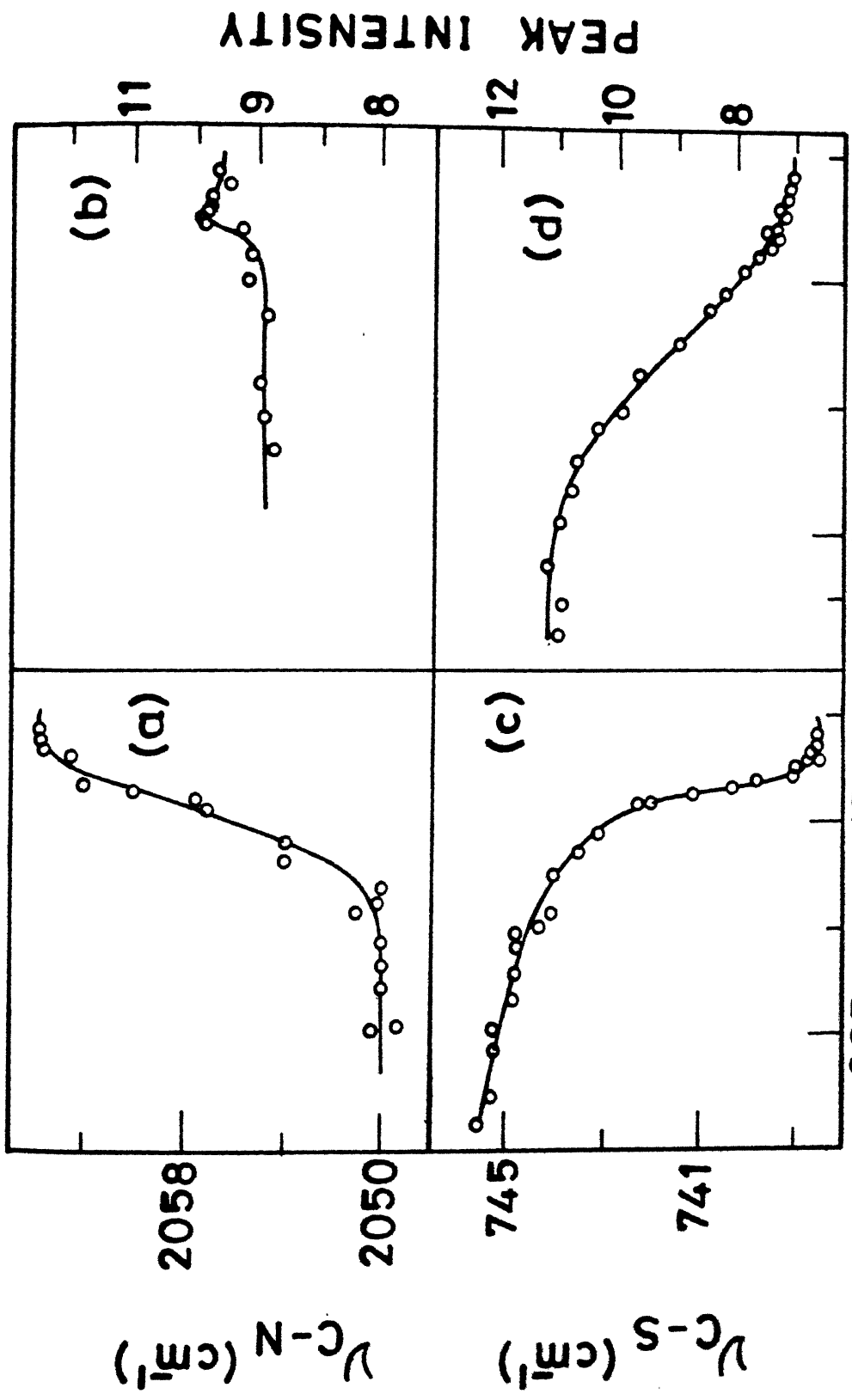

Figure 5.12: Temperature variations of the peak positions and intensities of IR, C-N and C-S stretching modes, (a) ν_{C-N} versus T (b) ν_{C-S} versus T (c) I_{C-N} versus T and (d) I_{C-S} versus T.

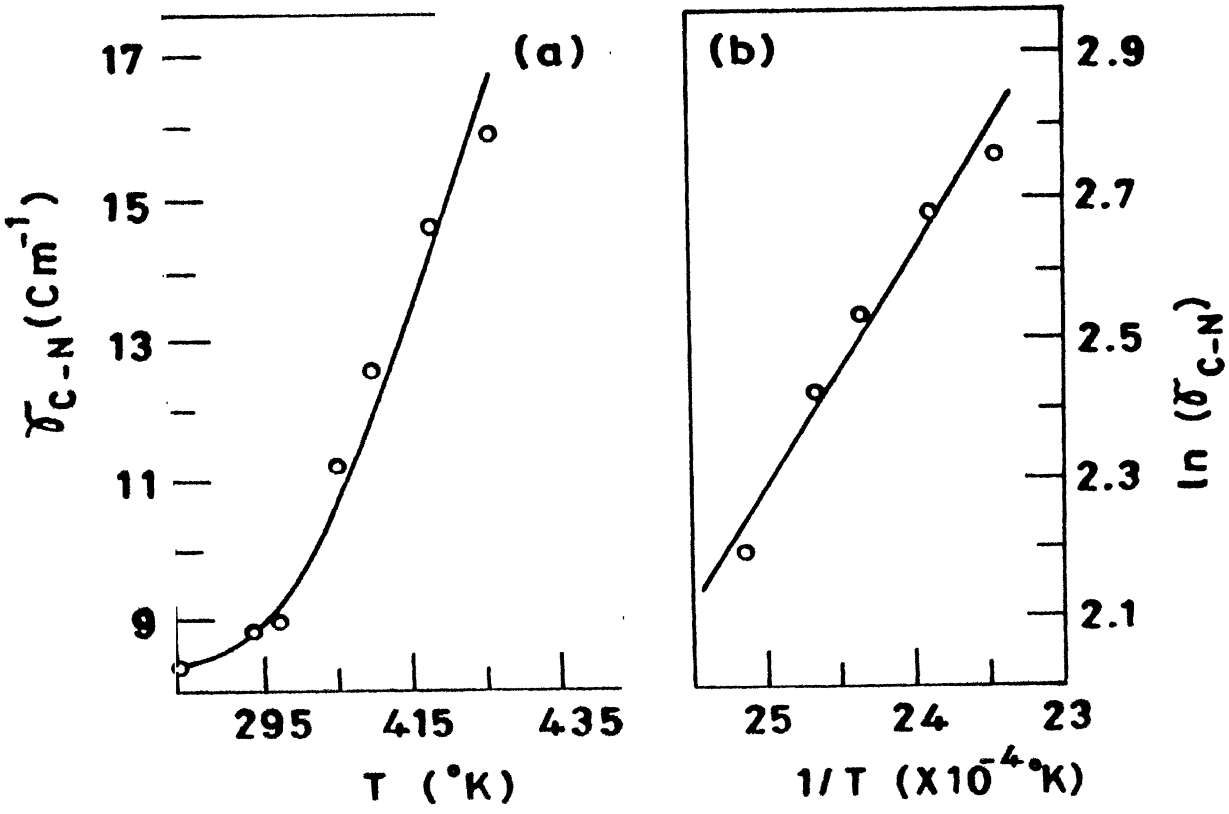

Figure 5.13: Rapid increase in the badnwidth (γ_{C-N}) of C-N stretching (Raman) mode near T_c. (a) γ_{C-N} versus T and (b) $\ln(\gamma_{C-N})$ versus $\frac{1}{T}$.

CHAPTER 6

VIBRATIONAL SPECTROSCOPY OF STRUCTURAL PHASE TRANSITIONS AND RAMAN EVIDENCE OF LIBRATIONAL FLUCTUATIONS IN THALLIUM THIOCYANATE

Abstract

The detailed analysis of Raman and IR spectra of Thallium thiocyanate (TlNCS) in the temperature range 293-438^{o}K has been carried out. Peak positions, bandwidths and relative strengths of almost all the vibrational modes have been measured. A careful search of the Raman spectra very close ($\geq$ 7 cm^{-1}) to the incident laser frequency revealed no soft modes. However, indirect manifestations of orthorhombic to tetragonal structural phase transition (SPT) have been found in large changes of bandwidths, peak positions and relative intensities of many thermosensitive internal and external modes near T $\simeq$ 367^{o}K (=T_c). More precisely, the linear variations in reduced peak intensities (I_2^r & I_3^r) of Raman external modes ν_2, ν_3 and complete disappearance of ν_2 mode at T_c symbolize the progressive reorientational disordering processes as T approaches T_c (from below). The values of β obtained from these measurements are (0.46 $\pm$0.04 and 0.45 $\pm$ 0.04) strikingly consistent. The characteristic temperature dependence of I_3^r for T above T_c has been attributed to thermal variations of correlation length and a mean field type correlation length exponent, $\nu \simeq 0.46 \pm 0.04$ has been extracted from the data. An abrupt increase in bandwidths of some of the external and internal modes near T_c has been attributed to the orientational disordering of NCS^- ions. An activation

energy $U \simeq 0.32 \pm 0.02$ ev, for the reorientational motion of NCS^- ions, has been calculated from the large changes in bandwidth of ν_3 near T_c. Like RbNCS, the appearance of side bands in the ν_{C-N}, ν_{C-S} and δ_{N-C-S} mode regions of Raman spectra can be related to splitting due to an internal field in the ordered orthorhombic phase. The continuous growth in the relative intensities and decrease in splitting energies reveal the gradual diminution of internal field as T approaches T_c.

Publications based on the material contained in this chapter are the following:

[A] S. Sathaiah, V.N. Sarin and H.D. Bist, Proc. Int.Conf. Raman Spectr. XI, England, 459 (1988).

[B] S. Sathaiah and H.D. Bist, J. Chem. Phys. (submitted).

6.1 Introduction

The general role of thermally activated disordering processes and critical fluctuations near an order-disorder SPT can be investigated spectroscopically by recording changes in the band profiles of thermosensitive external as well as internal modes [1-3]. A study of relationship between the spectral manifestations of disorder in regions of both the internal and external modes is expected to enhance the amount of information that can be deduced from such investigations [4-6]. With these points in view, a comprehensive temperature (T) dependent vibrational study of SPT in TlNCS in the range 293-438^{o}K has been carried out. The spectroscopic characterizations of disorder in TlNCS are presented here for the first time.

6.2 Crystal Structure

At room temperature (RT), TlNCS crystallizes in an ordered orthorhombic structure. The symmetry of the structure has been related to the space group Pbcm (D_{2h}^{11}) with four formula units in the primitive cell [7,8]. From thermal (DTA and DSC) [9] and x-ray diffraction [10] studies TlNCS was found to undergo a transition around $T_c \simeq 363^{o}$K from orthorhombic structure to disordered tetragonal phase (I). The transition has been identified as second order on the basis of continuous changes in volume and latent heat of transformation.

6.3 Experimental

For Raman spectral measurements, 514.5 nm radiation of $\simeq$ 20 mW power, from an Ar^{+} laser was used to excite the sample; a

Spex Ramalog system to record the spectra. IR spectra were recorded using Perkin Elmer 580 double beam spectrometer. The details of the experimental set up are same as given in chapter 2. The average heating rates in the present Raman and IR measurements were $\simeq$ 0.3 and 0.5^{o}K min^{-1}, respectively.

6.4 Results

6.4.1 Raman Spectrum at Room Temperature

The room temperature Raman spectrum of TlNCS powder is shown in Figure 6.1. The predominant bands below 150 cm^{-1} correspond to lattice modes and all other above 150 cm^{-1} are due to internal and multiphonon modes. Peak frequencies, relative strengths and probable mode assignments of all bands are listed in Table 6.1. Given mode assignments are inferred by comparing RT and T dependent data of TlNCS with other reported data on isomorphous MNCS (M=K, Rb) systems [11,12]. The lattice modes at ν_1=26, ν_2=40.5 & ν_4=142 cm^{-1} can be attributed to translatory modes. Whereas, the stronger band at ν_3=73 cm^{-1} is due to in-plane (N-C-S containing plane) rotatory mode (whose bandwidth is highly thermosensitive). The weaker feature at 57 cm^{-1} is probably a multiphonon mode.

In the internal mode region, stronger bands at ν_{C-N} = 2029 and ν_{C-S} = 736 cm^{-1} are C-N and C-S stretching modes, whereas $\delta^{a}_{N-C-S} \simeq$ 463 and $\delta^{b}_{N-C-S} \simeq$ 456 cm^{-1} are in-plane and out-of-plane bending modes of NCS^{-} ions. The bands at 916 and 930 cm^{-1} are the overtones of δ_{N-C-S} fundamentals. Bands at ν'_{C-N} = 1987 and

2007cm^{-1} ; and ν'_{C-S} = 728 cm^{-1} are C-N and C-S stretching modes of N-^{13}C-S and ^{15}N-C-S isotopic species. The weaker and broader features are probably due to multiphonon processes involving $\nu_{C-N} \pm L_{cp}$ (L_{cp} represents the critical point frequencies of lattice modes). Like RbNCS, the side bands at 2046, 731 and 460 cm^{-1} display increase in relative strength, gradual decrease in separation and merging into the main bands as T approaches T_c. So the appearance of these side bands at RT can be related to splittings due to an internal field in the orthorhombic TlNCS.

6.4.2 IR Spectrum at RT

The unpolarized IR transmittance spectrum of TlNCS is given in Figure 6.2. The dominant bands at ν_{C-N} = 2060 and ν_{C-S} = 745 cm^{-1} are C-N and C-S stretching modes. Whereas δ^{a}_{N-C-S} = 483 and δ^{b}_{N-C-S} = 469 cm^{-1} are in-plane and out-of-plane bending modes. Bands at 949 and 967 cm^{-1} are the overtone and combination modes of δ_{N-C-S} fundamentals. The weaker feature at 2015 cm^{-1} is a C-N stretching mode of N-^{13}C-S isotope. The shoulders at 767 and 2080 cm^{-1} are probably due to multi-phonon processes involving ν_{C-N} and L_{cp}.

6.4.3 Thermal Behaviour of Raman Modes

Thermal evolution of Raman spectra of TlNCS powder in the external mode region is shown in Figure 6.3, for various temperatures below and above T_c. On increasing temperature, gradual changes in the spectra can be seen. The most interesting

(Figure 6.6(b)) of $\log I_2^r$ versus $\log|T-T_c|$ gives an exact straight line with a slope of 0.91 ± 0.08. So the peculiar linear variation in I_2^r can be represented as $I_2^r \propto (|T-T_c|)^{2\beta}$ with an order parameter exponent $\beta \simeq 0.46 \pm 0.04$ for $300 \leq |T-T_c| \leq 367^oK$. The characteristic linear behaviour of I_2^r has been verified by repeating the experiment. The values of β and T_c obtained by the repeated experiment are $\beta \simeq 0.46 \pm 0.04$ and $T_c = 365^oK$. Similar linear variation in the reduced peak intensity I_3^r has been observed for ν_3 mode. But I_3^r does not become zero, it only changes in its slope at T_c, and then decreases slowly for $T>T_c$. Typical changes in the normalized $[I_3^r - I_D^r]$ versus T are plotted in Figure 6.6(c) for $300 \leq T \leq 367^oK$. Where I_D^r represents intensity contribution from the order parameter fluctuations near T_c and it has been extracted from the T dependence of I_3^r for $367 \leq T \leq 400^oK$ (the detailed description is given in section 6.5.3). A log-log plot of $[I_3^r - I_D^r]$ versus $(|T-T_c|)$ gives an exact straight line (Figure 6.6(d)) with a slope of 0.9 ± 0.08. Thus a consistent value of $\beta \simeq 0.45 \pm 0.04$ has been obtained by expressing $[I_3^r - I_D^r] \propto |T-T_c|^{2\beta}$.

Raman spectra in the internal mode region, at various temperatures above and below T_c, are given in Figure 6.7. As T increases, peak intensities of all internal modes decrease, while their bandwidths increase with some gradual variations in peak positions. It is interesting to note that the side band ($\simeq$ 2046 cm^{-1}, at RT) on the higher frequency side of the main ν_{C-N} mode (Figure 6.7(a)) grows in its relative intensity at the expense of decrease in the peak intensity of the main ν_{C-N} mode as T

(Figure 6.6(b)) of $\log I_2^r$ versus $\log|T-T_c|$ gives an exact straight line with a slope of 0.91 ± 0.08. So the peculiar linear variation in I_2^r can be represented as $I_2^r \propto (|T-T_c|)^{2\beta}$ with an order parameter exponent $\beta \simeq 0.46 \pm 0.04$ for $300 \leq |T-T_c| \leq 367^oK$. The characteristic linear behaviour of I_2^r has been verified by repeating the experiment. The values of β and T_c obtained by the repeated experiment are $\beta \simeq 0.46 \pm 0.04$ and $T_c = 365^oK$. Similar linear variation in the reduced peak intensity I_3^r has been observed for ν_3 mode. But I_3^r does not become zero, it only changes in its slope at T_c, and then decreases slowly for $T>T_c$. Typical changes in the normalized $[I_3^r - I_D^r]$ versus T are plotted in Figure 6.6(c) for $300 \leq T \leq 367^oK$. Where I_D^r represents intensity contribution from the order parameter fluctuations near T_c and it has been extracted from the T dependence of I_3^r for $367 \leq T \leq 400^oK$ (the detailed description is given in section 6.5.3). A log-log plot of $[I_3^r - I_D^r]$ versus $(|T-T_c|)$ gives an exact straight line (Figure 6.6(d)) with a slope of 0.9 ± 0.08. Thus a consistent value of $\beta \simeq 0.45 \pm 0.04$ has been obtained by expressing $[I_3^r - I_D^r] \propto |T-T_c|^{2\beta}$.

Raman spectra in the internal mode region, at various temperatures above and below T_c, are given in Figure 6.7. As T increases, peak intensities of all internal modes decrease, while their bandwidths increase with some gradual variations in peak positions. It is interesting to note that the side band ($\simeq$ 2046 cm^{-1}, at RT) on the higher frequency side of the main ν_{C-N} mode (Figure 6.7(a)) grows in its relative intensity at the expense of decrease in the peak intensity of the main ν_{C-N} mode as T

approaches T_c. In addition, bandwidths and peak positions of the main ν_{C-N} modes increase abruptly near T_c. Finally, a single and broader band can be seen in the ν_{C-N} region for $T>T_c$. Similarly, the structure on the low frequency sides of ν_{C-S} (Figure 6.7(b)) and δ_{N-C-S} (Figure 6.7(c)) gradually increase in their strengths as T approaches T_c. Finally, for $T>T_c$, broad bands with large asymmetric wings on the low frequency sides can be seen in the ν_{C-S} and δ_{N-C-S} regions.

Typical changes in peak intensity I_{C-N}, bandwidth γ_{C-N} of C-N stretching mode and peak frequencies of all the internal modes with T are plotted in Figure 6.8. I_{C-N} decreases continuously (Figure 6.8(a)) with a change in the slope around T_c. Whereas, γ_{C-N} [denoted by O or Δ in Figure 6.8(a)] increases linearly with T showing an abrupt jump near T_c. There are only marginal changes in the peak positions for T well below T_c. As T approaches T_c, ν_{C-N} increases anomalously (Figure 6.8(b)) while there is a continuous decrease in ν_{C-S} (Figure 6.8(c)) and δ_{N-C-S} (Figure 6.8(d)) modes. All the observed changes in Raman spectra are reversible during heating and cooling cycles without any hysteresis in T_c value.

6.4.4 Temperature Dependence of IR Spectra

IR spectra in the internal mode region are presented in Figures 6.2 and 6.9 for different temperatures below and above T_c. As T increases gradual changes in the band profiles of ν_{C-N} (Figure 6.9(a)), ν_{C-S} (Figure 6.9(b)) and δ_{N-C-S} (Figure 6.9(c)) can be seen. Typical changes in peak intensities, bandwidths and peak positions of the internal modes are plotted in Figure 6.10.

The peak intensity of the side band ($\simeq$ 2083 cm^{-1}) in the ν_{C-N} region (Figure 6.9(a)) increases continuously with T (Figure 6.10(a)). Whereas, the peak intensity of the main ν_{C-N} mode remains constant (Figure 6.10(b)) throughout the studied T range. The peak intensity I_{C-S} of ν_{C-S} mode (Figure 6.10(c)) decreases continuously with a change in its slope around 365°K ($\simeq T_c$). There is only a marginal variation in I_{C-S} between 365-385°K and it decreases anomalously for T>385°K. Peak intensity of δ^a_{N-C-S} mode remains constant till 355°K and then decreases continuously with a change in its slope around 367°K (Figure 6.10(d)). Between 367-390°K it shows a marginal variation and an anomalous diminution for T>390°K . Peak intensity of δ^b_{N-C-S} remains almost constant except for a small jump around 367°K (T_c) (Figure 6.10(d), o points). Figures 6.10(e)and(f),respectively, show the increase in the band width γ_{C-N} and peak frequency ν_{C-N} of C-N stretching mode near and above T_c.Whereas peak frequencies ν_{C-S} [Figure 6.10(g)] and δ^a_{N-C-S}[Figure 6.10(h)] remain almost constant until 390°K, decrease anomalously between 390-415°K and once again become constant for T > 415°K. Peak frequency δ^b_{N-C-S} remain constant throughout the studied temperature range (293-438°K) [Figure 6.10(h)].

6.5 Discussion

All observed changes in Raman spectra, e.g. (i) the anomalous enhancement in bandwidths γ_{C-N} and γ_3, (ii) significant changes in peak frequencies ν_{C-N} and ν_3, (iii) linear decrease in relative intensities I^r_2 and I^r_3 and (iv) the complete disappearance of ν_2 mode around 367°K reveal an order-disorder

SPT at that temperature. Similarly, changes in the IR spectra indicate the transition to be at 367 ± 2°K. The T_c values obtained from both experiments are in good agreement with the reported $T_c \simeq 363^{o}K$ from x-ray and thermal investigations [10]. Consistent spectral results in both heating and cooling cycles without any hysteresis in T_c values are in accordance with the reversibility and second order nature of the transition. The IR spectral changes in the ν_{C-S} and δ_{N-C-S} modes indicate another possible transition around $410^{o}K$, which needs further investigation.

6.5.1 Anomalous Increase in γ_3 and Calculation of Activation Energy

A careful search of the Raman spectra closer to (i.e. ≥ 7 cm^{-1}) the incident laser frequency revealed no soft modes associated with the transition. Generally, in order-disorder transitions, the soft mode is likely to be a diffusive large amplitude motion which may be too low in frequency to be observed by Raman spectroscopy [13,14]. However, an indirect manifestation of this relaxational motion has been observed in the large changes of bandwidth (γ_3) of a rotatory mode ν_3. The anomalous increase in γ_3 (Figure 6.11(a)) in the vicinity of T_c (i.e. $358 \leq T \leq 367^{o}K$) can be fitted in the (Arrehenius law) expression $\gamma_3 \propto e^{-U/K_BT}$, where U = activation energy for the re-orientational motion of NCS^- ions and K_B= Boltzmann constant. A plot of $\ln\gamma_3$ versus 1/T (Figure 6.11(b)) gives an exact straight line. The value of U ≃ 0.32 ± 0.02 ev extracted from the slope is

in good agreement with the values, U = 0.41, 0.29 ± 0.02 ev obtained for KNCS [15] and RbNCS [Chapter 5] systems, respectively.

6.5.2 Raman Activity of Hard Mode

The existence of soft modes in Raman spectra is the most interesting manifestation of SPTs in solids. But it is by no means the only striking spectral change induced by SPTs [16]. The most striking spectral manifestations of SPTs occur for some of the modes which are not directly involved in the phase transition. These modes are called hard modes and they consist in either activation of silent modes and/or splitting of degenerate modes below T_c. As described in chapter 1, a quantitative account of mode splittings, relative strengths of new bands and their temperature dependences can be made on the basis of an evaluation of the coupling between the order parameter and other relevant degrees of freedom.

In TlNCS, the external mode ν_2 is found to be Raman active below T_c and inactive above T_c. It is interesting to note that the reduced peak intensity I_2^r of ν_2 mode varies linearly with T {i.e. $I_2^r \propto |T-T_c|^{0.9}$}, like square of the order parameter (η). This peculiar linear behavior of I_2^r suggests that the thermodynamic potential involving η^2 as one of its lowest invariants may describe the effects induced by SPT in TlNCS. Indeed such an expression for free energy involving η^2 invariants has been proposed by Schranz et.al [17] to explain some of the experimental results in an isomorphous KNCS system.

6.5.3 Critical Scattering and Correlation Length Exponent

Deep in the ordered phase, the reduced peak intensity I_3^r of ν_3 mode also varies linearly with T, implying that it is solely governed by long-range order. But as T approaches T_c there is an additional contribution to I_3^r evidently from the fluctuations of η. Fluctuating clusters of η appear and enhance in their sizes as T approaches T_c. The size of these clusters can be described by a correlation length $\xi \propto (|T-T_c|)^{-\nu}$, where ν is the correlation length exponent. The effect of fluctuating clusters has been considered by Dultz [18] to explain the critical light scattering intensity near an order-disorder transition in KCN system. According to that theory the Raman scattered intensity in the disordered phase can be related to ξ by

$$I^r = a + b\left[\, 1 - \frac{\tan^{-1} k_o\xi}{k_o\xi} \,\right] \qquad (6.1)$$

Where a and b are temperature independent parameters and k_o is the radius of a small spherical region in k space around the critical wave vector k_c (i.e. k_o is the wave vector where fluctuations become critical). To select only small number of phonons with wave vectors near k_c, the peak height has to be considered in the quantitative analysis instead of integrated intensity. Along similar lines, the I_3^r in TlNCS, for $T \geq T_c$ can be assumed to depend only on temperature via ξ. The product $k_o\xi$ at different temperatures between 367-400^{o}K has been obtained by fitting the data on temperature dependence of I_3^r (Figure 6.12(a)) to the expression (6.1). A log-log plot (Figure 6.12(b)) between $k_o\xi$

and $(T-T_c)$ gives an exact straight line with a slope of (-0.46 ± 0.04). The product $k_o\xi$ in Figure 6.12 represents the actual correlation length (ξ) measured in the units of reciprocal radius k_o^{-1}. So, the temperature dependence of ξ can be expressed as $\xi \propto (|T-T_c|)^{-\nu}$ with $\nu = 0.46 \pm 0.04$. The observed exponents $\beta \simeq 0.46 \pm 0.04$ and $\nu \simeq 0.46 \pm 0.04$ are strikingly consistent with mean field values.

6.5.4 Raman Internal Modes and Local Field

Like in RbNCS, the appearance of side bands and characteristic changes in relative intensities and peak frequencies of ν_{C-N}, ν_{C-S} and δ_{N-C-S} modes can be explained by considering the existence of an internal field ($E_\uparrow$) in the ordered orthorhombic phase of TlNCS. The stronger bands in ν_{C-N}, ν_{C-S} and δ_{N-C-S} regions, at RT, can be attributed to Raman transitions from NCS^- groups which form an aligned ($E_\uparrow$) dipole configuration. Whereas, the side bands at higher frequency side of the main ν_{C-N} or lower frequency sides of main ν_{C-S} and δ_{N-C-S} modes correspond to the spectral components of the counter aligned ($E\downarrow$) dipole configuration. The gradual growth in relative strengths of side bands at the expense of decrease in the relative intensities of corresponding main bands reveals an increase in the population of the counter aligned dipoles while the main electric field diminishes as T approaches T_c. The anomalous increase (or decrease) in the main ν_{C-N} (or ν_{C-S} or δ_{N-C-S}) mode and the gradual merging of the main and side bands into a broad singlet are also in accordance with [Equations (5.1) and (5.2)], the

internal field diminution, as T approaches T_c. Additionally, the appearance of side bands at the lower frequency sides of the main ν_{C-S} and δ_{N-C-S} modes and the gradual decrease in the peak frequencies of main bands as $T \longrightarrow T_c$, in contrast to ν_{C-N} modes, suggest that the internal field influences C-N; and C-S and N-C-S oscillators in an opposite manner.

References

[1] J.P. Lemaistre, R. Ouillon B. Perrin and P. Ranson in "Dynamical processes in condensed molecular systems", eds. J. Klafter, J. Jortner and A.Blumen, (World Scientific, Singapore, 1989).

[2] J.B. Sokoloff, Phys. Rev. B. 5 (12), 4962 (1971).

[3] V.L. Ginzburg, A.P. Levanyuk and A.A Sobyanin, Phys. Reports 57 (3), 151 (1980).

[4] A.D. Bruce, W. Taylor and A.F. Murray, J. Phys. C: Solid St. Phys. 13, 483 (1980).

[5] P.da. R. Andrade, A.D. Prasad Rao, R.S. Katiyar and S.P.S. Porto, Solid St. Comm. 12, 847 (1973).

[6] D. Durand, L.C. Scavarda do Carmo and F. Luty, Phy. Rev. B39, 6096 (1989).

[7] W. Büssem, P. Günther and R. Tubin, Z. Phys. Chem. B 24, 1 (1934).

[8] C. Akers, S.W. Peterson and R.D. Willet, Acta Crystallogra B 24, 1125 (1968).

[9] W. Klement Jr. and C.W.F.T. Pistorius, Bull. Chem. Soc. Jpn. 49, 2148 (1976).

[10] R. Lippman and R. Rudman, J. Chem. Phys., 79 (7), 3457 (1983).

[11] S.S. Ti, S.F.A. Kettle and Ø. Ra, spectrochimica Acta. 32A, 1603 (1976).

[12] M.J. Joyce and F. Ninio, Aust. J. Phys. 42, 389 (1989).

[13] J.F. Scott, Rev. Mod. Phys. 46, 83, (1974).

[14] Z. Iqbal and C.W. Christoe, J. Chem. Phys. 62, 3246 (1975).

[15] F.J. Owens, Solid St. Commun. 29, 789 (1979).

[16] J. Petzelt and V. Dvorak in "Vibrational Spectroscopy of Phase transitions" eds. Z. Iqbal and F.J. Owens (Academic Press, Orlando, 1984) p. 76.

[17] W. Schranz, H. Warhanek and P. Zielinski, J. Phys. Condens. Matter. 1, 1141 (1989).

[18] W. Dultz, J. Chem. Phys. 65 (7), 2812 (1976).

Table 6.1 : Vibrational frequencies, relative strengths and tentative assignments of Raman active modes in TlNCS at room temperature

(a) External and Internal modes

	Vibrational fequency (cm^{-1})	Relative strength	Mode assignment †
External Modes	26	ms	T
	40.5	ms	T
	57	sh	multi-phonon ?
	73	vs	R
	142	vs	T
Internal Modes	456	w	δ^{b}_{N-C-S}
	460	w	$\delta^{a}_{N-C-S}{}^{(E\downarrow)}$
	463	w	$\delta^{a}_{N-C-S}{}^{(E_{\uparrow})}$
	731	m	$\nu_{C-S}{}^{(E\downarrow)}$
	736	s	$\nu_{C-S}{}^{(E_{\uparrow})}$
	2029	vs	$\nu_{C-N}{}^{(E_{\uparrow})}$
	2046	m	$\nu_{C-N}{}^{(E\downarrow)}$

(b) Multi-phonon modes and internal modes of isotopic species

	Vibrational fequency (cm^{-1})	Relative strength	Mode assignment	Critical point L_{cp} frequency
Multi-phonon Modes	916	w	$2\delta^{b}_{N-C-S}$	
	930	m	$2\delta^{a}_{N-C-S}$	
	1960	vw	$\nu_{C-N}{}^{-L}{}_{cp}$	69
	2066	w	$\nu_{C-N}{}^{+L}{}_{cp}$	37
	2109	vw	$\nu_{C-N}{}^{+L}{}_{cp}$	80
Internal Modes of Isotopic Species	728	m	$^{13}C\ \nu'_{C-S}$	
	1987	m	$^{13}C\ \nu'_{C-N}$	
	2007	w	$^{15}N\ \nu'_{C-N}$	

† Inferred from [11,12]

Table 6.2 Vibrational frequencies and assigments of IR active internal and multi-phonon modes in TlNCS at 298°K

Vibrational fequency (cm^{-1})	Relative strength	Mode assignment
469	m	δ^{b}_{N-C-S}
483	s	δ^{a}_{N-C-S}
745	s	ν_{C-S}
767	w	Multi-phonon
949	w	$\delta^{a}_{N-C-S}+\delta^{b}_{N-C-S}$
967	w	$2\delta^{a}_{N-C-S}$
2015	w	$^{13}C\ \nu'_{C-N}$
2060	vs	ν_{C-N}
2080	sh	Multi-phonon

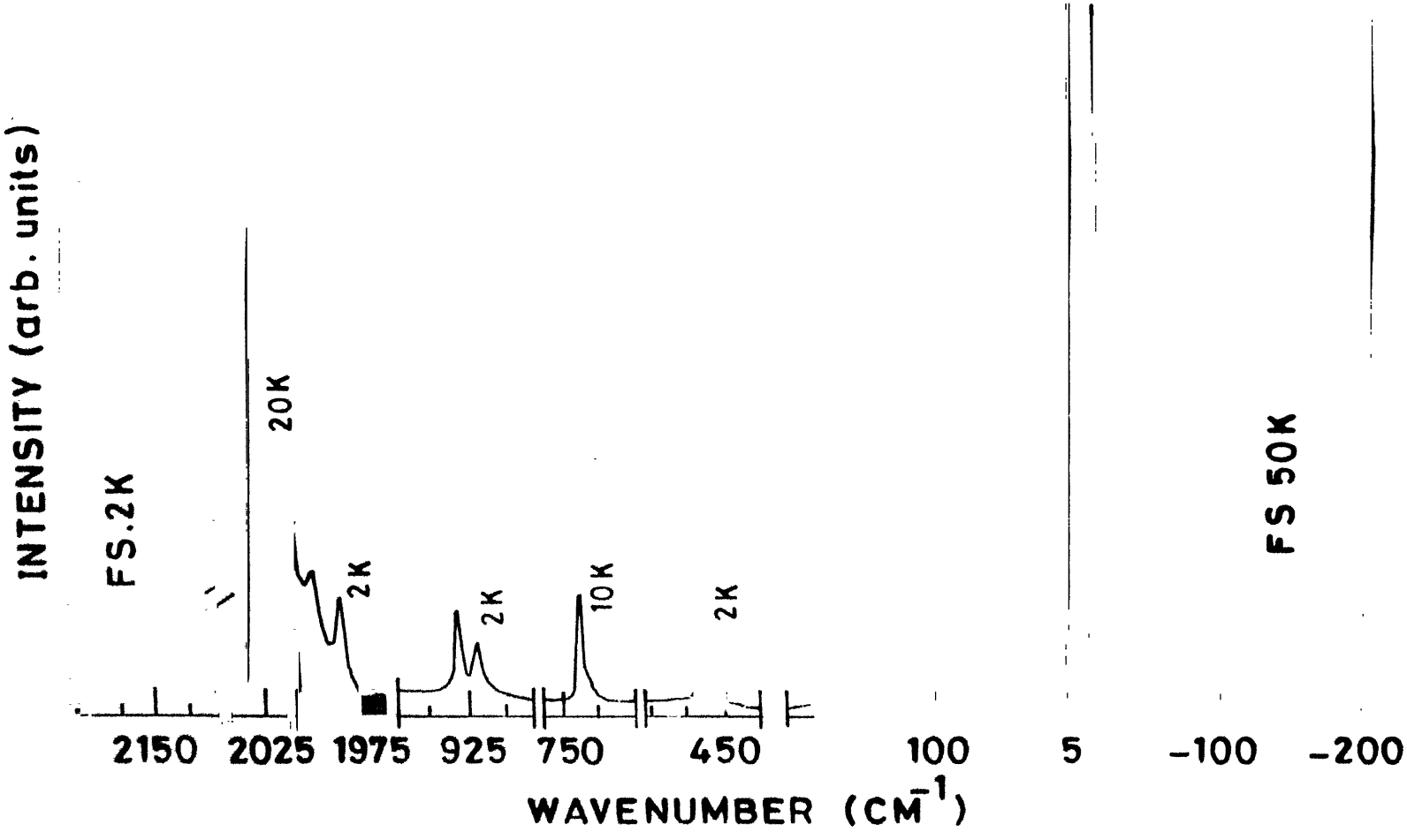

Figure 6.1: Unpolarized Raman spectrum of TlNCS powder at room temperature (i.e. 298°K). FS: 50K, 20K, 10K and 2K are the recording sensitivities (photon counts/sec.).

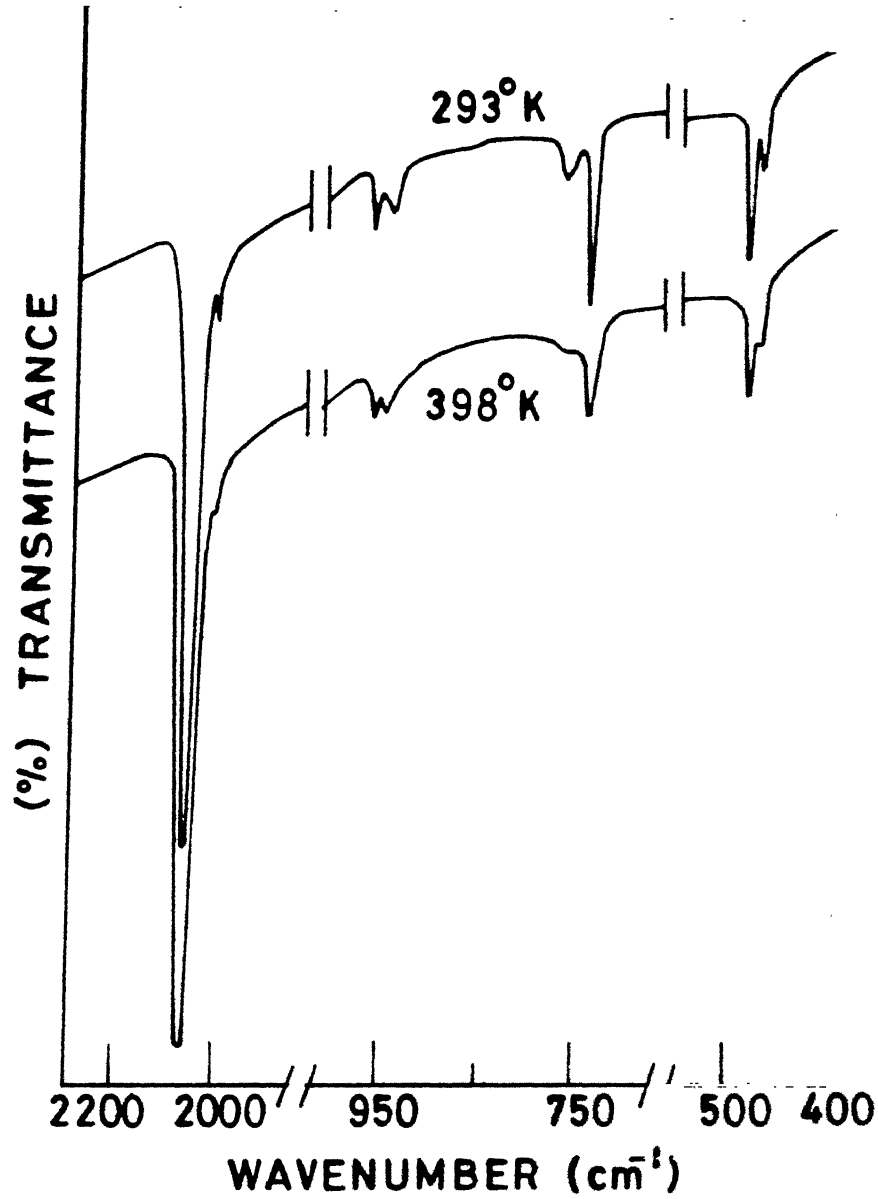

Figure 6.2: Infrared spectra of TlNCS at 293°K and 398°K.

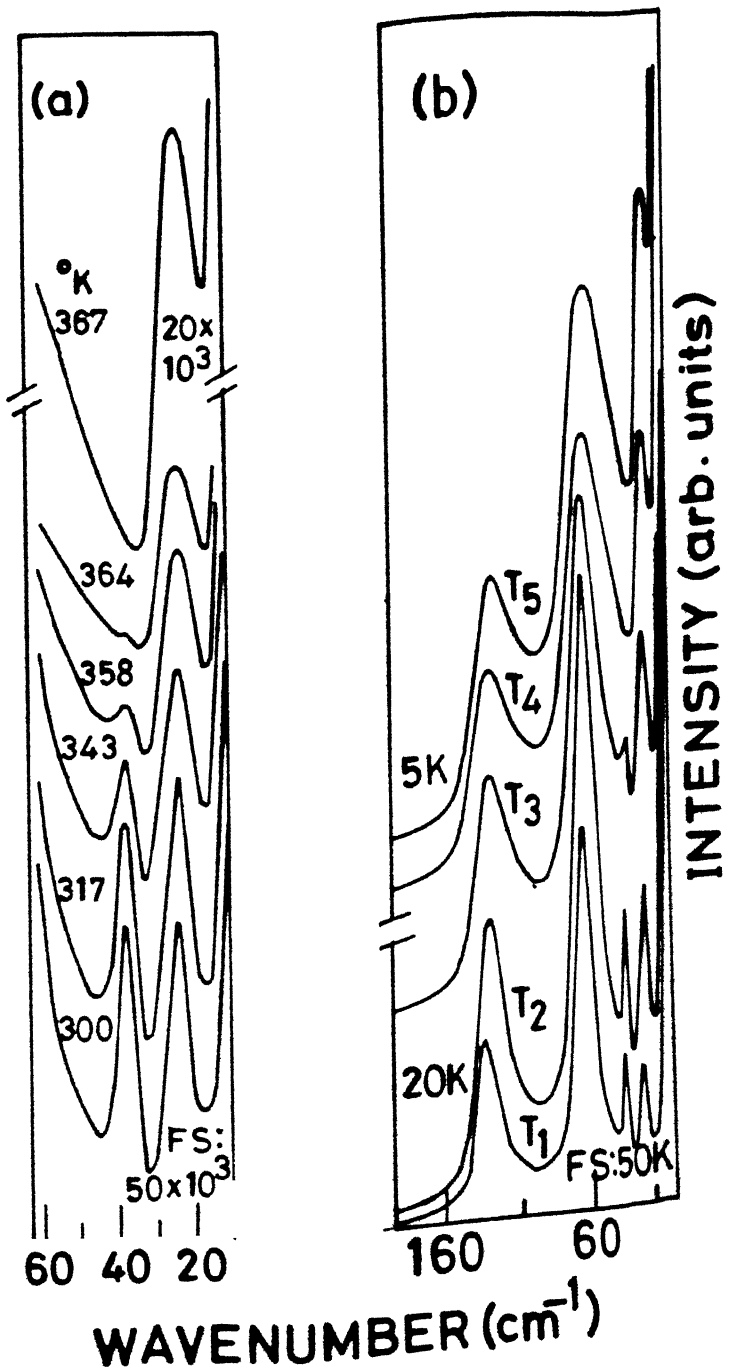

Figure 6.3: Temperature evolution of Raman spectra in th external mode (a) 5 - 55 cm^{-1} and (b) 5 - 180 cm^{-1} regions. T_1 t T_5 are the temperatures 297, 324, 354, 365 and 390°K, in the order.

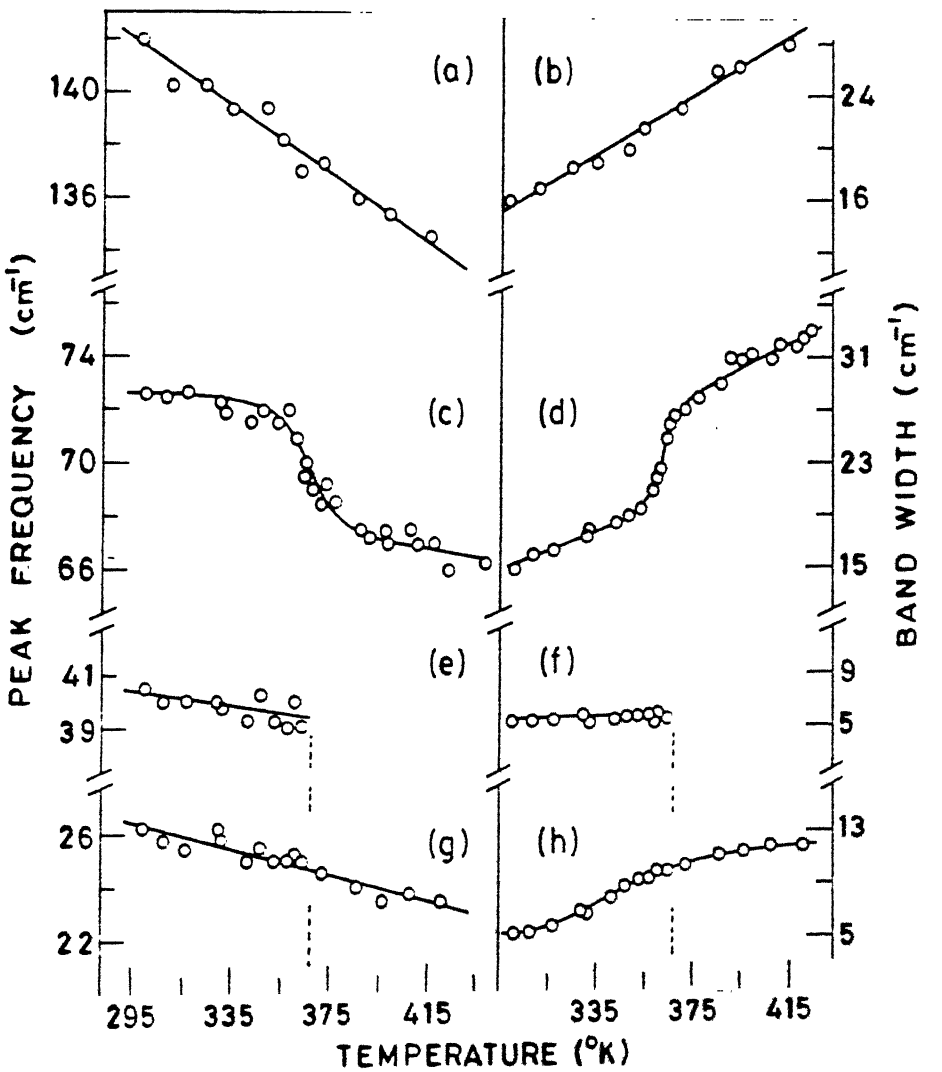

Figure 6.4: Temperature dependence of the peak positions (ν_i) and bandwidths (γ_i) of Raman external modes. (a)ν_4, (b) γ_4, (c) ν_3, (d) γ_3, (e) ν_2, (f) γ_2, (g) ν_1, and (h) γ_1 versus T, respectively.

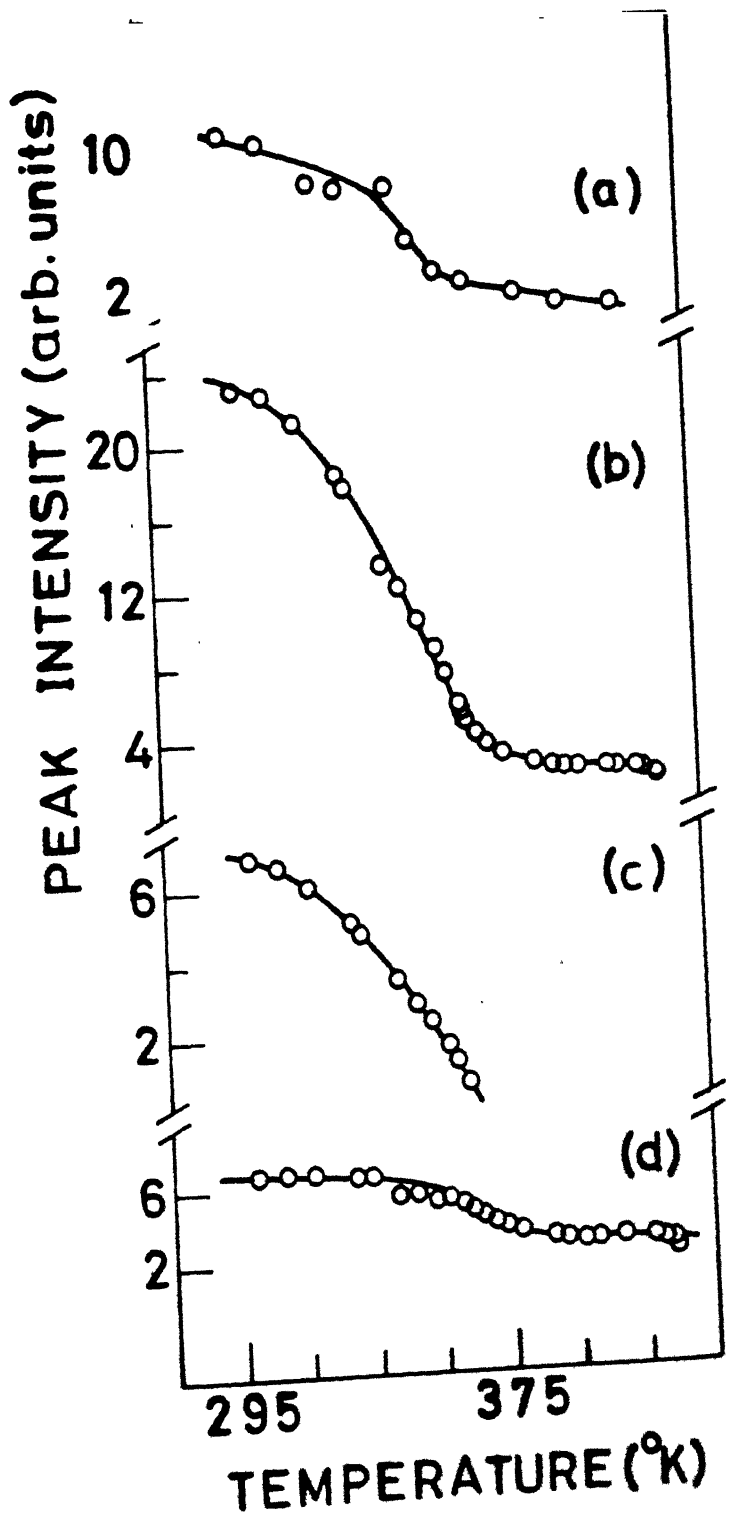

Figure 6.5: Peak intensities of Raman external modes. (a) I_4, (b) I_3, (c) I_2 and (d) I_1 versus T, respectively.

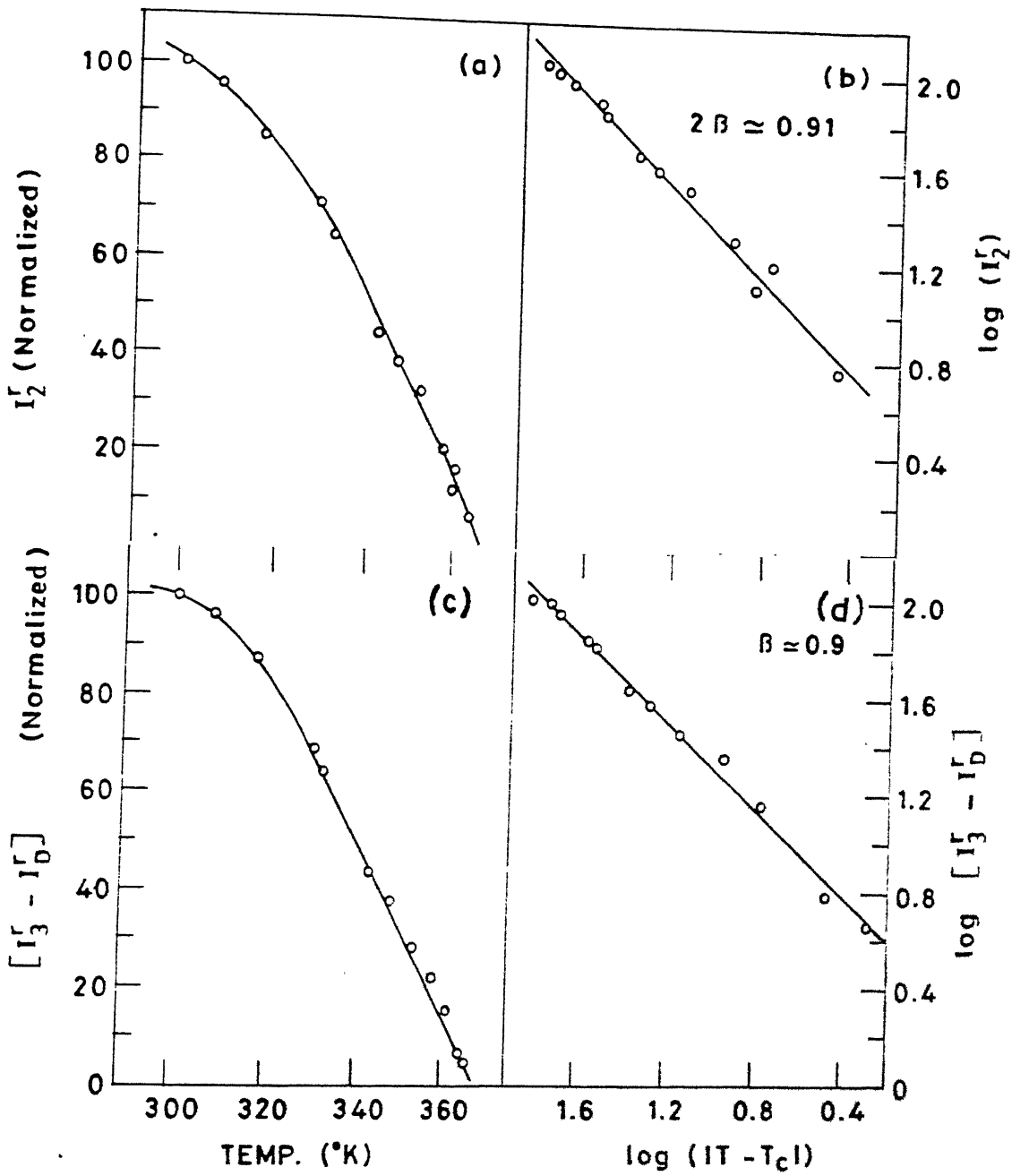

Figure 6.6: The linear variation in the reduced peak intensities (I_2^r and I_3^r) of Raman external modes with T. (a) I_2^r (normalized) versus T, (b) log(I_2^r) versus log(|T-T_c|), (c) (I_3^r-I_D) versus T and (d) log(I_3^r-I_D) versus log(|T-T_c|)

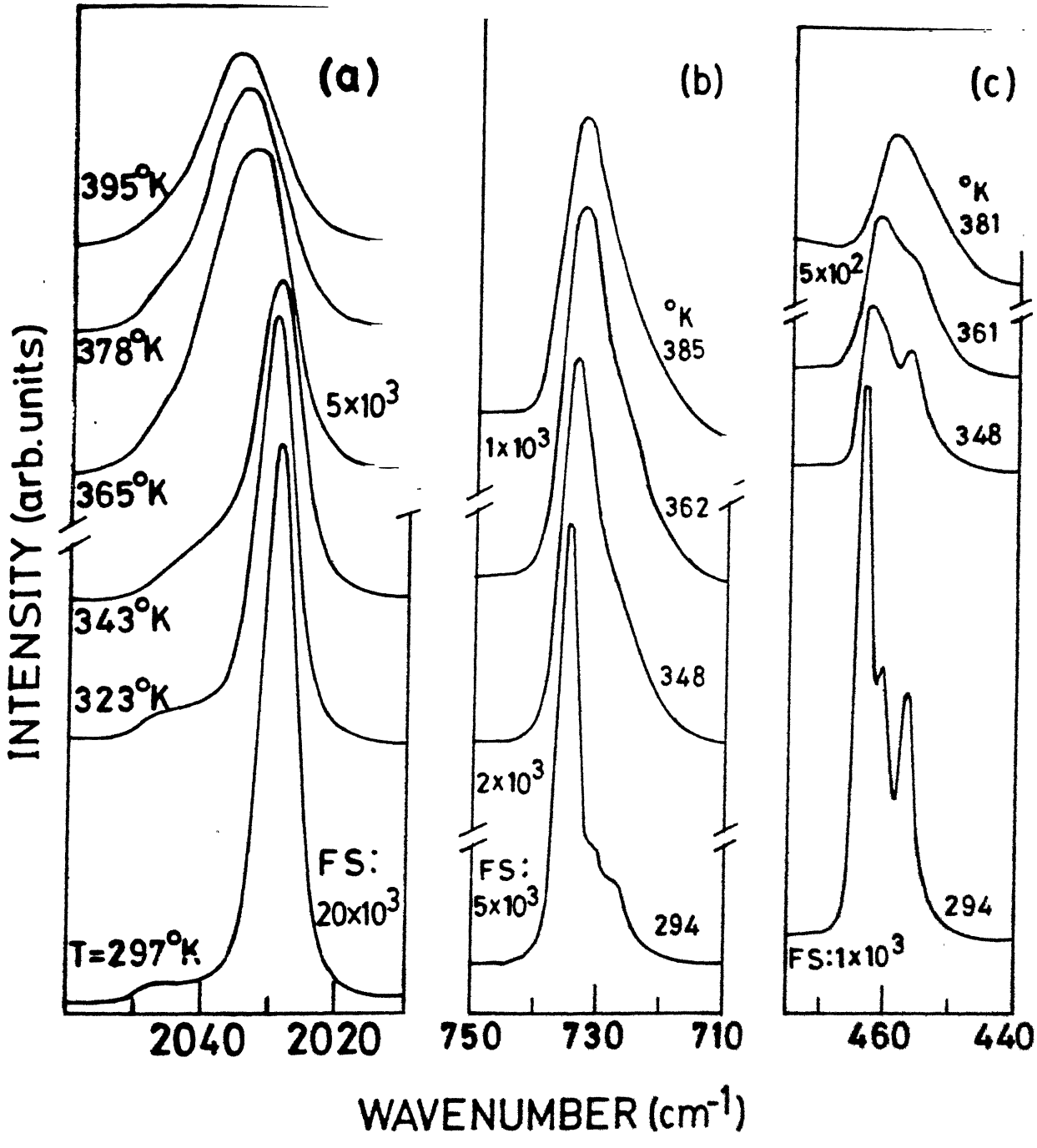

Figure 6.7: Thermal evolution of Raman spectra in the (a) C-N stretching, (b) C-S stretching and (c) N-C-S bending mode regions.

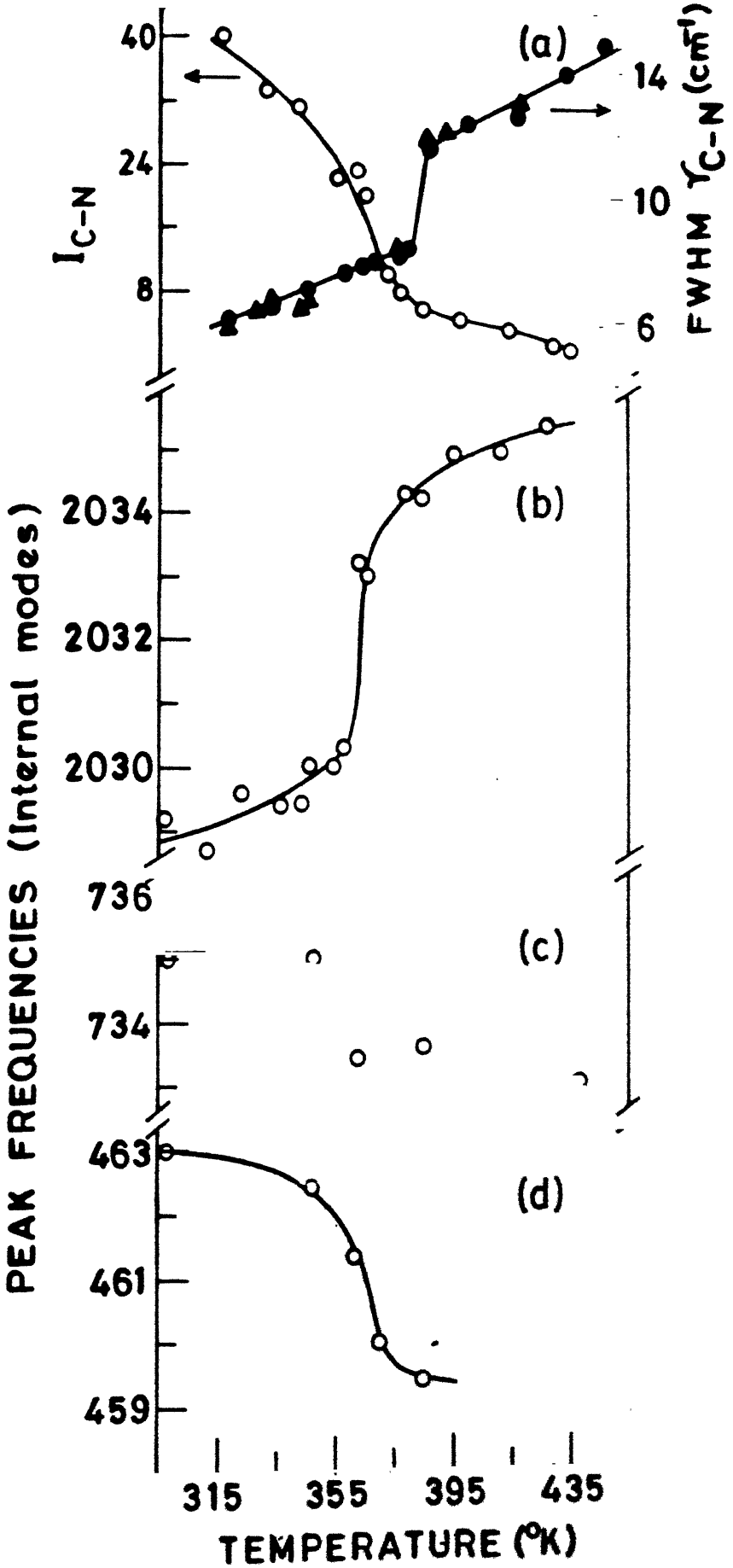

Figure 6.8: Typical changes with temperature in: (a) the peak intensity I_{C-N} (0-points)and bandwidth γ_{C-N} (O & Δ represent data in heating and cooling cycles, respectively); and peak positions: (b) ν_{C-N}, (c) ν_{C-S} and (d) δ_{N-C-S} of Raman internal modes.

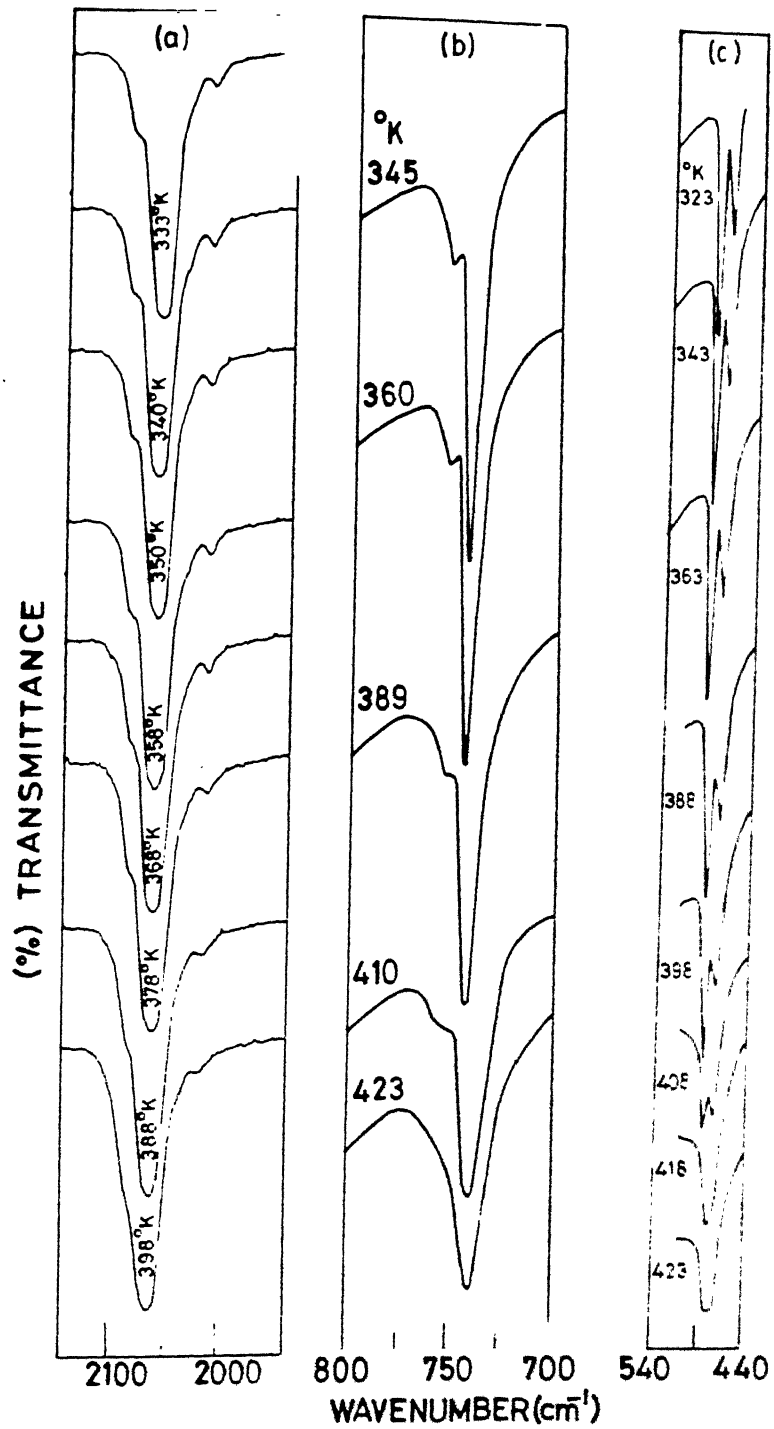

Figure 6.9: Thermal behaviour of IR spectra in the (a) C-N stretching (b) C-S stretching and (c) N-C-S bending mode regions.

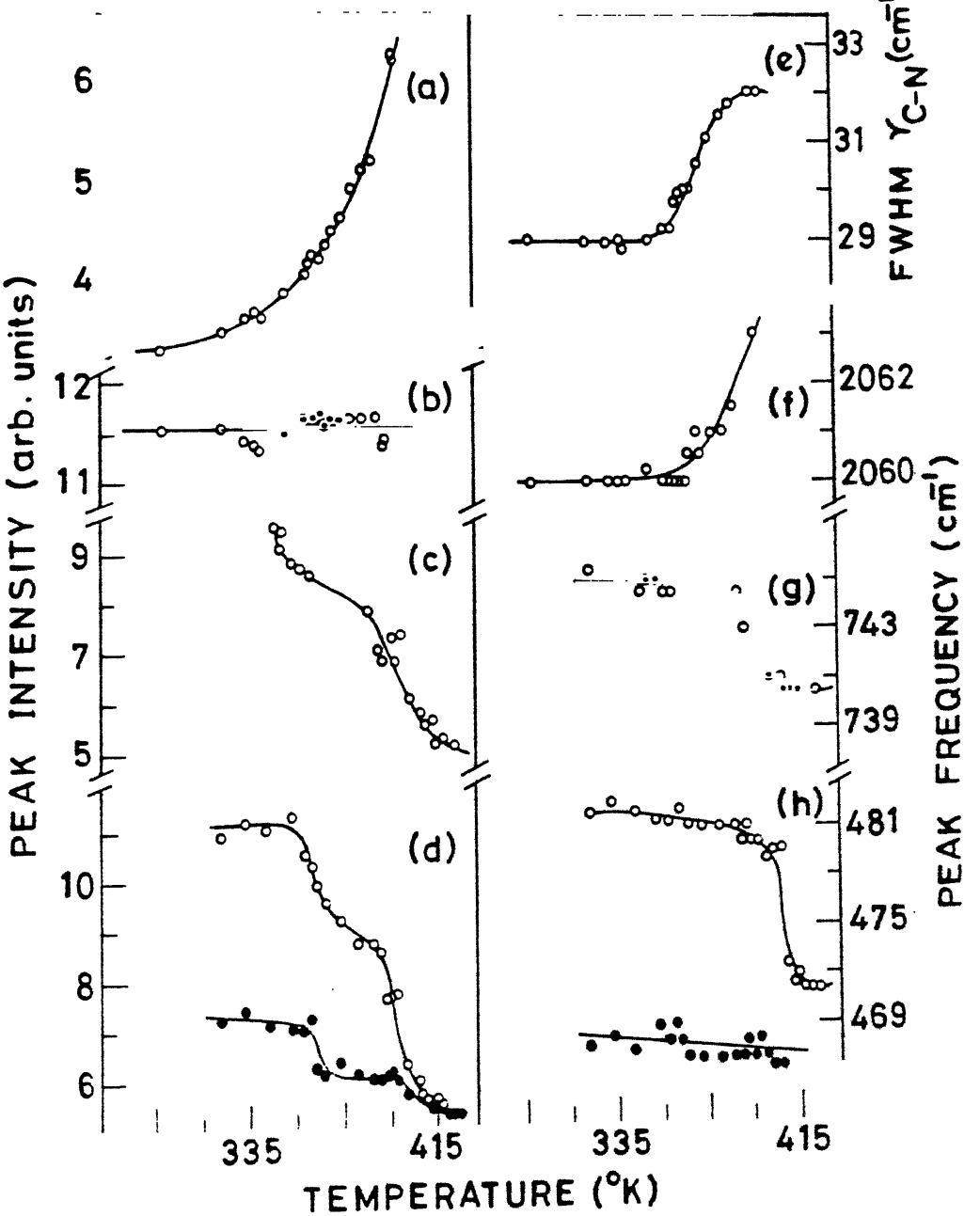

Figure 6.10: Typical changes in the peak frequencies, intensities and halfwidths of IR internal modes: Peak intensities of (a) a shoulder at 2080 cm^{-1}, (b) C-N stretching (ν_{C-N}), (c) C-S stretching (ν_{C-S}) and (d) in-plane bending (δ^{a}_{N-C-S}) and out-of-plane bending (δ^{b}_{N-C-S}) modes versus temperature; (e) Bandwidth γ_{C-N} versus T; and peak frequencies (f) ν_{C-N}, (g) ν_{C-S} and (h) δ^{a}_{N-C-S} & δ^{b}_{N-C-S} (denoted by O points) versus T.

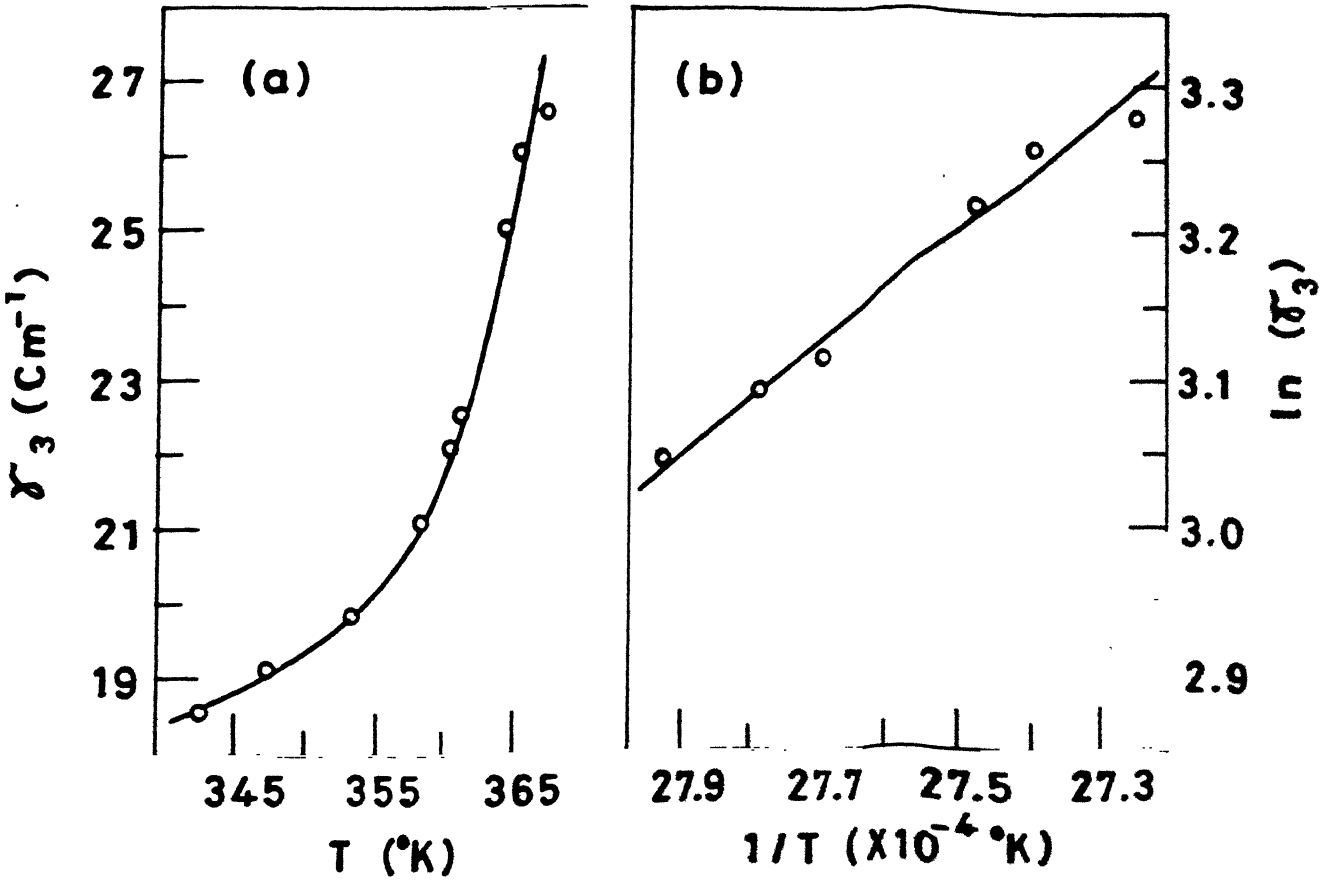

Figure 6.11: Exponential increase in the bandwidth (γ_3) of Raman librational mode (a) γ_3 versus T and (b) ln γ_3 versus 1/T (x 10^{-4} ^{o}K).

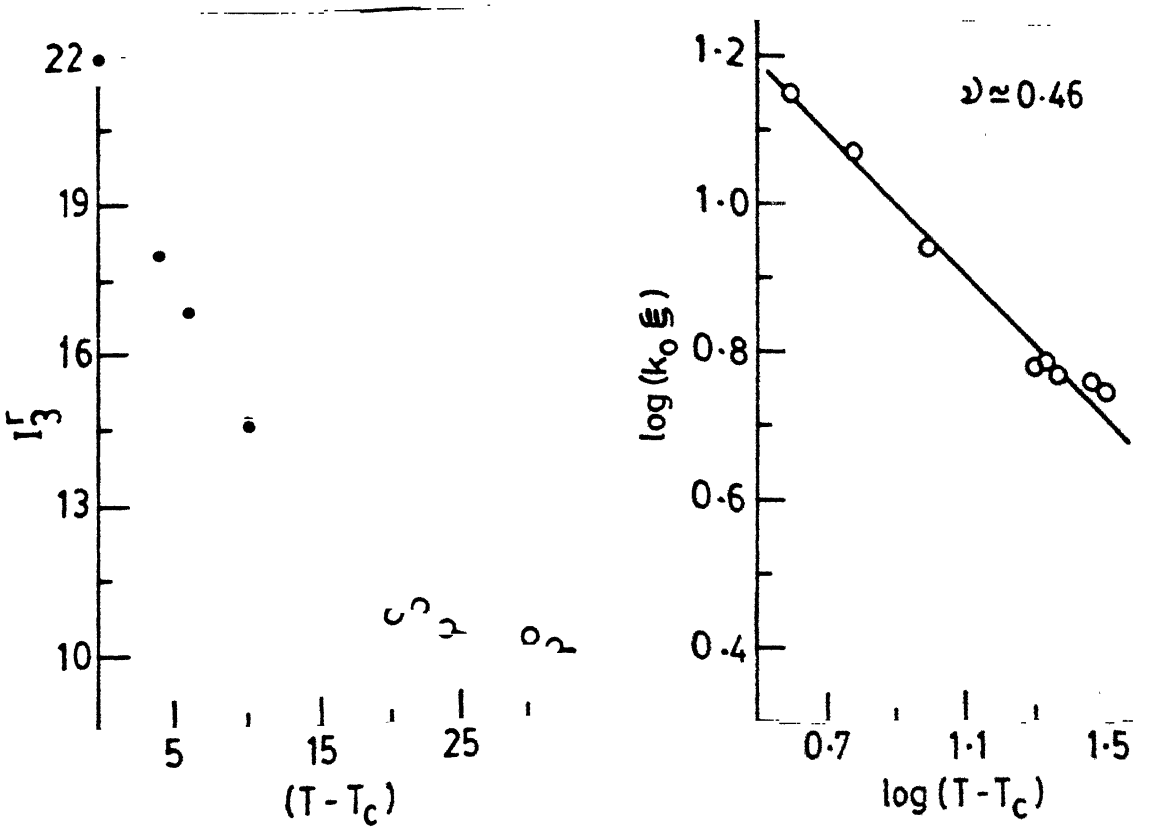

Figure 6.12: (a) Reduced peak intensity I_3^r of Raman librational mode versus T and (b) log $(k_o \xi)$ versus $(T-T_c)$ for $367 \leq T \leq 400^{\circ}K$.

CHAPTER 7

SUMMARY AND CONCLUSIONS

In this thesis a detailed analysis of (i) vibrational (Raman and IR) spectroscopy of SPTs in CsNCS, RbNCS and TlNCS; and (ii) "Period doubling" like oscillatory instabilities near the SPT in CsNCS crystal have been carried out. The results have been discussed in the context of known theoretical models.

Vibrational spectra of MNCS (M=Na, K, Rb, Cs, NH_4 and Tl) systems reveal considerable anharmonic effects even at room temperature. The peak frequencies of C-S and C-N stretching modes show strong cationic dependence. Whereas, the peak frequency of the bending mode is almost same for all the MNCS systems. It is interesting to note that C-N stretching frequency (ν_{C-N}) of alkali thiocyanates varies linearly with cationic radius as shown in Figure 7.1

Prior to the present work, vibrational studies of SPTs have been reported only for KNCS and NH_4NCS systems. Careful analysis of the temperature dependent Raman spectra of NaNCS crystal indicated that the orthorhombic NaNCS allows a reasonable amount of disorder but the sample gets melted before it had a chance to change the structure [1].

Vibrational spectroscopy of SPTs in RbNCS, CsNCS and TlNCS revealed no soft modes associated with the transitions. However, the indirect spectral manifestations of order-disorder SPTs have been found in the large changes of bandwidths, peak intensities and frequencies of many thermosensitive modes.

Exponential increase in the bandwidths of some of the vibrational modes near T_c have been used to extract activation energies (U) for the re-orientational motion of NCS^- ions. The values of U obtained for RbNCS, TlNCS and CsNCS are 0.46, 0.29 and 0.32 ± 0.02ev, respectively. These values are in good agreement with the previously reported (U ≃ 0.4lev) value for KNCS system [2]. Similarly, order parameter exponent (β) and correlation length exponent ν have been extracted from the characteristic changes in the integrated (or reduced peak) intensities of some of the thermosensitive vibrational modes. The value of β obtained for CsNCS, RbNCS and TlNCS are 0.35, 0.45 and 0.46 ± 0.04, respectively. The value of $\nu \simeq 0.46 \pm 0.04$ for TlNCS is strikingly consistent with the mean field exponent.

Comparison of present studies with known ones in other systems reveals an "antiferroelectric" like structure and the existence of internal field in the ordered orthorhombic phases of RbNCS and TlNCS. Moreoever, the observed spectral changes suggest that the order-disorder transitions, in all the studied samples, occur as both cation and anion are in motion. This mechanism for the phase transition involving a co-operative dynamic re-orientational disordering near T_c as both ions are in motion [Figure 7.2] is consistent with previously reported X-ray [3,4] and neutron diffraction studies [5]. More experiments have to be performed to understand clearly the anharmonic interactions and to establish all the possible couplings in these materials. Further, it would be interesting to extend the present work to SPTs in mixed crystal alkali thiocyanates.

Among all the SPTs in MNCS systems, the transition in CsNCS is found to be completely different. The large entropy change at T_c, the first order character of the transition, the cubic symmetry, enhanced anharmonicities near T_c and highly disordered nature of the phase I are unique features of CsNCS sample among all the MNCS systems. The most interesting and novel aspect is the observation of laser induced temporal oscillations and cascade of period doublings as a function of laser irradiation time near the SPT in CsNCS crystal. From the striking similarities between the observed phenomenon and period doubling bifurcations which occur in diverse nonlinear physical, chemical and biological systems, different oscillatory regions in CsNCS crystal have been related to successive instabilities as some internal parameter of the system changes with the irradiation time in a self-controlled manner. Considering thermal and photo induced changes as the major sources, probable nonlinear interaction mechanisms for the observed phenomenon have been proposed.

More experiments are needed to understand the mechanisms involved and to find out the parameters which control the stability of periodic oscillations in CsNCS crystal. Further work is planned to obtain well controlled time series data for quantitative analysis. Finally, it should be emphasized that the observed oscillatory scattering in CsNCS crystal is the first of its kind. In order to explain all the observations quantitatively, a theoretical model is needed which takes into account the combined effects of structural and photo-induced changes on the optical characteristics of CsNCS crystal.

References

[1] S. Sathaiah, V.N. Sarin and H.D. Bist, "Raman scattering studies of NaNCS single crystal above room temperature", presented at Int. Conf. Raman Spectr. Calcutta (1988).

[2] F.J. Owens, Solid St. Commun. 29, 789 (1979).

[3] R. Lippman and R. Rudman, J. Chem. Phys. 79(7), 3457 (1983).

[4] S. Yamamoto, M. Sakuno and Y. Shinnaka, J. Phys. Soc. Jpn. 56(12), 4393 (1987).

[5] B.K. Moss, S.L. Mair, C.J. Mcintyre and R.K. McMullan, Acta. Crystallogr. B43, 16 (1987).

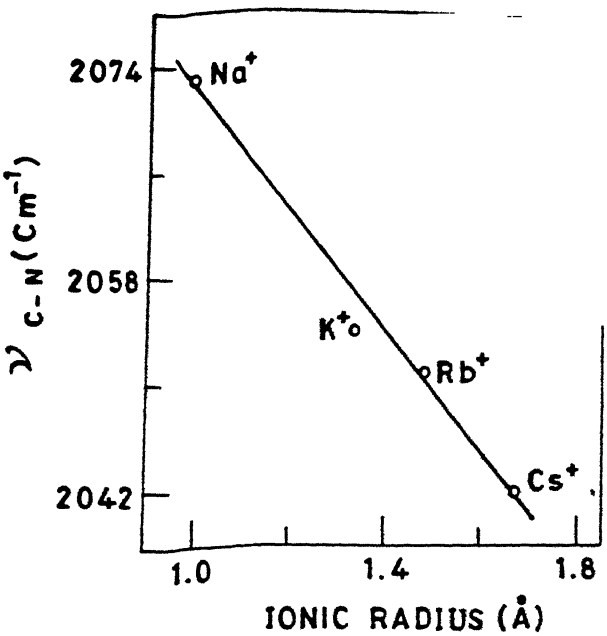

Figure 7.1: Variation in the peak frequency of C-N stretching mode (ν_{C-N}) with cationic radius for four alkali thiocyanate (NaNCS, KNCS, RbNCS and CsNCS) systems.

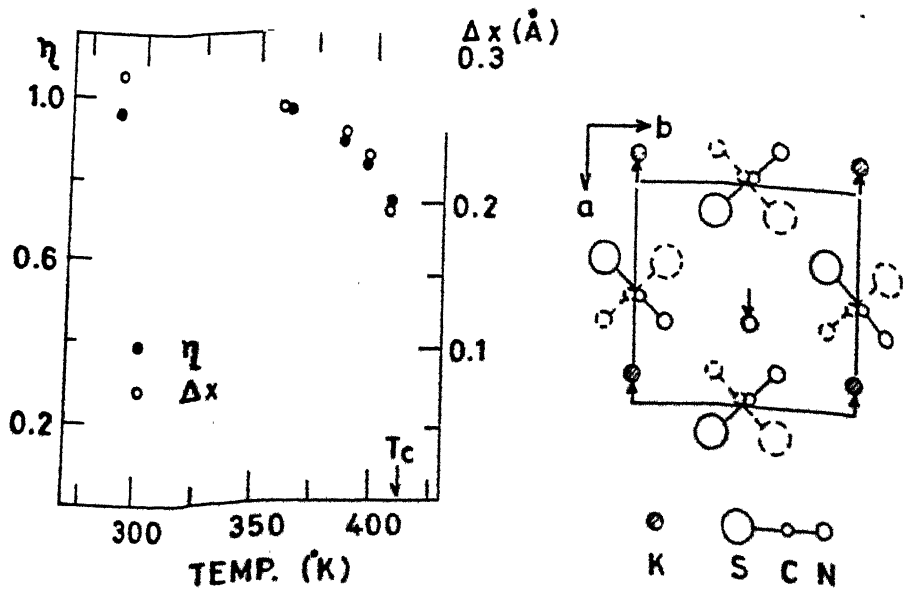

Figure 7.2: Temperature dependences of the order parameter η of NCS^- and the spontaneous displacement Δx of K^+ in KNCS system. Both are scaled at 363°K [4]